



3 1293 01409 8663

THESIS

Z

LIBRARY
Michigan State
University

This is to certify that the

dissertation entitled

"Substrate Morphology's Influence on the
Overlayer Structure and Oscillator Strength"

presented by

Hong Wang

has been accepted towards fulfillment
of the requirements for

Ph.D. degree in Physics

Major professor

R. Tobin

Date January 9, 1995

**PLACE IN RETURN BOX to remove this checkout from your record.
TO AVOID FINES return on or before date due.**

DATE DUE	DATE DUE	DATE DUE
_____	_____	_____
_____	_____	_____
_____	_____	_____
_____	_____	_____
_____	_____	_____
_____	_____	_____
_____	_____	_____

**SUBSTRATE MORPHOLOGY'S INFLUENCE ON THE
OVERLAYER STRUCTURE AND OSCILLATOR
STRENGTH**

By

Hong Wang

A DISSERTATION

Submitted to
Michigan State University
in partial fulfillment of the requirements for the degree of

DOCTOR OF PHILOSOPHY

Department of Physics and Astronomy
and Center for Fundamental Materials Research

1995

ABSTRACT

SUBSTRATE MORPHOLOGY'S INFLUENCE ON THE OVERLAYER STRUCTURE AND OSCILLATOR STRENGTH

By

Hong Wang

I used infrared spectroscopy (IRS) and electron energy loss spectroscopy (EELS) to probe the influence of substrate morphology on the interaction strength among coadsorbates and hence on the overlayer structure and on the oscillator strength. We compared the coadsorption behavior of H and CO on both steps and terraces of the Pt(335) surface, and compared our results with previous studies on similar surfaces. We also compared the cross section and Stark tuning rate of edge and terrace CO.

Our infrared spectroscopy study of coadsorption of H and edge CO on Pt(335) show that along the step edges of the Pt(335) surface, coadsorbed H and edge CO actually mixed together. In contrast, on Pt(111) and Pt(112) surfaces, coadsorbed CO and H segregate into islands. We proposed an overlayer structure model to explain our data, in which adsorbed H continuously shifts CO from atop to bridge binding. The different results on Pt(112) and Pt(335) mean that the interaction strength among the coadsorbates changes with the terrace width.

With EELS, we directly verified the proposed CO site shift. We also surprisingly found that coadsorbed H produced no observable effect on the HREEL spectra of terrace CO.

With IRS and EELS, we found that edge atop CO has twice the cross section of terrace atop CO, and that edge atop CO's Stark tuning rate is also twice that of terrace atop CO. We explained these and several previous results with an electrostatic model.

This model also partly accounts for the much smaller difference found on surfaces with much wider terraces.

Our data show that the screening of IR and static fields is different, whether by changing coadsorbate coverage or by changing the substrate sites. This is not explained by the standard dipole-dipole coupling model. We also found that the Stark tuning rate measured in electrochemical cells is 3 times larger than our data if standard models of electrochemical double layers are used. Coadsorption of H also produces different effects in the two environments. These results require much better understanding of how the adsorbate responds to the applied fields.

ACKNOWLEDGMENTS

I am grateful to Professor Roger G. Tobin, my thesis adviser, for his support, encouragement, and efforts to provide me with a complete training in scientific research, and especially for his patience. I learned greatly from both his scientific insight and his way of life.

I am also grateful to Drs. David K. Lambert and Galen B. Fisher, my advisors in General Motors Research and Development Center, for their support for my work as well as for my career. I have benefited a great deal from their very different yet individually successful styles of research.

Drs. Tobin, Lambert and Fisher's contribution and their spirits are reflected throughout this work. Without their help, it is impossible for me to carry out this research.

I would also like to thank Craig L. DiMaggio, for teaching me how to run many instruments carefully and correctly, and for his help in carrying out many experiments. For my 3 years in GM research, many people there have given me candid advice on both research and many personal issues. I would like to thank particularly Drs. P. C. Wang, D. Y. Wang, L. Green, D. L. Partin, C. M. Thrush, T. Perry, Y. T. Cheng, D. N. Belton and T. E. Moylan.

I enjoyed the friendship and support from other members of Roger's group, Dr. C.Chung, Dr. J. S. Luo, K. C. Lin, D. E. Kuhl, J. Gemmell, E. Krastev. I thank Dennis, John and Ati especially for their caring about my future. I would like to thank John particularly for correcting the English for a large portion of this dissertation.

I would like to thank other Chinese students here in the Physics Department for their support, especially, Q. Yang, Q. F. Zhu, J. D. Chen, B.Y. Chen, Dr. Y. Cai, Dr. W.Q. Zhong. I would also like to thank P. H. Liu, C. C. Wang, P. C. Liao, Y. L. Yeh, S.

Liu, and many other friends who make the five years at Michigan State a very memorable period of my life.

All that I accomplished is given by my parents, who, even in the most difficult years, taught me the importance of education and knowledge. They have always been my mental support and the origin of my strength to face the challenges. They have given me the most parents can give.

Finally, I want to thank my wife, Mei, the source of my happiness. She warms my heart with her smile. Without her love, I could not have done nearly as much.

This work is partially supported by The Petroleum Research Fund, administered by the American Chemical Society, and the National Science Foundation under Grant # DMR-9201077. It is also partially supported by General Motors.

TABLE OF CONTENTS

LIST OF FIGURES	ix
LIST OF TABLES	xv
1. INTRODUCTION	1
References	10
2. EXPERIMENTAL TECHNIQUES	12
2.1 Scattering mechanisms and selection rules for RAIRS and HREELS	14
2.2 HREELS	15
2.2.1 Operation of the HREELS system	17
2.3 Infrared spectroscopy	18
2.3.1 RAIRS with polarization modulation	21
2.3.1.1 Quantitative analysis of polarization modulated RAIRS	23
2.3.2 Electroreflectance Vibrational Spectroscopy (EVS)	25
2.3.2.1 Quantitative analysis of EVS	26
2.3.3 Determination of the Stark tuning rate	27
2.3.4 Measurement of the <i>E</i> -field	29
2.4 TPD	30
2.5 Sample preparation and characterization	33
References	48
3. COADSORPTION OF HYDROGEN AND CO ON Pt(335): STRUCTURE AND VIBRATIONAL STARK EFFECT	50
1. Introduction	50
2. Experiment	51
3. Experimental results	54
3.1 TPD	54
3.2 ir spectra	56

4. Structural model of the CO + H overlayer	56
5. Vibrational Stark effect and coadsorbates	61
5.1 Background	61
5.2 Our experiment	66
5.3 Comparison with electrochemical experiments	69
6. Summary	70
References	83
4. H-CO INTERACTION ON THE TERRACES AND STEP EDGES OF THE Pt(335) SURFACE	89
1. Introduction	89
2. Experiment	90
3. Results and discussion	91
3.1 Coadsorption of H and CO on the step edge	91
3.2 Coadsorption of H and CO on the terrace	94
4. Summary	98
References	107
5. VIBRATIONAL INTENSITY AND STARK TUNING RATE OF EDGE AND TERRACE CO ON Pt(335)	110
1. Introduction	110
2. Experiment	112
3. Results	113
3.1. RAIRS and EVS	113
3.2. HREELS	114
3.3. Analysis of the atop intensity	115
4. Discussion	116
5. Conclusion	123
References	130

6. CONCLUSIONS	132
References	136

LIST OF FIGURES

Chapter 1

- Figure 1-1.** **8**
Side view of the Pt(335) surface.
- Figure 1-2** **9**
Atop and bridge CO on Pt(111).

Charter 2

- Figure 2-1.** **35**
Dipole moment perpendicular to the metal surface is reinforced, dipole moment parallel to the surface is screened.
- Figure 2-2.** **36**
Block diagram of an electron energy loss spectrometer (Luo [30]).
- Figure 2-3.** **37**
Schematic diagram of the system for high resolution electron energy loss spectroscopy in this work (B. A. Sexton [34]).
- Figure 2-4.** **38**
The surface electric field E/E_0 in (a), and the quantity $(E/E_0)^2/\cos\theta$ in (b) for platinum at 2100 cm^{-1} ($\epsilon = -375 - 200i$) as a function of the incidence angle θ (Bradshaw and Schweizer [2]).
- Figure 2-5.** **39**
The process of a RAIR spectrum: comparing the scans with clean sample and with adsorbate (CO) (Luo [30]).
- Figure 2-6** **40**
Optical set up for RAIRS and EVS showing detector D, sample S, and electrode E, polarizers P_1 and P_2 (Lambert [27]).

Figure 2-7	41
Schematic diagram of computer-controlled wavemeter for laser frequency calibration. Back-to-back hollow corner cube reflectors are mounted on a ball slide translation stage driven by a stepping motor. The stage moves freely except near the end of its travel where a beaded chain coupling becomes rigid and reverses its motion. (Evans and Lambert [21])	
Figure 2-8.	42
Schematic of the system used for polarization modulated reflection absorption infrared spectroscopy (RAIRS) (Luo [30]).	
Figure 2-9	43
Process of measuring the EV spectrum by modulating the <i>E</i> -field applied to the surface (Luo [30]).	
Figure 2-10	44
Schematic of the system used for electroreflectance vibrational spectroscopy (EVS) (Luo [30]).	
Figure 2-11	45
Schematic of the system used for temperature programmed desorption (TPD) (Luo [30]).	
Figure 2-12	46
TPD spectrum for saturation coverage of NO on Pt(335). The highest peak is from edge NO and the rest are from terrace NO. All the terrace NO stays at identical sites before heating. (Wang <i>et al.</i> [32])	
Figure 2-13	47
C(4×2) structure of 0.5 ML CO on Pt(111) (Luo [30]).	

Chapter 3

Figure 3-1.	73
--------------------	-----------

a) TPD spectra obtained by desorbing CO from the Pt(335) surface (without H). The CO dosages used to prepare (a)–(d) were 20, 1.5, 1.0 and 0.5 L, respectively.

b) Fit of two Gaussians (one from edge CO and the other from terrace CO) to the 20 L TPD spectrum.

Figure 3-2. 74

TPD spectra obtained by desorbing H₂ from the Pt(335) surface (without CO). From top to bottom the dosages used to prepare the surface were 40, 20, 10, 3, 1.5, 0.8, 0.5, 0.3 and 0.1 L.

Figure 3-3. 75

TPD spectra obtained by desorbing H₂ from the Pt(335) surface (with and without CO). In a) $\theta_{\text{CO}} = 0$, $\theta_{\text{H}} = 0.35$ ML; in b) $\theta_{\text{CO}} = 0$, $\theta_{\text{H}} = 0.25$ ML; in c) $\theta_{\text{CO}} = 0.05$ ML, $\theta_{\text{H}} = 0.31$ ML; and in d) $\theta_{\text{CO}} = 0.16$ ML, $\theta_{\text{H}} = 0.30$ ML. The hydrogen doses were a) 0.5 L, b) 0.3 L, c) 0.8 L and d) 4.5 L.

Figure 3-4. 76

Measured H occupancy of edge sites vs H₂ dosage with various pre-coverages of CO. The data with ●, ▲ and ■ were obtained by pre-dosing with 0.5, 1.0 and 1.5 L of CO, respectively.

Figure 3-5. 77

RAIR and EVS spectra of CO coadsorbed with H on Pt(335). The CO coverage was 0.16 ML for all of the spectra. From top to bottom the spectra are for $\theta_{\text{H}} = 0.06$, 0.10, 0.16, 0.18, 0.21, 0.29, and 0.06 ML. The lowermost spectrum was obtained after the sample had been heated to 420 K to desorb the H but leave the CO in place.

Figure 3-6. 78

Data showing the effect of coadsorbed H on the resonant frequency of the C-O stretch vibration at atop sites, for CO and H coadsorbed on Pt(335).

Figure 3-7. 79

Data showing the effect of coadsorbed H on integrated intensity S of the C-O stretch vibration at atop sites, for CO and H coadsorbed on Pt(335).

Figure 3-8. 80

Data showing the effect of coadsorbed H on the Stark tuning rate (dv/dE) of the C-O stretch vibration at atop sites, for CO and H coadsorbed on Pt(335).

Figure 3-9. 81

Data showing the effect of coadsorbed H on the integrated intensity S for atop CO on Pt(335). With each CO coverage, the data have been normalized by S_0 , the value of S at the lowest H coverage. The data with 0.06, 0.12 and 0.16 ML of CO are represented by ●, ▲ and ■, respectively.

Figure 3-10. 82

Data showing the effect of coadsorbed H on the screening factors (●) γ_{ir} and (◆) γ_{dc} for CO on Pt(335). We assume that $\gamma_{ir} = 1$ and $\gamma_{dc} = 1$ at the lowest coverage, and that $\gamma_{ir} \propto \sqrt{S/\theta_{atop}}$ and $\gamma_{dc} \propto (dv/dE)$.

Chapter 4

Figure 4-1. 99

TPD spectra obtained by desorbing H_2 from the Pt(335) surface (without CO). From top to bottom, the relative dosages used to prepare the surface were 10, 5, 2.5, 1, 0.5, 0.25, and 0.1. The absolute dosages are uncertain because a doser was used, but a relative dose of 1 is approximately 1×10^{-6} torr s.

Figure 4-2. 100

EEL spectra of edge CO on Pt(335) as a function of H coverage. The CO coverages in (a) and (b) are 0.07 and 0.13 ML, respectively. The spectra are arranged so H coverage increases up the page. In (a) the H coverages are 0.02, 0.10, 0.14, 0.18, 0.22, and 0.24 ML; in (b) 0 ($\theta_{CO} = 0$ also), 0.01, 0.06, 0.10, 0.13, 0.22, and 0.40 ML.

Figure 4-3. 101

(a) Ratio I_B/I_{tot} of bridge to total (bridge +atop) single-loss EELS intensity as a function of H coverage, for the spectra in Fig. 4-2. (b) Ratio I_B/I_E where I_E is the elastic EELS intensity, as a function of H coverage, for the spectra in Fig. 4-2.

Figure 4-4. 102

EEL spectra at various CO coverages after predosing with 0.25 ML H to block the edge sites. The spectra are arranged so CO coverage increases up the page: $\theta_{CO} = 0.05, 0.08, 0.13, 0.19, 0.28,$ and 0.36 ML.

Figure 4-5. 103

Ratio I_B/I_{tot} as a function of CO coverage, for terrace CO, with the edge saturated with H (for the EEL spectra in Fig. 4-4). Also shown is the bridge CO coverage, calculated assuming that the EELS cross section of terrace atop CO is a factor 1.8 times that of terrace atop CO.

Figure 4-6. 104

EEL spectra of 0.05 ML terrace CO as a function of postdosed H coverage. The spectra are arranged so θ_H increases up the page: $\theta_H = 0.24, 0.46, 0.70,$ and 0.70ML.

Figure 4-7. 105

Ratio I_B/I_{tot} from EELS intensity for terrace CO, as a function of H coverage, for three CO coverages: \blacktriangle 0.05 ML, \bullet 0.13 ML, and \blacksquare 0.19 ML.

Figure 4-8. 106

TPD spectra obtained by desorbing a saturation coverage H_2 from the Pt(335) surface and by desorbing 0.48 ML of H on clean surface. In (a) $\theta_{CO} = 0$ ML, $\theta_H = 1.0$ ML; in (b) $\theta_{CO} = 0.05$ ML, $\theta_H = 0.69$ ML; in (c) $\theta_{CO} = 0.13$ ML, $\theta_H = 0.55$ ML; and in (d) $\theta_{CO} = 0.19$ ML, $\theta_H = 0.45$ ML; (e) $\theta_{CO} = 0$ ML, $\theta_H = 0.48$ ML.

Chapter 5

Figure 5-1. 125

RAIR and EV spectra for 0.16 ML CO on a Pt(335) surface precovered with 0.72 ML of H, before and after annealing the sample at 420 K. Upon H desorption, the CO moves to edge sites.

Figure 5-2. 126

RAIR and EV spectra for 0.14 ML CO on a Pt(335) surface predosed with 0.1 L, before and after annealing the sample at 260 K. Upon annealing, the CO moves from terrace sites to edge sites, while the O moves to terrace sites.

Figure 5-3. 127

HREEL spectra for 0.16, 0.13, 0.08, 0.05 ML CO (from top to bottom) on a Pt(335) surface precovered with 0.25 ML of H, before and after annealing at 420 K.

Figure 5-4. 128

Calculated E field normal to the average surface plane, as a function of fractional distance across the terrace. The field is normalized to the field on a flat surface, and is calculated along a line one-half step height above the terrace, as shown in the inset. The dotted curve represents a surface with narrow terraces similar to Pt(335); the solid curve represents a surface with much wider terraces, similar to that used in Refs. 8 and 9 of Chapter 5.

Figure 5-5. 129

EV and RAIR spectrum for 3.5 L (0.26 ML) CO on clean surface. Strong EV features are seen corresponding to both of the peaks in the RAIR spectrum, indicating that edge and terrace CO have comparable Stark tuning rates. The zero-crossings in the EV spectrum occur at the same frequencies as the peaks in the RAIR spectrum. These results are in contrast to those reported in Ref. 4 of Chapter 5.

LIST OF TABLES

Table I. **72**

Summary of the ir spectra with only CO on Pt(335). Here θ_{CO} is the CO coverage, ν is the frequency of the peak in the ir spectrum, $(\Delta R)/R$ is the maximum CO-induced reflectivity change in the RAIR spectrum, $S = \int (\Delta R) / R d\nu$, and $(d\nu/dE)$ is the Stark tuning rate in terms of the externally applied E -field.

Table II. **124**

Ratios of vibrational intensity, vibrational cross section, and Stark tuning rate of edge atop CO compared to terrace atop CO. The intensity and Stark tuning rate ratios are determined directly from the experimental data. The cross section ratios include corrections for loss of CO during annealing and for migration between bridge and atop sites, as discussed in the text.

Chapter 1

Introduction

This work deals with chemisorption and coadsorption of several simple molecules and atoms on a stepped Pt(335) surface and how their interactions change over site differences of atomic scale. This work demonstrates that the existence of monatomic steps profoundly influences the adsorption and coadsorption behavior of adsorbates on the surface. Not only the adsorption on step edges, but the adsorption on the terraces also differs from that on a flat surface.

Chemisorption of gas molecules and atoms on metal surfaces is a very important issue in catalysis, coating and anti-corroding [1]. Transition metals, like Pt, are among the most commonly used catalysts. The real catalysts used in applications are polycrystalline and have a large concentration of steps, defects and kinks. A study on a regularly stepped surface like (335) is an important step toward understanding real situations. One can compare the different behavior of adsorbate on terraces and steps and even compare them with flat surfaces gaining insight into the chemical and physical processes that happen on real catalyst surfaces. Meanwhile, more than one kind of species is present on the catalyst under real conditions. A coadsorption study should also be very beneficial in understanding the interaction between the adsorbed species on the surface and how the interactions change with site differences at the atomic scale.

The Pt(335) crystal, Pt(s)[4(111)×(100)] in step-terrace notation, is shown in Fig. 1-1. The (335) surface consists of 4 atom wide (111) terraces, separated by monatomic (100) steps.

The essential tool in this study is vibrational spectroscopy. Vibrational spectroscopy is based on the fact that the constituent atoms of a molecule, solid, or combination of the two execute multidimensional, quasiperiodic motion over potential

energy surfaces that are determined by the electronic/chemical state of the system, when the energy content of the motion is substantially less than the electronic or chemical dissociation energies of the bound system [2]. The low-lying vibrationally excited eigenstates associated with energies in the $\sim 50 - 250$ meV ($400 - 2000$ cm^{-1}) range involve light atoms such as H, C, N, and O which are of obvious chemical importance. Transitions between these states give rise to a spectrum which is a characteristic signature of both the chemical species being interrogated and its local environment. The corresponding frequency of the quasiperiodic motion of the (usually heavy) atoms comprising the substrate is usually much less than the intramolecular frequencies. Consequently the vibrational modes of the admolecules retain much of their free space character, which permits species identification. The small deviations from free space behavior, such as in frequencies and line widths, carry information about the local environment such as bond site or molecular orientation and the characteristics of the adsorbate-substrate interaction[2].

Adsorption on the surfaces can be atomic and molecular and can have many different bonding situations. For the species in this study, CO stays in molecular form on Pt(335), hydrogen dissociates on this surface, and oxygen stays in molecular form below 150 K but dissociates above 200 K [15]. Because CO adsorption is most heavily studied and hence most clearly understood, I will use it as an example to illustrate the general concepts of adsorption. Let us first look at CO on Pt(111), a flat surface. Studies have shown that CO binds vertically on this surface with the C atom at the bottom [3]. (It is relatively easy to understand, since CO donates charges to the metal, but oxygen is unlikely to do this.) At low coverage, all the CO stay straight on top of a Pt atom. At high coverage CO can occupy two-fold bridge sites[16], as shown in Fig. 1-2. The binding energy for atop CO is slightly higher than that of bridge CO, 1 kcal/mol (0.043 eV). When a step is introduced, as on our sample, the binding energy at the step is significantly larger, because of the lower coordination number for the substrate atom

there. So the adsorption takes place first at the steps and then on the terraces. On Pt(335), both edge and terrace CO can have atop and bridge bondings. Experiment has also found that CO does not tilt away from the surface normal by more than 10° [4].

Spectroscopy techniques used in this study were polarization modulated reflection absorption infrared spectroscopy (RAIRS), electroreflectance vibrational spectroscopy (EVS) and high resolution electron energy loss spectroscopy (HREELS). Temperature programmed desorption spectrometry (TPD) was also extensively used. Detailed discussion about the techniques will be given in Chapter 2.

In this work, I studied adsorption of CO, and coadsorption of H and CO, O and CO, on Pt(335) with the above mentioned experimental techniques, with the focus on comparison between edge and terrace sites. The existence of the steps profoundly changes not only the morphology of the surface but also the surface electronic states. Consequently, adsorption and coadsorption on step sites and terrace sites show different character as compared with each other. I performed several experiments to investigate the difference between steps and terraces and compare them with a flat surface. First, I successfully showed that the interaction between coadsorbed species on step edges is different from that on flat surfaces. Furthermore, this interaction is modulated by the terrace width; and the interaction on the terraces is also different from that on flat surface. Second, I demonstrated that the vibrational cross section of the same species is different for step and terrace sites, and that the difference is mostly from the field enhancement on the step and screening on the terraces. The difference between the chemical environment of the two sites is very small.

The general motivation of this work comes from many previous studies that demonstrate differences between step and terrace sites. In particular, before our work, all coadsorption studies of CO and hydrogen on single crystal Pt surfaces have found them to be strongly repulsive: CO and hydrogen segregate on both Pt(111) [5,6] and along the step edges of Pt(112) [7]. When segregation happens, CO is compressed together by

coadsorbed hydrogen, thus, the hydrogen-induced change in the spectrum for CO is similar to the change caused by increased CO coverage on a clean surface. On Pt(111), with increasing CO coverage, CO first occupies atop sites and then bridge sites. The vibrational frequency also increases with CO coverage as a result of stronger coupling between the CO molecules[16]. Segregation of CO and H on Pt(111) is evidenced by the CO site shift, frequency shift and IR peak shape changes [6] and by thermal energy atom scattering (TEAS) and low energy electron diffraction (LEED) [5]. Edge CO on Pt(112) is studied by electron stimulated desorption ion angular distribution (ESDIAD), which probes the direction of the adsorbate's axis on the surface [7]. Along the step edges of Pt(112), edge CO exhibits complex tilting angles with increasing coverage. Segregation of edge CO and H on Pt(112) is evidenced by the CO pattern change with increasing H coverage, which follows the same pattern change as the CO density increases [7]. Previous experimental evidence and theoretical calculations have shown that H-CO interaction on the surface can only be mostly indirect, or through-metal. This kind of interaction depends strongly on the perturbation of the charge density of the substrate metal by the adsorbates. It is conceivable that the terrace width can influence the strength of this kind of interaction by curbing off the charge density perturbation at the steps.

I performed a RAIRS and EVS study on coadsorption of edge CO and H on Pt(335), which is structurally similar to Pt(112) and Pt(111) [17]. The results are presented in Chapter 3. My results clearly show that even though the interaction between edge CO and coadsorbed H is repulsive, the strength of this repulsion is weaker compared to the CO-CO, and H-H repulsion. Edge CO and H mix together within the hydrogen region, and my experimental evidence implies that CO stays only on bridge sites within such islands, while outside such islands CO is unperturbed by H and stays on atop sites. This result, compared with the (112) result, proves that the interactions between edge coadsorbates are influenced by the terrace width.

I performed HREELS experiments to directly verify the site shifting of edge CO by the coadsorbed H [18]. I also studied the coadsorption of terrace CO and H with HREELS [18]. The results are presented in Chapter 4. I found that the site shifting of CO is accompanied by a significant change in bridge CO's cross section. The experiments also show H did not produce any observable effect to the terrace CO, different from both the flat surface result and the edge CO result. These results show that the interactions between coadsorbates are much more complex than previously believed. A subtle change in surface morphology can radically change the formation of the adsorbed layer.

Another direct motivation of this work is the controversy over whether there is significant *E*-field enhancement at the step edges. One possible difference between the edge and terrace species is that they may have different cross sections, which may have physical or chemical origins. A previous IR study of CO on Pt(335) has shown that the increase of IR intensity with CO coverage is 2.7 times slower when terrace CO appears than for edge CO [8]. Greenler *et al.* explained this with a classical electrodynamics calculation of *E*-field enhancement at the step edges [9]. On the other hand, Lambert and Tobin compared the cross section of edge CO on Pt(335) with CO on Pt(111) and found them to be similar [10], which seems to contradict Greenler *et al.*'s explanation. Furthermore, Reutt-Robey *et al.*, with a time-resolved IR study, reported that the cross section of edge CO and terrace CO is the same within 5% on Pt(S)[28(111)×(110)] and that put a serious question on whether there is any difference on edge and terrace CO's cross sections [11,12].

In most of the above mentioned comparisons, terrace CO coexists with edge CO. Strong intensity coupling between the two makes it difficult to separate the contribution to the total intensity from edge and terrace CO. I performed both RAIRS and EVS as well as HREELS experiments to compare the cross section of terrace and edge CO directly, on Pt(335) [19]. The results are presented in Chapter 5. The terrace CO is

produced by blocking the step edges with H or O at low temperature. After heating the overlayer to a certain higher temperature, terrace CO will move to edge sites. The questions I wanted to answer were first whether there is difference in edge and terrace CO's cross section, second, if there is, whether it is from chemical origin or from physical origin?

I found clearly that edge CO has a cross section twice as large as terrace CO on Pt(335). I also performed classical E -field calculations to show that the difference in cross section mostly originates from field strength difference at the two sites, which consists of both the enhancement at the edge and screening on the terrace. My calculation also shows that screening on the terraces decrease rapidly with the increasing of the terrace width. This explains half the difference between our result and the result on Pt(s)[28(111)×(110)].

This work is also significant in reconfirming the previous finding of different screening of static and IR fields by coadsorbates[13], which is not in agreement with the present understanding of surface electrostatics. Furthermore, I find that the screening by the metal of the static and IR fields is also different, which again disagrees with the current understanding of electrostatics. These findings reveal that the current understanding of surface electron response to applied E -field and the depolarization effect by coadsorbates is still very incomplete.

This work is also important in providing a comparison between the response of adsorbates to applied static E -field in ultrahigh vacuum (UHV) and in an electrochemical environment. Lambert [14] has measured the Stark tuning rate of CO on a flat Ni surface in vacuum and it is in agreement with current models of the double layer between metal and electrolyte in the electrochemical cell. However, from the first direct comparison between the same adsorbate on same substrate in UHV and electrochemical cell, CO on Pt(111) [13], the Stark tuning rate measured in UHV is a factor of two smaller than that from the electrochemical measurement.

My measurement of CO's Stark tuning rate on Pt(335) provides another direct comparison with the electrochemical experiment [20]. I also found that the Stark tuning rate from the UHV measurement is much too small compared to that from electrochemical measurements to be explained by current double layer models. The coadsorbed H also produces different results in the two environments. In UHV the CO's Stark tuning rate is not influenced by H while in the electrochemical experiment, CO's Stark tuning rate goes to zero in the classical hydrogen region. These profound differences demonstrate that the current understanding of the double layer between the metal and the electrolyte needs significant correction.

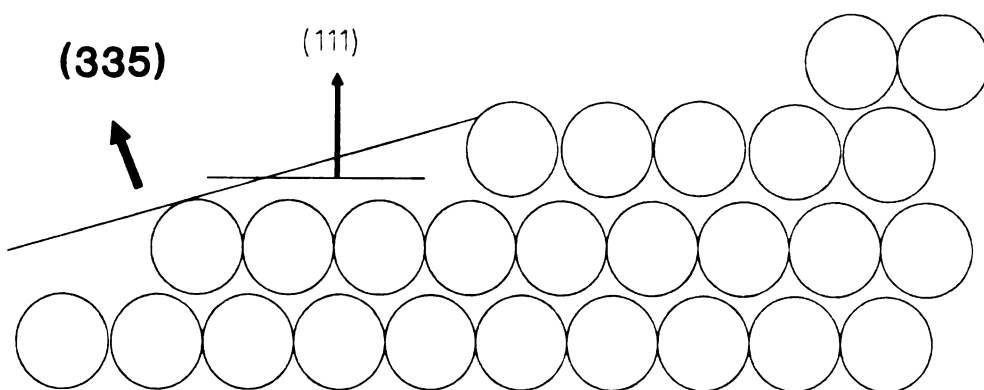


Figure 1-1. Side view of the Pt(335) surface.

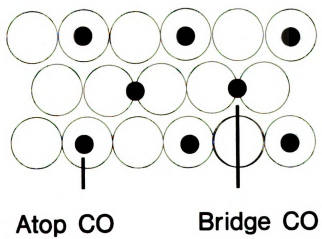


Figure 1-2. Atop and bridge CO on Pt(111).

References

1. G. A. Somorjai, *Chemistry in Two Dimensions: Surfaces*, (Cornell University Press, Ithaca, New York, 1981).
2. J. W. Gadzuk, in *Vibrational Spectroscopy of Molecules on Surfaces*, edited by J.T. Yates, Jr. and T. E. Madey, (Plenum, New York, 1987).
3. P. Hoffman, S. R. Bare, N. V. Richardson, and D. A. King, *Solid State Commun.* **42**, 645 (1982).
M. Trenary, S. L. Tang, R. J. Simonson, and F. R. McFeely, *Surf. Sci.* **124**, 555 (1983).
4. J. S. Somers, T. Linder, M. Surman, A. M. Bradshaw, G. P. Williams, C. F. McConville, and D. P. Woodruff, *Surf. Sci.* **183**, 576 (1987).
5. S. L. Bernasek, K. Lenz, B. Poelsema, and G. Comsa, *Surf. Sci.* **183**, L319 (1987).
6. D. Hoge, M. Tüshaus, and A. M. Bradshaw, *Surf. Sci.* **207**, L935 (1988).
7. M. A. Henderson and J. T. Yates, Jr., *Surf. Sci.* **268**, 189 (1992).
8. B. E. Hayden, K. Kretzschmar, A. M. Bradshaw, and R. G. Greenler, *Surf. Sci.* **149**, 394 (1985).
9. R. G. Greenler, J. A. Dudek, and D. E. Beck, *Surf. Sci.* **145**, L453 (1984).
10. D. K. Lambert, and R. G. Tobin, *Surf. Sci.* **232**, 149 (1990).
11. J. E. Reutt-Robey, Y. J. Chabal, D. J. Doren, and S. B. Christman, *J. Vac. Sci. Technol.* **A7**, 2227 (1989).
12. J. E. Reutt-Robey, Y. J. Chabal, D. J. Doren, and S. B. Christman, *J. Chem. Phys.* **93**, 9113 (1990).
13. J. S. Luo, R. G. Tobin, and D. K. Lambert, *Chem. Phys. Lett.* **204**, 445 (1993).
14. D. K. Lambert, *J. Chem. Phys.* **89**, 3847 (1988).
15. H. Wang, R. G. Tobin, G. B. Fisher, C. L. DiMaggio, D. K. Lambert, unpublished.
16. B. E. Hayden and A.M. Bradshaw, *Surf. Sci.* **125**, 787 (1983).
17. H. Wang, R. G. Tobin, and D. K. Lambert, *J. Chem. Phys.* **101**, 4277 (1994).

18. H. Wang, R. G. Tobin, D. K. Lambert, G. B. Fisher, C. L. DiMaggio, submitted to *Surface Science*.
19. H. Wang, R. G. Tobin, D. K. Lambert, G. B. Fisher, C. L. DiMaggio, to be submitted to *J. Chem. Phys*
20. C. S. Kim, W. J. Tornquist, and C. Korzeniewski, *J. Phys. Chem.* **97**, 6484 (1993)..

Chapter 2

Experimental Techniques

Spectroscopy techniques used in this work include two forms of IR spectroscopy, RAIRS and EVS, as well as HREELS. TPD is also extensively used in this work.. RAIRS, HREELS and TPD are among the most commonly used techniques in surface science study. Review articles on RAIRS, HREELS are readily available [1,2,3,4,5,6,7]. There are also several articles about the quantitative analysis of TPD[8,9]. The EVS system used is the only one in the world that can measure the first order Stark effect of adsorbed molecule in vacuum. It was built by Dr. D. K. Lambert at GM R&D center.

In HREELS, a monochromatic electron beam with energy of several eV is focused onto the surface at a relatively large angle, between 45-70°, and the energy distribution of the outgoing beam is analyzed. The electrons lose energy due to long range dipole scattering from the adsorbed molecules and excitation of the vibrational modes of the adsorbed molecules. By analyzing the energy loss spectrum, one can then gain information about the surface layer.

HREELS has several advantages. Among them are high sensitivity, wide dynamic range, and relatively quick data taking. Also, because the technique is quite mature, good HREEL spectrometers are commercially available. HREELS also has several disadvantages, the most evident of these are, low resolution, usually between 40-80 cm^{-1} in routine operations; less reliable absolute intensity due largely to work function variation caused by difference in the surface layer and ordering of the adlayer; and the requirement of vacuum. (By trading off sensitivity, recent advances by Ibach [10] in HREELS design have achieved 7.9 cm^{-1} resolution. Commercially available instruments have also recently arrived at the same level [11].) Because of the low resolution in our

HREELS, step and terrace species usually can not be distinguished as the frequency difference is only in the order of 20 cm^{-1} .

RAIRS is also a very widely used technique. In RAIRS, an IR beam is directed onto the sample at a near grazing angle. The interaction between the IR field and the vibration modes of adsorbates on the surface results in absorption of IR intensity at certain frequencies. By analyze the intensity distribution as a function of frequency, one can gain much information about the surface layer. In addition to high sensitivity, RAIRS has very high resolution, typically 1 cm^{-1} . High resolution is necessary in site assignment, in studying frequency shifts as the result of interaction between the adsorbates, which are usually of 10 cm^{-1} order, and in line shape studies which are particularly important in understanding the dynamics behind vibrational modes. Since RAIRS uses photons as the probe instead of electrons as in the HREELS, vacuum is not required for the technique itself. This significantly widens the applicable area to include applied studies. The biggest limitation to the current RAIRS technique is the lower frequency limit which can be reached. It is very difficult to apply RAIRS to frequencies lower than 800 cm^{-1} mainly due to the low intensity of the source and very high ambient noise. There has been much progress in this area, synchrotron sources which are several orders brighter than the conventional sources [12] can be used and ambient noise can be reduced by reducing the temperature of the whole system [13].

TPD has been widely used in studying kinetic parameters, like activation energy, pre-exponential factor, as well as in adsorbate coverage measurement and site assignment for admolecules desorbing from the surface. In TPD, the sample is heated from a low temperature to a higher temperature, and the partial pressure increases for the molecules of interest in the vacuum chamber are monitored as a function of the sample temperature. The various chemisorbed phases can be distinguished by the order in which they desorb. Population of individual phases can be deduced from the integration of the particular peak in the spectrum. It is dangerous to draw conclusions based on TPD alone, because

TPD is a technique that changes the surface condition, unlike RAIRS or HREELS. When admolecules of one chemisorbed phase begin to desorb, all the admolecules in phases with lower activation energy have already desorbed and the sample temperature is high enough for the admolecules in this phase to rearrange. So in many cases, TPD can only be used as a reference with RAIRS or EELS required to supply crucially needed information.

In this Chapter, I will discuss in detail the principles of the three techniques and the actual experimental set up in my work. I will also discuss briefly the sample preparation and characterization at the end. Because of the unique nature of the polarization modulated RAIRS and EVS, discussion concerning them will be lengthier than that of HREELS and TPD.

2.1 Scattering mechanisms and selection rules for RAIRS and HREELS

When an adsorbate chemisorbs on a metal surface, there is usually some charge transfer δe between the adsorbate and the substrate. The dipole moment due to the transferred charge and its image in the substrate is [6]

$$\mu = 2\delta e(S_0 + q(t)). \quad (2.1.1)$$

where S_0 is the equilibrium location of the static charge centroid from the image plane and q is a possible oscillatory small displacement about this equilibrium point. Since energy transfer will not occur in a static field, the static portion of μ does not contribute to the interaction with an electron or photon. Only the time varying part of μ , the dynamic dipole-moment does. When the adsorbate vibrates on the surface, an oscillatory field will be set up in the vacuum above the surface. The time varying field interacts with an incoming photon or electron, resulting in the absorption of the photon or the energy loss of the electron. This is the basic scattering mechanism behind RAIRS or HREELS.

Because of the high mobility of electrons inside metal, the component of the E field parallel to the surface is almost perfectly screened, as discussed later in detail in section 2.3. The response of the metal surface that screens the parallel field will also

screen out any dynamic dipole moment appearing on the adsorbate in a direction parallel to the surface. This is illustrated in Figs. 2-1 and 2-4. The combination of the two screening effects, which are actually the same physically, results in only ‘perpendicular’ vibrations being observed in RAIRS or HREELS.

There are exceptions for this rule, under special circumstances. In EELS, electrons can lose energy through “impact scattering”, *i.e.* direct scattering off the ion cores of the adsorbates. The incident electron feels the full atomic details of the adsorbates, and can excite dipole forbidden modes. The scattered wave is diffuse rather than directed, as in dipole scattering, which makes it easier to observe this kind of scattering at off specular angles. Examples of impact scattering are given in ref. [14]

Recent IR studies have also observed formally dipole-forbidden vibrational modes [15]. The origin of this effect is explained by Persson and Volokitin based on the “surface resistivity” concept [16]. Scattering of the electron from the adsorbates results in a broad band absorption in the IR light [17]. When the IR frequency ω coincides with the resonance frequency ω_0 of the parallel adsorbate vibrations, the molecules move in resonance with the collective drift motion of the electrons; hence the additional surface resistivity vanishes and the IR reflectivity reaches the original value of the clean surface. this results in an anti-absorption peak which is observed at the frequency ω_0 of the molecular vibration parallel to the surface (frustrated translation or rotation).

Certain parallel vibrations with dynamic dipole perpendicular to the surface can also be observed in HREELS and RAIRS. For example, molecular oxygen lies down on the Pt(111) surface: when the O-O stretch mode is active, charge transfers back and forth between the substrate and the molecule. This produces a perpendicular dipole moment. This mode has been observed in both HREELS [36] and RAIRS [13].

2.2 HREELS

HREELS was one of the main probes in this study. HREELS was used to confirm the site shift of CO by coadsorbed H as the bridge CO vibrational frequency was out of

the active range of the diode laser used in the IR study. HREELS is also used in studying the different cross sections of terrace and edge CO, and coadsorption of terrace H and terrace CO.

Low energy electrons, with energy of several eV, are the probe in HREELS. The beam energy used was always 2.257 eV in this study. As an adsorbate on the surface vibrates, it modulates the electric dipole moment of its environment in a time-dependent fashion. An electron in the vacuum above the crystal senses a long-ranged dipole electric field, and that produces small angle scattering typically substantially more intense than the scattering with large deflection angles. One observes a 'lobe' of inelastically scattered electrons sharply peaked about the specular direction [5].

Schematic diagrams of the HREELS instrument used in this study are shown in Fig. 2-2 and 2-3. Two 127° cylindrical deflector analyzers (CDA) are used in this system, one as the monochromator, the other as the energy analyzer. Since the resolution requirement of the electron beam is in the order of several meV ($1\text{meV} \approx 8\text{ cm}^{-1}$), a monochromator must be used capable of selecting an electron beam with a very narrow energy distribution. A lens system is used after the selector to allow the electron energy at the sample to be independently chosen from the pass energy of the selector. For the vibrational measurement, we are interested in the electrons coherently reflected from the surface and events in which essentially no momentum is transferred are confined to a small cone about the specularly reflected beam. The beam is then retarded and focused into a dispersive energy analyzer.

Sensitivity and resolution are the most important requirements for a surface science analysis technique. Sensitivity is important because the adlayer we want to study is usually less than a monolayer, so the total amount of particle responding to the probe is small. With a cross section close to atomic dimensions [3], HREELS has quite high sensitivity, and is able to study a surface layer in 0.1% monolayer order. The other important index is the resolution, which is absolutely necessary in site and species

assignment. High resolution is especially required in line shape studies. The typical resolution of HREELS is between 40 to 80 cm^{-1} , by trading off sensitivity, 8 cm^{-1} resolution has been achieved [10]. The ultimate resolution of a HREELS system is decided by the resolution of the monochromator and the energy analyzer. Several analyzer designs have been used, including a 42° cylindrical mirror analyzer (CMA), a 180° concentric hemispherical analyzer (CHA) and a 127° cylindrical deflector analyzer (CDA). The relative merits of each of them is discussed by Avery [3] and by Ibach and Mills [5].

Since the kinetic energy of the electron beam in the selector is as low as several hundred meV, any magnetic field present can potentially destroy the sensitivity and the resolution of the HREELS system. OFHC copper was used to make the bulk parts of the system and the earth's field is screened by a cylindrical layer of mu-metal 0.014 in. thick surrounding the instrument. The electron filament heater leads are also twisted to provide a noninductive winding [34]. The whole system is also degaussed every time when it is taken out of vacuum.

2.2.1 Operation of the HREELS system

Tuning of HREELS is an art. There are more than 25 adjustables controlling the optics. I have found the best process is finding the elastic peak first and adjusting every variable (except the bias voltage between the sample and the HREELS instrument) to optimize the peak. The same process is repeated several times until I get a symmetric, strong ($> 2 \times 10^4$ counts/sec) elastic peak. The first tuning can take as much as 1 to 2 hours. Usually within the day, if the work function of the surface has not radically changed, the tuning of subsequent scans is easy, usually taking less than 1 min., as long as I return the sample back to the same position.

Major re-tuning is necessary if the work function has changed or major change in overlayer ordering occurs. Some experimentalists advocate compensation by changing the bias voltage on the sample. I, however, have not found that method as reliable as re-

tuning, in agreement with Avery [3] and several GM researchers[18]. Besides, changing the bias voltage can potentially destroy the consistency of HREELS and sometimes even cause the reflection of the electron beam without inelastic surface interaction. By keeping the bias voltage unchanged, the tuning is quite reproducible.

Quantitative analysis of the HREELS intensity is usually done by measuring the height of the inelastic peak and comparing it with the height of the elastic peak. The rationale behind this practice is that HREELS resolution is significantly wider than the intrinsic line width of the vibrational mode. I found that the loss peaks were almost always wider than the elastic peak and integrated both the loss and elastic peaks over frequency in this study. This is the common practice in infrared spectroscopy for obtaining the integrated intensity. Examples of HREEL spectra can be seen in Chapters 4 and 5.

2.3 Infrared spectroscopy

Interaction between the electromagnetic field of infrared radiation and the oscillating dipole associated with a particular normal mode excites the vibration of ad molecules on the surface. The excitation manifests itself in the absorption of the radiation. This is the basis of reflection absorption infrared spectroscopy (RAIRS). In RAIRS, the adlayer we are interested consists of only $\sim 10^{14}$ molecules (atoms), significantly less than the number of molecules in a bulk sample or in a traditional high surface area sample in the transmission IR experiment. Therefore, certain special experimental conditions are necessary in order to observe the small absorption, at times smaller than 0.1%.

There have been many theoretical considerations and review articles [1,2] pertaining to such experimental conditions. The most important consideration is that only the p-polarized component (with the polarization in the incidence plane, while the s-polarization is perpendicular to the incidence plane.) of the IR beam is able to interact with the adsorbate and such interaction is most strong at near-grazing incidence [19].

The dependence of absorption strength on incidence angle was first considered by Greenler [20] for reflection from a clean and highly reflective surface with classical electrodynamics. It is then straightforward to calculate the strength of the field on the surface with the Fresnel equations. In Fig. 2-4, the dependence of the electric field strength E (normalized to the strength of the incoming beam) on the incidence angle θ is shown on a platinum surface at 2100 cm^{-1} . The p-polarized light is further split into two components in Fig 2-4, $E_{p\perp}$ and $E_{p\parallel}$, perpendicular and parallel to the surface, respectively. The strength of the p-polarized light increases with θ and falls rapidly to zero at 90° after a maximum at about 86° . The more important quantity is the total luminosity on the surface, $E^2/\cos(\theta)$, because the number of molecules with which the incoming incident beam can interact is proportional to $1/\cos(\theta)$. The total absorption is then given by $\Delta R \propto (E_{p\perp})^2/\cos(\theta)$, because both E_s and $E_{p\parallel}$ are much smaller than $E_{p\perp}$, especially at high incidence angles, as can be clearly seen in Fig. 2-4. This, as a result of the high conductivity of the metal and the boundary conduction on the surface, is a well known result and also decides the dipole selection role in the RAIRS and HREELS experiments, as discussed in section 2.1. ΔR is also plotted in Fig. 2-4; it is very clear that in order to get high sensitivity, the experiment has to be done at near-grazing angle.

Two scans are necessary in the conventional RAIRS, one is on the clean surface, and the other on the surface covered with adsorbates. The reflectance change is then obtained by subtracting the first spectrum from the second one, as illustrated in Fig. 2-5. The absorption signal can be as small as 0.1%. Because of the subtraction involved, how small a signal can be detected crucially depends on the stability of the system. There are three obvious noise sources in conventional RAIRS. The first is the true noise associated with short term fluctuations, like shot noise of the source, Johnson noise of the detector and noise from other electronics instruments. This kind of noise can be reduced by averaging over a longer period of time. The instability of the system over longer time scales, for example, the temperature fluctuation of the thermal source or a drift in the

optical alignment, can significantly change the look of a spectrum. In my RAIRS, the sensitivity was really limited by these kinds of instabilities of the system.

The optical system used in both RAIRS and EVS is shown in Fig. 2-6. The diode laser was used as the IR source. Not all the components shown are in place during RAIRS and EVS. Beam splitter B and mirror M3 are in place only during calibration of the laser with the wavemeter and are moved during RAIRS and EVS. Mirror M6 is in place only during alignment, when the beam cross section profile can be measured with the pinhole A2. With M6 removed, a visible laser beam, collinear with the IR beam, is used to check the focusing of the IR beam on the sample and measure the angle of incidence. The angle of incidence is about 86°.

The diode laser is stepped through a set of predetermined laser currents and heat sink temperatures. The current is between 0.05 to 0.1 A. The heat sink temperature is slowly raised from about 70 to 100 K. The frequency of each single mode output is calibrated by the wavemeter [21]. The wavemeter, shown in Fig. 2-7, is operated open loop under computer control and is essentially a variable path length Michelson interferometer in which the two separated beams reflect from back-to-back corner cube reflectors on a translation stage. The beam splitter, B, is used to combine the IR beam and the visible beam from a 0.6328 μm He-Ne laser into a single collinear beam incident to the wavemeter. The beam splitter in the wavemeter is ZnSe coated for use at the Brewster angle in the 4-12 μm range and at 0.6328 μm . Separated IR and visible light interferograms are recorded by a HgCdTe detector and a silicon photodiode. The interferograms are fed into a counter-timer to determine their frequency ratio. The frequency of the diode laser is determined as [21]

$$\omega_{IR} = \omega_{vis} \frac{n_{vis}}{n_{IR}} \times \frac{f_{IR}}{f_{vis}}. \quad (2.3.1)$$

Where, f_{IR}/f_{vis} is the measured ratio of fringes from the IR laser to fringes from the He-Ne laser; n_{vis} and n_{IR} are the refraction index of air at the He-Ne laser and the IR

frequencies; and ω_{IR} and ω_{vis} are the frequency of the IR and visible beam, respectively. The largest systematic error observed by Lambert is 0.034 cm^{-1} [22].

The diode laser used in this study is a stripe-geometry double-heterostructure diode laser, grown by MBE on a PbTe substrate with $\text{Pb}_{0.9885}\text{Eu}_{0.0015}\text{Te}_{0.9881}\text{Se}_{0.0019}$ active region. The laser can be tuned from about 1750 to 2050 cm^{-1} with gaps of about 2 cm^{-1} with several mW power.

2.3.1 RAIRS with polarization modulation

Since only the p-polarized component of the IR radiation interacts with adsorbate on the surface, in principle the absorption spectrum can be seen with polarization modulation in which we compare the reflectance of the s and p-polarized light from the surface. The experimental set up for this polarization modulated RAIRS is shown schematically in Fig. 2-8. A photo-elastic modulator (PEM) is used for polarization modulation. A PEM operates [23] by applying an oscillating stress to a transparent material (zinc selenide), which causes the difference in optical path between light polarized parallel and perpendicular to the stress direction to likewise oscillate. The light intensity transmitted by the PEM and a subsequent polarizer is then modulated by an amount proportional to the difference between incident intensity of p- and s- polarized light. The polarization modulation technique has been used previously by several other groups [24,25] and is discussed fully by [24].

In Fig. 2-8, lock-in A gives the difference between the p- and s- polarized lights, $(I_p - I_s)$, lock-in C gives the total light intensity $(I_p + I_s)$. The only difference between I_p and I_s should be from the absorption of I_p by the adsorbate on the sample. $(I_p - I_s) / (I_p + I_s)$ gives the spectrum of the adsorbate on the surface because fluctuations in the source intensity and attenuation by gas phase molecules in the optical path are all canceled out. A spurious signal has been observed from lock-in A, possibly from ambient radiation modulated also by the PEM. This signal is removed by lock-in B, referenced at the chopper frequency.

In principle, only one scan is necessary to get the vibrational spectrum when polarization modulation is used. In practice, I still need to subtract the spectrum of the clean surface from the spectrum of the adsorbate covered surface, due to the variation of the polarization of the IR ray at different frequencies. Since polarization modulated RAIRS measures the difference in intensity between p- and s-polarized light, anything which changes this difference will appear in a single spectrum, and should be avoided. Sources of such irreproducibility include change in the polarization state of the light from the laser and the focal point of the light on the sample. We use two polarizers, P_1 and P_2 in the optical path before the UHV chamber to minimize the change in the polarization state of the light incident on the sample. The maximum variation is reduced to 1.8° when the polarization of the incident light is changed by 90° [22]. The PEM is oriented with its stress axis 45° from the direction of p-polarization. I also tried to keep the sample position unchanged. Unfortunately, changing sample position is sometimes unavoidable. The sample has to be moved up and down in taking TPD and in dosing. The sample position is also believed to move slightly in the heating and cooling process. Irreproducibility was the major obstacle in this system in getting good RAIRS spectrum.

Another major noise source in the polarization modulated RAIRS is from a Fabry-Perot effect. The IR signal varies with IR frequency in a cycle of 1 cm^{-1} . This effect is apparently caused by a component of $5 \text{ mm}/n$ thick, where n is the reflective index. We have not been able to locate this component. This noise is not very serious in the baseline region while it is very serious in the peak region because of the large slope of the profile there.

In optical alignment, we first set P_1 , P_2 to pass only the p-polarized light. Then the PEM stress amplitude was adjusted so that the detector wave form, as monitored on an oscilloscope, was nearly sinusoidal at twice the stress oscillation frequency. The lock-in A, referenced to twice the stress oscillation frequency of the PEM, is adjusted in phase to give maximum signal. During RAIRS, polarizers P_1 and P_2 are rotated to null the

signal from the lock-in A, so that both s- and p-polarized light are incident onto the sample with equal intensity. In principle, the PEM stress amplitude should be varied to keep the optical phase modulation unchanged during the course of a scan. In practice, the stress amplitude has been kept constant and the resulting variation in the optical phase modulation is quite small because only a very small frequency range is scanned.

2.3.1.1 Quantitative analysis of polarization modulated RAIRS

Quantitative analysis method for polarization modulated RAIRS has been developed by Lambert [22]. The material in this section is largely based on refs. 22 and 30.

The objective of RAIRS is to measure the effect of adsorbate on the reflectance of p-polarized light, R_p . The corresponding physical quantity can be denoted as [22]

$$\frac{\Delta R}{R} = \frac{R_p \text{ with CO} - R_p \text{ without CO}}{R_p \text{ without CO}} \quad (2.3.2)$$

First consider the effect of the PEM and P_3 on the transmitted light. Let I_s (I_p) be the transmitted intensity when the PEM is turned off and P_3 is set to pass only the s-polarized (p-polarized) light. Let Δ be the ellipsometric phase difference between the optical E -fields of the s- and p-polarized light incident on the PEM. Let $\phi(t)$ be the optical phase difference induced by the PEM to the component of transmitted light polarized along and perpendicular to the stress axis. The PEM is assumed to be oriented with its stress axis 45° from the direction of p-polarization. The intensity $I(t)$ transmitted with P_3 set to pass p-polarized light is [22]

$$I(t) = \frac{I_p + I_s}{2} + \frac{I_p - I_s}{2} \cos[\phi(t)] + \sqrt{I_s I_p} \sin(\Delta) \sin[\phi(t)] \quad (2.3.3)$$

with polarizers P_1 and P_2 set to pass only the p-polarized light, Eq 2.3.1 becomes

$$I_+(t) = I_p \frac{1 + \cos[\phi(t)]}{2} \quad (2.3.4)$$

Let f_M be the stress oscillation frequency of the PEM. The wave form of $I_+(t)$ is most closely sinusoidal at $2f_M$ if the stress amplitude of the PEM is chosen so [22]

$$\phi(t) = \pi \cos(2\pi f_M t) \quad (2.3.5)$$

Setting the reference phase of the lock-in A (at $2f_M$) to obtain maximum signal and P_1 and P_2 to pass only p-polarized light makes the lock-in only sensitive to the $\cos(4\pi f_M t)$ Fourier component of the signal, since the orthogonal reference phase gives

$$\int_0^\pi \cos[\pi \cos(x)] \sin(2x) dx = 0 \quad (2.3.6)$$

With the lock-in phase and PEM amplitude set this way, the lock-in output is independent of Δ even if P_1 and P_2 are rotated to some other angle because

$$\int_0^\pi \sin[\pi \cos(x)] \cos(2x) dx = 0 \quad (2.3.7)$$

Consequently, the lock-in A output is proportional to $I_p - I_s$, the difference in reflectivity between p- and s-polarized light incident on the PEM.

Four scans are necessary to get the quantitative RAIRS spectrum. Two of them are for calibration purposes and are not sensitive to the surface condition. The essential scans include that of the clean surface and of the adsorbate-covered surface.

Let $V(2f_M)$ be the rms voltage measured by the lock-in B. Similarly, let $V(f_c)$ be the rms voltage measured by lock-in C, referenced at the chopper frequency f_c . Before beginning, with the laser operated near the center of the frequency range, polarizers P_1 and P_2 are set to null $V(2f_M)$. During the scan, both $V(2f_M)$ and $V(f_c)$ are measured. At optical frequency ν , for the scan on clean surface, define $Q_1(\nu)$ to be the ratio,

$$Q_1(\nu) = V(2f_M) / V(f_c) \quad (2.3.8)$$

From the measured $V(2f_M)$ and $V(f_c)$ taken during the scan of the adsorbate covered surface, we can similarly define $Q_2(\nu)$.

Polarizers P_1 and P_2 are set to pass only the p-polarized light in the calibration scans. During one of them, A, both $V(2f_M)$ and $V(f_c)$ are measured as in the surface sensitive scans and $Q_A(\nu)$ is defined similar to $Q_1(\nu)$. During the other scan, B, the PEM is turned off, and only $V(f_c)$ is measured. $Q_B(\nu)$ is defined as the ratio of $V(f_c)$ measured during the two calibration scans,

$$Q_B(\nu) = V_A(f_C) / V_B(f_C). \quad (2.3.9)$$

The quantitative polarization modulated RAIR spectrum is then

$$S_{\text{adsorbate}} = \frac{Q_2 - Q_1}{Q_A Q_B}. \quad (2.3.10)$$

The above formalism has been shown to give $\Delta R/R$ correctly in ref [22].

2.3.2 Electroreflectance Vibrational Spectroscopy (EVS)

In RAIRS, the surface reflectance change induced by the adsorbate is measured. In EVS, the surface reflectance change induced by an applied E -field is measured. By comparing the two measurements, one can measure the Stark shift of the vibrational mode of adsorbate on the surface. There should be no difference in reflectance outside the absorption region, since only the vibrational mode of the adsorbate responds to the applied E -field. Consequently, EVS has zero background.

The primary effect of the applied E -field is to shift the frequency of the vibrational mode by a value on the order of 10^{-3} cm^{-1} , under my experimental conditions. Because the shift is so small, EVS is basically a derivative technique, and slow changes in the RAIRS background will not show up. Only the absorption peaks with narrow line shape are observable. The Stark tuning rate $d\nu/dE$, where ν is the vibrational frequency and E is the applied field, for adsorbed molecules can be deduced from the comparison of RAIRS and EVS. The principle of EVS is illustrated in Fig. 2-9.

It is particularly important that a diode laser optical source is used in EVS. Because of the small frequency shift, the fractional change in the reflected signal intensity is on the order of 10^{-6} for CO on Ni or Pt, which are among the strongest lines studied in surface science. A conventional IR source (thermal black body source) is not bright enough to achieve this level of sensitivity.

The experimental setup for EVS is shown schematically in Fig. 2-10. The E -field is produced by an oscillating voltage across the gap of about 0.5 mm between the sample

and the facing electrode. The strength of the field is about 3×10^4 V/cm. The breakdown field in vacuum is about 10^5 V/cm [26]. Light reflected from the sample is modulated both by the mechanical chopper and the applied E -field. Lock-ins A and B are referenced to the oscillating field and to the chopper, respectively. The ratio of the two lock-in outputs is proportional to the reflectivity modulation induced by the applied field. The polarizers P_1 and P_2 are set to pass only the p-polarized light during EVS.

During the alignment, light from the laser is focused to the point on the sample where the E -field is strongest. As the first step in alignment, a visible laser beam, collinear with the IR beam, is used to determine the angle of incidence and to make sure that the IR beam is correctly focused.

2.3.2.1 Quantitative analysis of EVS

Quantitative analysis method of EVS has been developed by Lambert [22]. The material in this section is largely based on refs.22 and 30. The effect of the applied E -field to the surface reflectivity, R_p , of p-polarized light can be described as [22]

$$S_E = \frac{\text{rms variation of } R_p \text{ caused by } E}{R_p \text{ without } E}. \quad (2.3.11)$$

Let f_E be the frequency of the ac electric field applied to the surface, 100 kHz in this study. The rms voltage $V(f_E)$ measured by lock-in A, referenced at f_E , is

$$V(f_E) = BI(f_E)D(f_E)T(f_E)\cos(\delta_E). \quad (2.3.12)$$

where B is the time average of the fraction of incident power transmitted by the mechanical chopper. $I(f_E)$ is the rms modulation at frequency f_E of optical power incident on the detector when the beam is not blocked by the chopper and $D(f_E)$ is detector responsivity defined as (rms output voltage)/(rms optical power modulation), $T(f_E)$ is the voltage transfer function of the circuitry between the detector and the lock-in amplifier, and δ_E is the difference between the lock-in reference phase and the phase that would give the maximum output.

Let f_C be the frequency at which the mechanical chopper interrupts the light. The rms voltage $V(f_C)$ measured by lock-in B, referenced at f_C is [22]

$$V(f_C) = I_0 G D(f_C) T(f_C) \cos(\delta_C). \quad (2.3.13)$$

Here I_0 is the power incident on the detector when the light is not blocked by the chopper, $G = (\text{rms optical power modulation at } f_C \text{ caused by the chopper})/I_0$, δ_C is the deviation of the lock-in reference phase from the phase would give the maximum output. From the above equations,

$$S_E = \frac{I(f_E)}{I_0} = \frac{G D(f_C) T(f_C) \cos(\delta_C) V(f_E)}{B D(f_E) T(f_E) \cos(\delta_E) V(f_C)} \quad (2.3.14)$$

For the chopper used in this study, $B=0.50$, $G = \frac{\sqrt{2}}{\pi} = 0.45$ [22]. $D(f)$ has been measured by Lambert to be well fit by [22]

$$D(f) = \frac{A}{f_D^2 + f^2} \quad (2.3.15)$$

where to 90% confidence, $169 \text{ kHz} < f_D < 220 \text{ kHz}$, here f_D is the detector roll-off frequency. In this work, $D(f_C)/D(f_E) = 1.278 \pm 0.044$. The ratio $T(f_C)/T(f_E)$ is measured by replacing the detector with an attenuator with the same output impedance and comparing the rms voltage input with the rms voltage output of the network at f_C and f_E . The measurement gives $T(f_C)/T(f_E) = 4.4 \times 10^{-7}$, accurate to within 5%. δ_E and δ_C can be measured by comparing the signal output with the phase set as for the spectrum, with the signal output with phase changed by 90° . In most situations, $\cos(\delta_C)/\cos(\delta_E) \approx 1$. Then the equation (2.3.14) can be effectively rewritten as

$$S_E = 5.1 \times 10^{-7} \frac{V(f_E)}{V(f_C)} \quad (2.3.16)$$

Examples of EV spectra can be seen in Chapter 3.

2.3.3 Determination of the Stark tuning rate

The Stark tuning rate can be deduced from the comparison of RAIR and EV spectra. Let $\Delta(\nu, E = 0)$ be the quantity measured in RAIRS,

$$\Delta(\nu, E = 0) = \frac{\Delta R(\nu)}{R(\nu)} \quad (2.3.17)$$

let Δ_E be the quantity measured in EVS. The relationship between Δ_E and $\Delta(\nu, E)$ is [27]

$$\frac{\Delta_E}{\langle E \rangle} = \frac{d\Delta(\nu, E)}{dE} = \frac{\partial\Delta(\nu, 0)}{\partial\nu} \frac{d\nu_0}{dE} + \frac{\partial\Delta(\nu, E)}{\partial E}. \quad (2.3.18)$$

where ν_0 is the resonant frequency of the adsorbate. The first term is the change in $\Delta(\nu, E = 0)$ due to a vibrational frequency shift caused by the applied field, the second term is the change in the intensity of $\Delta(\nu, E = 0)$ caused by the applied field. In the small E limit, the above equation can be evaluated at $E = 0$. It is easier to compare the two terms in equation (2.3.18) by integrating it over frequency:

$$\frac{\int \Delta_E(\nu') d\nu'}{\langle E \rangle} = \left(\frac{d\nu_0}{dE} \right)_{E=0} \Delta(\nu, E = 0) + \frac{\partial}{\partial E} \int \Delta(\nu', E) d\nu' \Big|_{E=0}. \quad (2.3.19)$$

For CO on Ni and Pd, at frequencies near resonance, the second term in equation (2.3.19) has been shown to be 50 times smaller than the first term [27,28]. So the direct effect of the applied E -field to the RAIRS intensity is negligible. Taking away the second term, (2.3.18) changes to

$$\int \Delta_E d\nu' \approx \Delta(\nu, E = 0) \left(\frac{d\nu_0}{dE} \right) \langle E \rangle = \frac{\Delta R}{R} \langle E \rangle \left(\frac{d\nu_0}{dE} \right). \quad (2.3.20)$$

it is then clear that the RAIR spectrum is proportional to the integration of the EV spectrum. The ratio between them is the product of the rms E -field and the Stark tuning rate $\left(\frac{d\nu_0}{dE} \right)$. Knowing the rms field, it is then straightforward to calculate the Stark tuning rate from the peak heights of the RAIR and integrated EV spectra. A second method can also be used: integration of both side of equation (2.3.20) means the integrated intensity of the RAIR spectrum multiplied by the Stark tuning rate and the rms applied field equates to the double integration over the EV spectrum.

In principle, either method should give the same Stark tuning rate. In practice, variation in the baseline of the RAIR spectrum, and the fact that the baseline of the integrated EV spectrum is usually asymmetric due to missing data points in the laser gaps

near the peak region, introduces error into the determination of the peak heights and integrated intensities. Both methods have been used here to calculate the Stark tuning rate. The reported results are always the average of the two methods.

2.3.4 Measurement of the E -field

The rms applied E -field must be known in order to determine the Stark tuning rate. The field is produced by applying high voltage across the gap between the sample and a counterelectrode. The rms voltage is measured during each EVS scan. To measure $\langle E \rangle$, one must know several other quantities. The electric field strength varies with the position on the sample face, as does the intensity of the beam. In the good approximation of linear response, the reflectivity modulation caused by the actual electric field contribution is the same that would be produced by an uniform "effective field". This "effective field", $\langle E \rangle$ can be written as [27]

$$\langle E \rangle = \frac{\int E I dA}{\int I dA} \quad (2.3.21)$$

Where I is the power incident on the detector per unit reflecting area of the sample, and E is the externally applied field. Both I and E are functions of position on the sample.

The laser intensity distribution, I , can be measured by moving the focus of the light outside the UHV chamber. One then compares light detected after focusing through a 500 μm diameter pinhole with that detected with the pinhole removed. In the approximation of a Gaussian beam and geometrical optics, the fraction of incident power transmitted through the pinhole can be used to calculate the intensity distribution on the sample. Two other methods have been used previously [27], and both give similar results.

The E -field distribution on the sample was calculated using the method of images [29]. In doing so, the sample surface was approximated by an infinite plane. The gap between the sample and the counterelectrode, which is necessary in this calculation, is determined by measurement of a series of capacitances between the two using a

capacitance bridge. Detailed discussion of the capacitance measurement is given by Luo [30].

2.4 TPD

TPD was used in this study primarily to determine relative coverages of adsorbates on the surface, and the distribution among different chemisorbed phases (sites). I have also used TPD to study the mechanisms and products of certain chemical reactions. TPD can also supply information about the desorption activation energy and preexponential factor of desorption. Quantitative analysis methods of TPD are given in several reports[8,9], and the discussion here is largely based on them.

In TPD, the sample covered with an adlayer is heated from a low temperature to a higher temperature, usually but not necessarily at a constant heating rate. In this study, the heating rate is always 10 K/sec. As the sample temperature increases, the desorption rate increases and that causes the pressure in the chamber to increase. The adsorption of admolecules on the surface in vacuum is not under equilibrium, as desorbed gases are pumped away but no more adsorption occurs. The desorption flux is a product of desorption rate, which is a function of the sample temperature, and the population of that particular chemisorbed phase. The desorption rate increases with the sample temperature while the coverage decreases with the sample temperature, as a result, a peak in the partial pressure appears at certain temperature, and the activation energy can be calculated from the profile. I will give the formalism in detail later in this section.

The experimental setup for TPD experiments is shown schematically in Fig. 2-11. For the experiments performed in the IR chamber, the sample was not moved from the IR position, which is approximately at the center of the chamber and facing roughly 100° away from the mass spectrometer. For the experiments performed in the HREELS chamber, the sample was moved to face the mass spectrometer at a distance of about 1 cm away from the aperture of the nozzle covering the mass spectrometer. Due to the

proximity of the sample and the mass spectrometer, and because the desorbed gases go into the nozzle, which has much smaller volume than the whole vacuum chamber, the sensitivity of TPD is greatly enhanced. Since the sample is facing a small aperture, the desorption from the heater wire, edge and back of the crystal is not picked up by the mass spectrometer. The reason why this scheme was not adopted in the IR experiment is because the baseline of the IR spectrum was extremely sensitive to the sample position change. This is a major problem in RAIRS, which was discussed fully in section 2.3.1.

It has been shown [31] for a system with constant pumping speed, the relationship between the partial pressure profile and the desorption rate is

$$\frac{dn}{dT_s} = \frac{V}{AkT_g} \left[\frac{P_{sy} - P_{eq}}{\beta\tau} + \frac{dP_{sy}}{dT_s} \right], \quad (2.4.1)$$

and

$$\frac{dn}{dT_s} = \frac{v_0^{(m)} n^m \exp(-E_d / kT_s)}{\beta}, \quad (2.4.2)$$

where n is the molecular concentration on the surface, T_s and T_g are the temperatures of the surface and the gas, V is the volume of the system, A is the area of adsorption, P_{eq} and P_{sy} are the equilibrium partial pressure and the instantaneous pressure of the system, β is the heating rate and τ is the pumping time constant, E_d is the desorption activation energy, and $v_0^{(m)}$ is the preexponential factor for a desorption of order m . The order of desorption depends upon the limiting process of desorption. For example, CO adsorbs on Pt in molecular form, the desorption is first order, while adsorbed hydrogen on Pt(111) is in atomic form, the two H atoms have to come together before they can desorb, this desorption is second order.

Define

$$P = P_{sy} - P_{eq}, \quad (2.4.3)$$

which is plotted vs. T_s as the desorption spectrum. Combining the above two equations we get,

$$\frac{dP}{dT_s} + \frac{P}{\beta\tau} = \frac{v_0^{(m)} n^m \exp(-E_d / kT_s)}{\beta n_0} P_{\max}, \quad (2.4.4)$$

where $P_{\max} = \frac{AkT_s n_0}{V}$, is the maximum pressure observed during a desorption measurement in a closed system ($\tau = \text{infinity}$) for an initial surface coverage of n_0 . The parameters of desorption like E_d , v_0 , order of desorption m and relative population of admolecules originally on the surface can be obtained by fitting the experimental spectrum with this equation. The second term in the left hand of (2.4.4) is usually much larger than the first term and the latter can be neglected. In this case, $\frac{dn}{dT_s} \propto P$, and the amount of admolecules desorbed is then proportional to $\int_{T_1}^{T_2} P dT_s$, where T_1 and T_2 are the starting and stopping sample temperatures, respectively.

If there is more than one chemisorbed phase, then equation (2.4.4) changes to

$$\frac{dP}{dT_s} + \frac{P}{\beta\tau} = \sum_i \frac{v_{0i}^{(m)} n_i^m \exp(-E_{di} / kT_s)}{\beta n_{0i}} P_m^i, \quad (2.4.5)$$

where i is the label for each individual phase. From the resolved phases we can then usually assign sites for the molecules. Differences between the activation energies, molecules changing phase during the desorption process, the pumping speed of the system and the heating rate can all influence whether two different chemisorbed phases are resolved in TPD. The system parameters are almost unchangeable, so the most important factors are the activation energy and site movement. For example, atop and bridge CO cannot be distinguished in TPD. The activation energy difference between the two is about 1 kcal/mol (1 kcal/mol = 0.043 eV), and some bridge CO first changes to atop CO before desorbing. On the other hand, edge and terrace CO on Pt(335) can be clearly resolved, as their activation energies differ by about 6 kcal/mol and terrace CO doesn't move to edge sites before desorbing (because all the edge sites are still occupied).

In Fig. 2-12, I have plotted a TPD spectrum for saturation coverage of NO on Pt (335). The dotted lines are fit with Gaussian peaks, which give almost identical relative concentrations to equation (2.4.5). Oxygen and CO were used to verify that the NO peak near 220° C (500 K) is from the edge. When the edge sites were covered with oxygen or CO before exposing the sample to NO, the NO desorption peak near 220° C disappears while all three other peaks remain. HREELS experiments also found that the terrace peaks do not correspond individually with different NO sites. Actually all the terrace NO stays at the same sites before the desorption begins [32].

TPD alone cannot decide the absolute coverage of adsorbate on the surface. In practice, Low Energy Electron Diffraction (LEED) and other techniques are usually used to obtain absolute coverage information at certain particular coverages. The TPD spectra from these coverages are then used as references. By comparing other TPD spectra with a reference spectrum, one can then infer the absolute coverage of other situation. For CO on Pt(111), a $(\sqrt{3} + \sqrt{3})R30^\circ$ LEED pattern is observed for the maximum atop CO coverage of 0.33 ML, and a $c(4 \times 2)$ pattern is observed for the saturation coverage of 0.50 ML [33] which is shown in Fig. 2-13. All other coverages can be derived by comparing the TPD spectrum with the TPD spectrum from one of these two coverages.

Another method of getting absolute coverage is to use the absolute coverage information of another adsorbate and calibrate the mass spectrometer sensitivity between the two through one or more chemical reaction. This method involves larger errors than the above method.

2.5 Sample preparation and characterization

The Pt(335) sample was mounted in two separate UHV chambers in the IR and HREELS experiments. The surface was oriented to within 0.5° from the (335) direction, verified by Laue X-ray diffraction. In both chambers, the sample was spot welded to two Ta wires, which were used for heating and cooling. Auger spectroscopy was used to

check the surface cleanness. Common contaminants found on the sample were C, Ca, and O. C was usually removed by heating the sample in an oxygen environment. Chemisorbed oxygen could be removed by heating the sample to about 1100 K. Ca and oxide were removed by Ar ion sputtering at 300 K. After sputtering and oxygen treatments, the sample had to be annealed at high temperature to retain the surface morphology and remove small amounts of oxide. Care was taken so that C and Ca contaminants in the bulk do not move to the surface during the annealing. The balance between heating and oxygen treatment is very delicate. Sample cleaning is more of an art than a standard procedure. Detailed procedures used in the IR and HREELS experiment will be discussed in Chapters 3 and 4.

Dosing of the sample was usually done by leaking gas into the chamber through a controlled valve (leak valve), raising the chamber pressure. It is important to keep the chamber pressure low and the dosing time short, especially when dealing with species for which the pumping speed is low. A disadvantage of dosing this way is that other species adsorbed on the chamber walls may exchange with species we are interested in and result in an overlayer composition different from that expected. One way of reducing dosing pressure and time and avoiding the exchange problem is to use a doser which can produce much higher pressure in a much smaller volume than the total chamber volume. This way, residual pressure will not be high and with the sample very close to the doser, the exchange is minimal. The exposure can also be measured much more accurately this way because the time needed to move the sample close to and away from the doser is on the order of 1 second, much shorter than the time constant for the pressure to become stabilized, which is in the order of 1 minute. Detailed calculations for different doser designs are given in ref. 35. In the IR experiments, CO and hydrogen were dosed by back filling the chamber. Oxygen was dosed through a diffusive doser which has an enhancement factor of about 20. In the HREELS experiments, all the gases were dosed through individual dosers with enhancement factors close to 100.

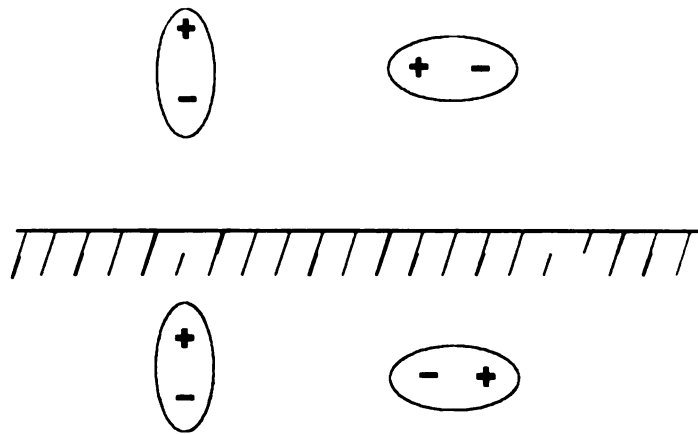


Figure 2-1. Dipole moment perpendicular to the metal surface is reinforced, dipole moment parallel to the surface is screened.

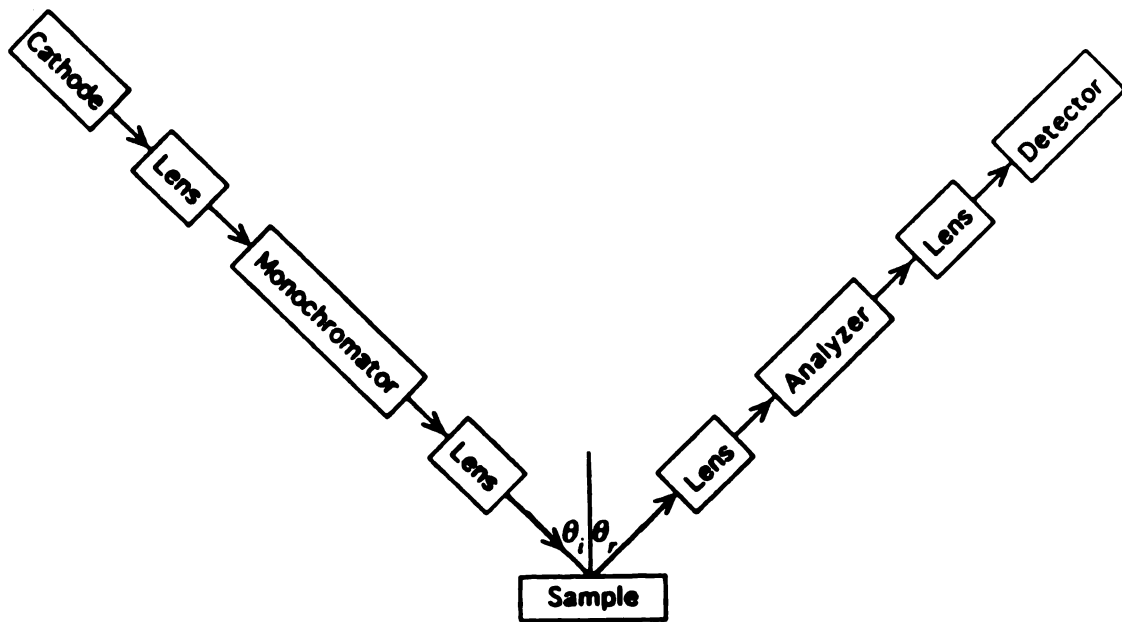


Figure 2-2. Block diagram of an electron energy loss spectrometer (Luo [30]).

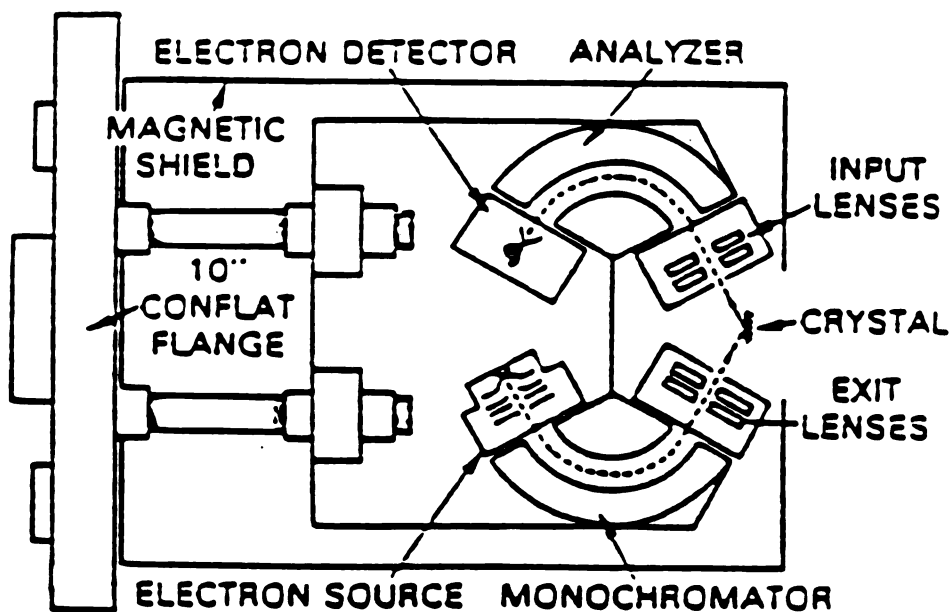


Figure 2-3. Schematic diagram of the system for high resolution electron energy loss spectroscopy in this work (B. A. Sexton [34]).

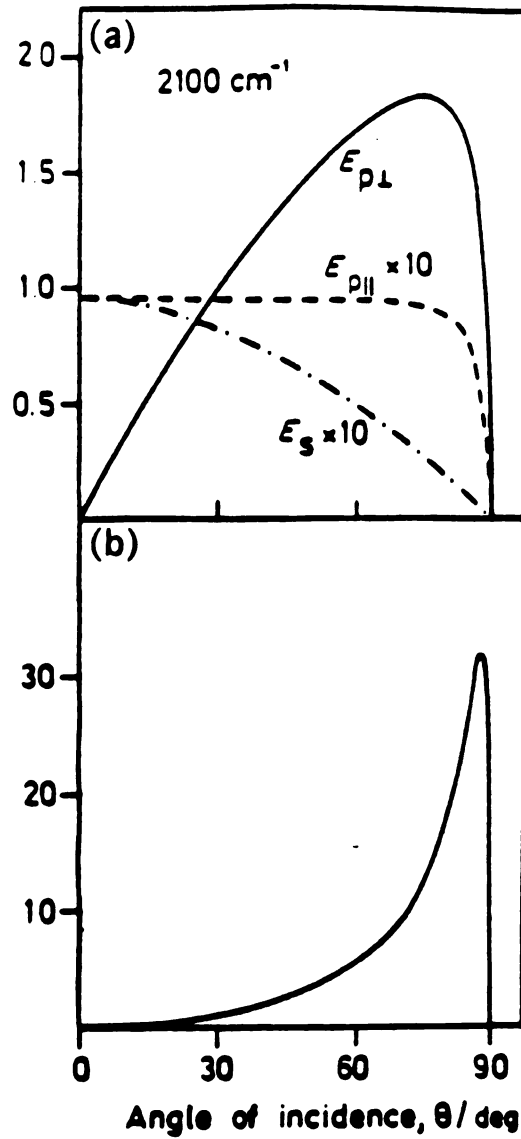


Figure 2-4. The surface electric field E/E_0 in (a), and the quantity $(E/E_0)^2/\cos\theta$ in (b) for platinum at 2100 cm^{-1} ($\epsilon = -375 - 200 i$) as a function of the incidence angle θ (Bradshaw and Schweizer [2]).

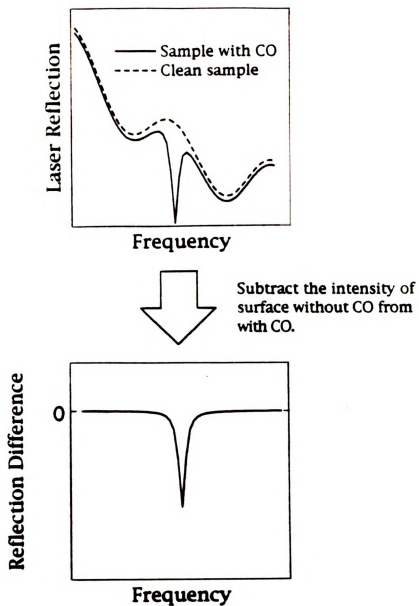


Figure 2-5. The process of a RAIR spectrum: comparing the scans with clean sample and with adsorbate (CO) (Luo [30]).

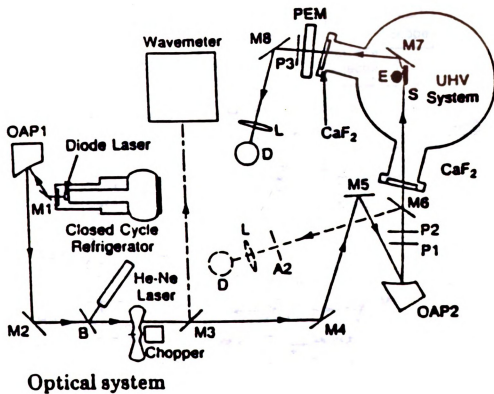


Figure 2-6 Optical set up for RAIRS and EVS showing detector D, sample S, and electrode E, polarizers P_1 and P_2 (Lambert [27]).

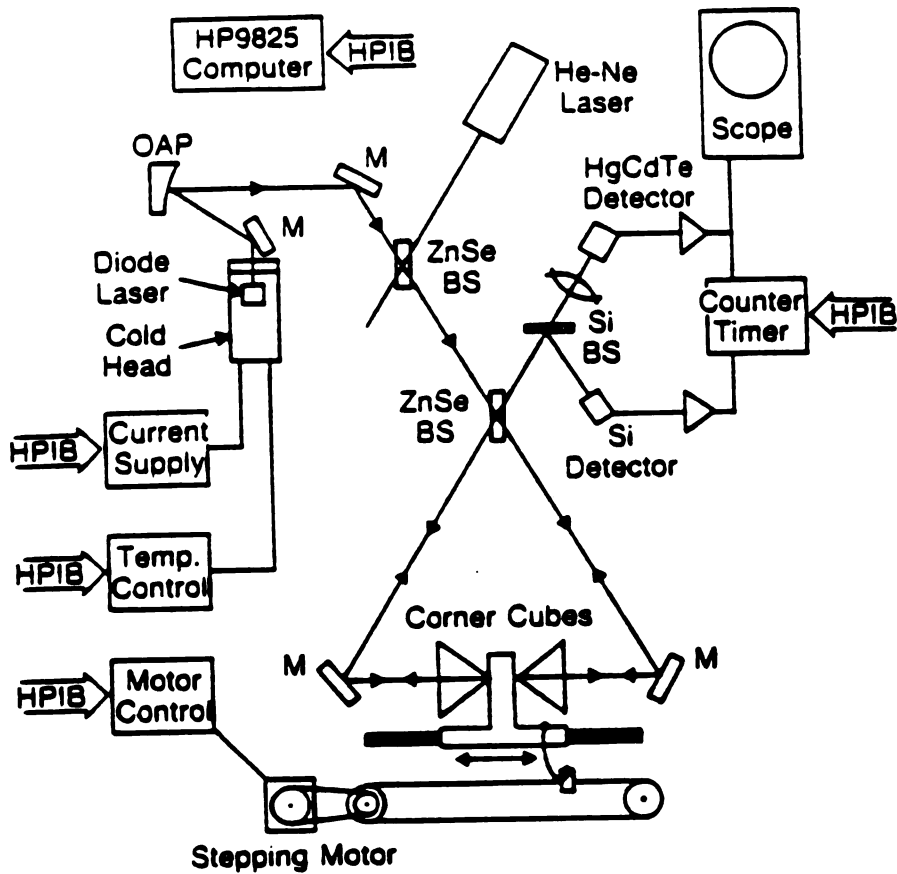


Figure 2-7 Schematic diagram of computer-controlled wavemeter for laser frequency calibration. Back-to-back hollow corner cube reflectors are mounted on a ball slide translation stage driven by a stepping motor. The stage moves freely except near the end of its travel where a beaded chain coupling becomes rigid and reverses its motion. (Evans and Lambert [21])

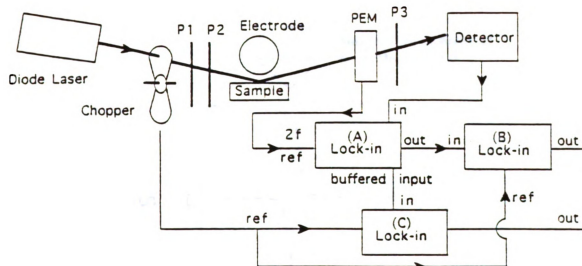


Figure 2-8. Schematic of the system used for polarization modulated reflection absorption infrared spectroscopy (RAIRS) (Luo [30]).

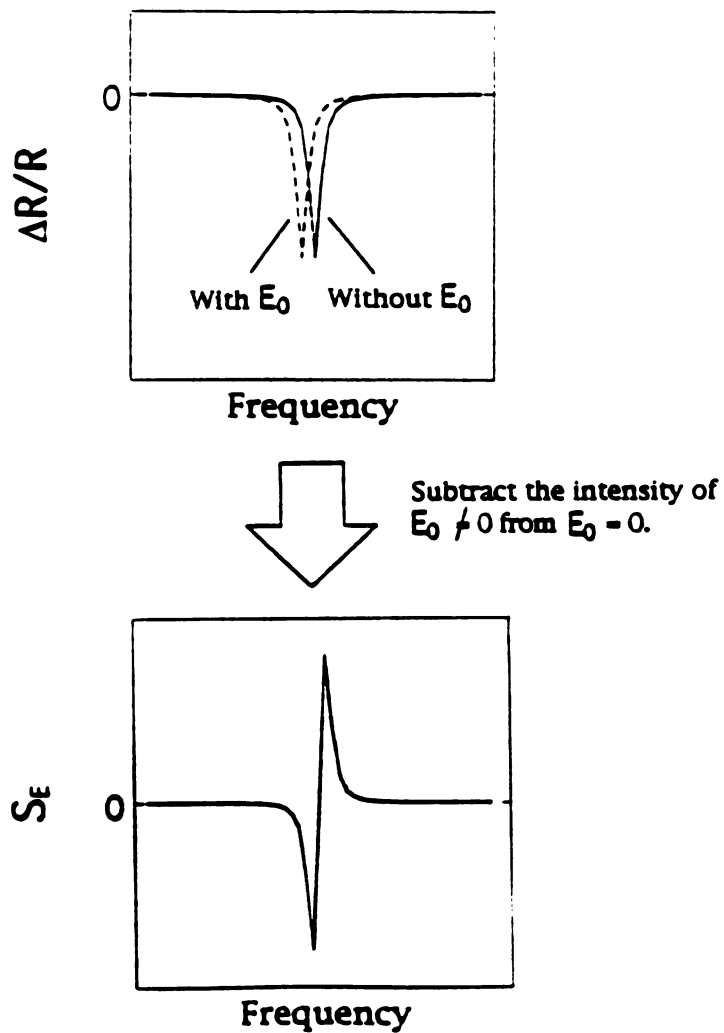


Figure 2-9 Process of measuring the EV spectrum by modulating the E -field applied to the surface (Luo [30]).

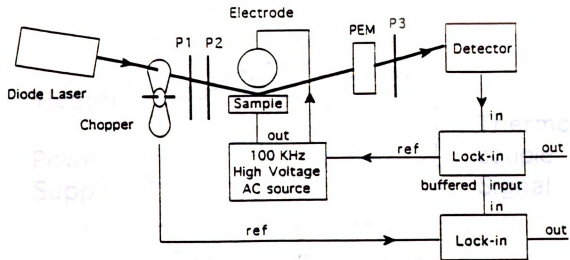


Figure 2-10 Schematic of the system used for electroreflectance vibrational spectroscopy (EVS) (Luo [30]).

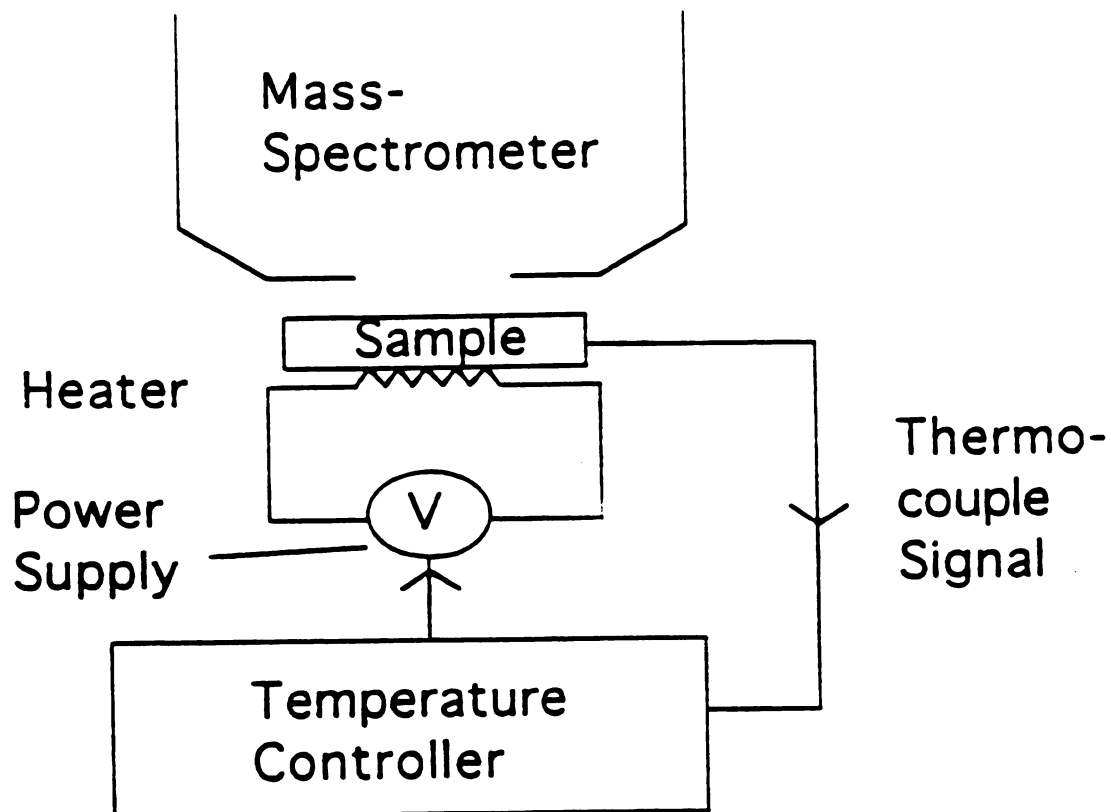


Figure 2-11 Schematic of the system used for temperature programmed desorption (TPD) (Luo [30]).

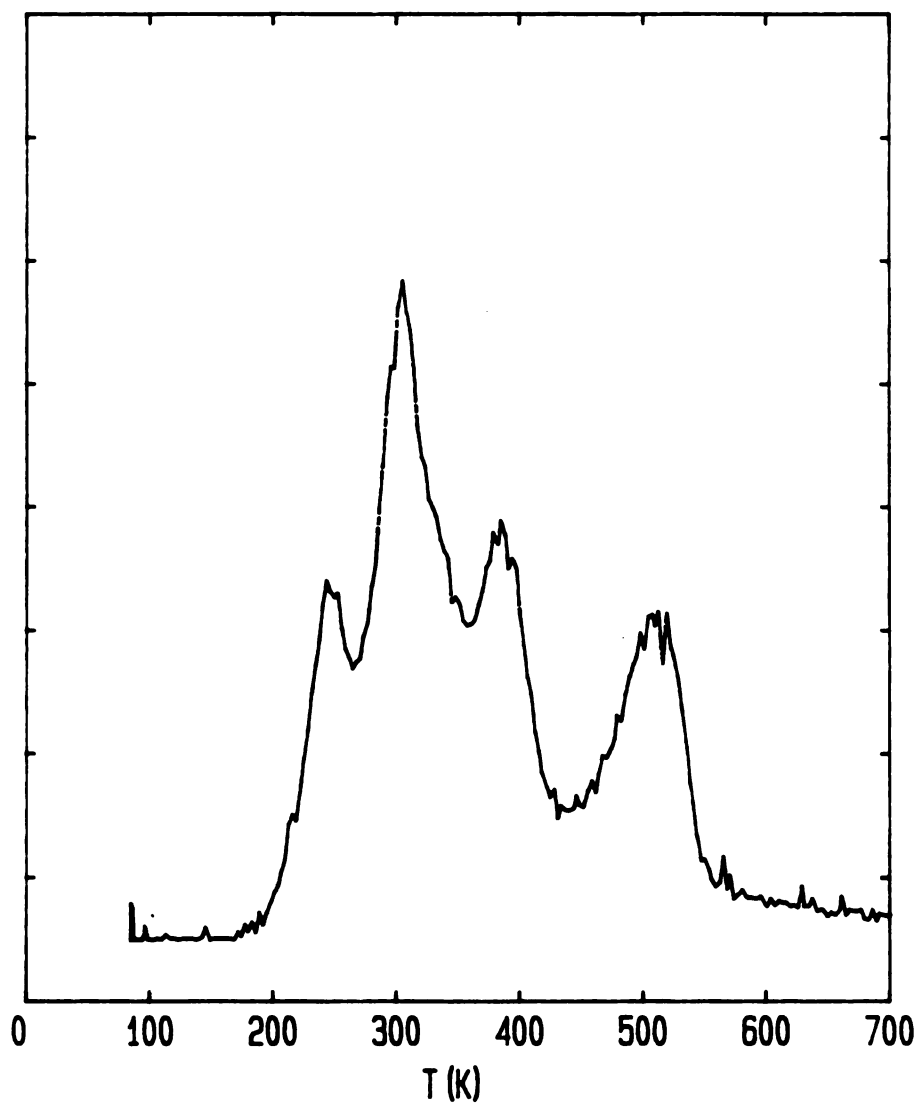


Figure 2-12 TPD spectrum for saturation coverage of NO on Pt(335). The highest peak is from edge NO and the rest are from terrace NO. All the terrace NO stays at identical sites before heating. (Wang *et al.* [32])

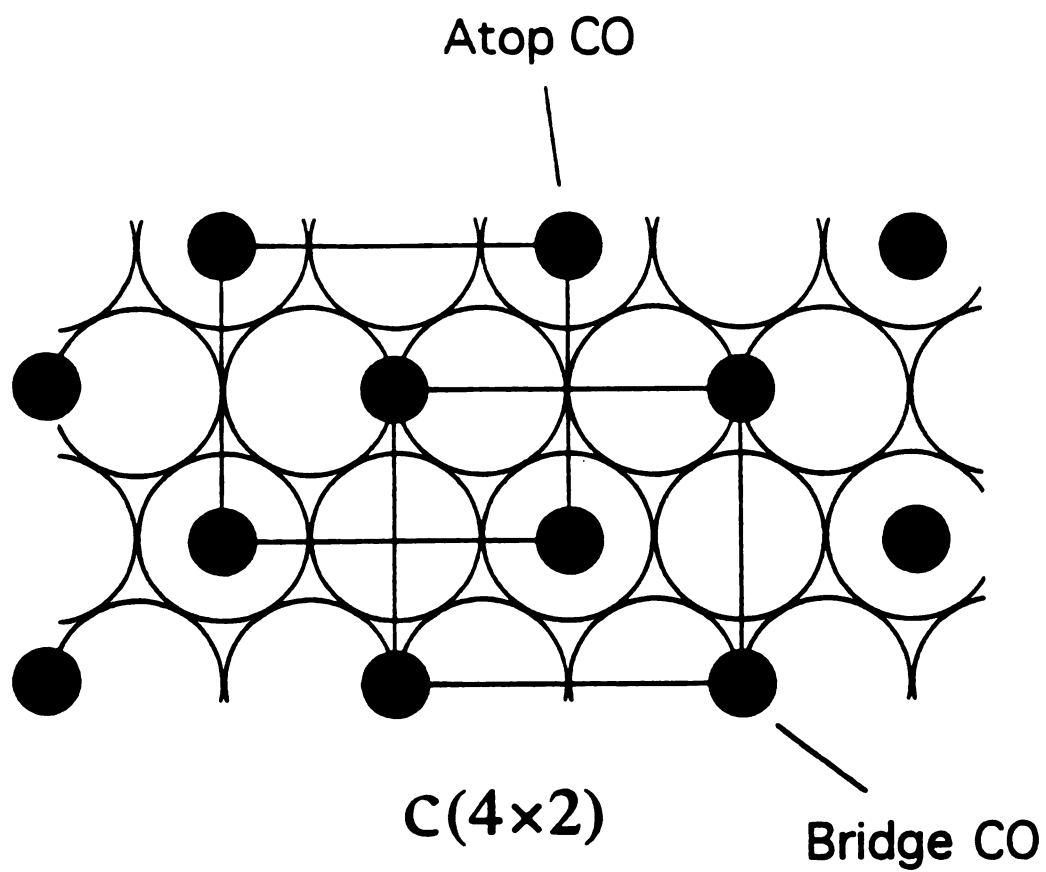


Figure 2-13 $c(4 \times 2)$ structure of 0.5 ML CO on Pt(111) (Luo [30]).

Reference

1. B. E. Hayden, in *Vibrational Spectroscopy of Molecules on Surfaces*, edited by J.T. Yates, Jr. and T. E. Madey (Plenum, New York, 1987).
2. A. M. Bradshaw and E. Schweizer, in *Spectroscopy of Surfaces*, edited by R. J. H. Clark and R. E. Hester (John Wiley & Sons, New York, 1988).
3. N. R. Avery, in *Vibrational Spectroscopy of Molecules on Surfaces*, edited by J.T. Yates, Jr. and T. E. Madey (Plenum, New York, 1987).
4. M. A. Chesters and N. Sheppard, in *Spectroscopy of Surfaces*, edited by R. J. H. Clark and R. E. Hester (John Wiley & Sons, New York, 1988).
5. H. Ibach and D. L. Mills, *Electron Energy Loss Spectroscopy and Surface Vibrations* (Academic, New York, 1982).
6. J. W. Gadzuk, in *Vibrational Spectroscopy of Molecules on Surfaces*, edited by J.T. Yates, Jr. and T. E. Madey (Plenum, New York, 1987).
7. P. Hollins and J. Pritchard, *Prog. Surf. Sci.* **19**, 275 (1985).
8. P. A. Redhead, *Vacuum* **12**, 203 (1962).
9. C. -M. Chan, and W. H. Weinberg, *Appl. Surf. Sci.* **1**, 377 (1978).
10. G. Kisters, J. G. Chen, S. Lehwald, H. Ibach, *Surf. Sci.* **245**, 65 (1991).
11. Vacuum Science Instruments, Delta 0.5 UREELS
12. For example, see C. J. Hirschmugl, G. P. Williams, F. M. Hoffmann and Y. J. Chabal, *Phys. Rev. Lett.* **65**, 480 (1990) and ref. 15.
13. Ph. D. thesis, Chilhee Chung, Michigan State University, 1993.
14. W. Ho, R. F. Willis, and E. W. Plummer, *Phys. Rev. Lett.* **40**, 1463 (1978).
15. C. J. Hirschmugl, Y. J. Chabal, F. M. Hoffmann, and G. P. Williams, *J. Vac. Sci. Technol.* **A12**, 2229 (1994).
16. B. N. J. Persson, and A. I. Volokitin, *Surf. Sci.* **310**, 314 (1994).
17. K. C. Lin, R. G. Tobin, P. Dumas, *Phys. Rev.* **B49**, 17 273 (1994).
18. C. L. DiMaggio, T. E. Moylan, private communication.

19. S. A. Francis and A. H. Ellison, *J. Opt. Soc. Amer.* **49**, 131 (1959).
20. R. G. Greenler, *J. Chem. Phys.* **44**, 310 (1966).
21. W. J. Evans, and D. K. Lambert, *Appl. Opt.* **25**, 2867 (1986).
22. D. K. Lambert, *Appl. Opt.* **27**, 3744 (1988).
23. K. W. Hipps, and G. A. Crosby, *J. Phys. Chem.* **83**, 555 (1979).
24. W. G. Golden, D. S. Dunn, and J. Overend, *J. Catalysis* **71**, 395 (1981).
25. L. F. Sutcu, J. L. Wragg, and H. W. White, *Phys. Rev.* **B41**, 8164 (1990).
26. P. A. Chatterton, "Vacuum Breakdown," in *Electrical Breakdown of Gases*, J. M. Meek and J. D. Craggs, Eds. (Wiley, New York, 1978), Chap. 2.
27. D. K. Lambert, *J. Chem. Phys.* **89**, 3847 (1988).
28. D. K. Lambert, *J. Chem. Phys.* **94**, 6237 (1991).
29. W. R. Smythe, *Static and Dynamic Electricity*, 3rd ed. (McGraw-Hill, New York, 1968), pp. 131,132.
30. J. S. Luo, Ph. D. thesis, Michigan State University, 1992.
31. L. D. Schmidt, *Catal. Rev.-Sci. Eng.* **9**, 115 (1974).
32. H. Wang, R. G. Tobin, G. B. Fisher, C. L. DiMaggio, and D. K. Lambert, unpublished
33. H. Steininger, S. Lehwald, and H. Ibach, *Surf. Sci.* **123**, 264 (1982).
34. B. A. Sexton, *J. Vac. Sci. Technol.* **16**, 1033 (1979).
35. D.E. Kuhl, and R. G. Tobin, *Review of Scientific Instruments*, to be published, and references therein.
36. J. L. Gland, B. A. Sexton, and G. B. Fisher, *Surf. Sci.* **95**, 587(1980).

Chapter 3

Coadsorption of hydrogen and CO on Pt(335): structure and vibrational Stark effect

1. Introduction

The material presented in this Chapter is largely based on our paper published in the *Journal of Chemical Physics* [112].

Important applications involve CO and H coadsorbed on Pt surfaces from a gaseous ambient, [1,2] and these have stimulated a variety of experimental studies in vacuum. Our experiment studies CO and H coadsorbed on Pt(335) using ir spectroscopy (electroreflectance and polarization modulation), temperature programmed desorption (TPD), and low energy electron diffraction (LEED). As shown in Fig.1-1 of Chapter 1, the Pt(335) surface consists of (111) terraces, four atoms wide, separated by monatomic (100) steps: Pt(S)[4(111) × (100)] in step-terrace notation. Adsorbed hydrogen dissociates on Pt surfaces. [3,4]

One motivation to study a highly stepped surface like Pt(335) is to understand the polycrystalline surfaces used in applications. Both CO and H preferentially bind at a step edge. At the low CO coverages discussed here, CO occupies only edge sites. We are also interested in how CO's response to electrostatic and ir fields is changed by coadsorbed H. Our data for CO and H on Pt(335) in vacuum are compared with spectroelectrochemical data obtained by Kim *et al.* [5,6] for CO and H on Pt(335) in aqueous electrolyte.

There have been previous studies of CO on Pt(335) in vacuum, [7-14] but we are not aware of any with coadsorbed H. However, studies of CO coadsorbed with H on Pt(112) [15] and Pt(997) [16] in vacuum have been reported. Both surfaces are vicinal to (111) and differ from Pt(335) mainly in terrace width. In step terrace notation Pt(112) and Pt(997) are Pt(S) [3(111) × (100)] and Pt(S) [9(111) × (111)], respectively. Bridge

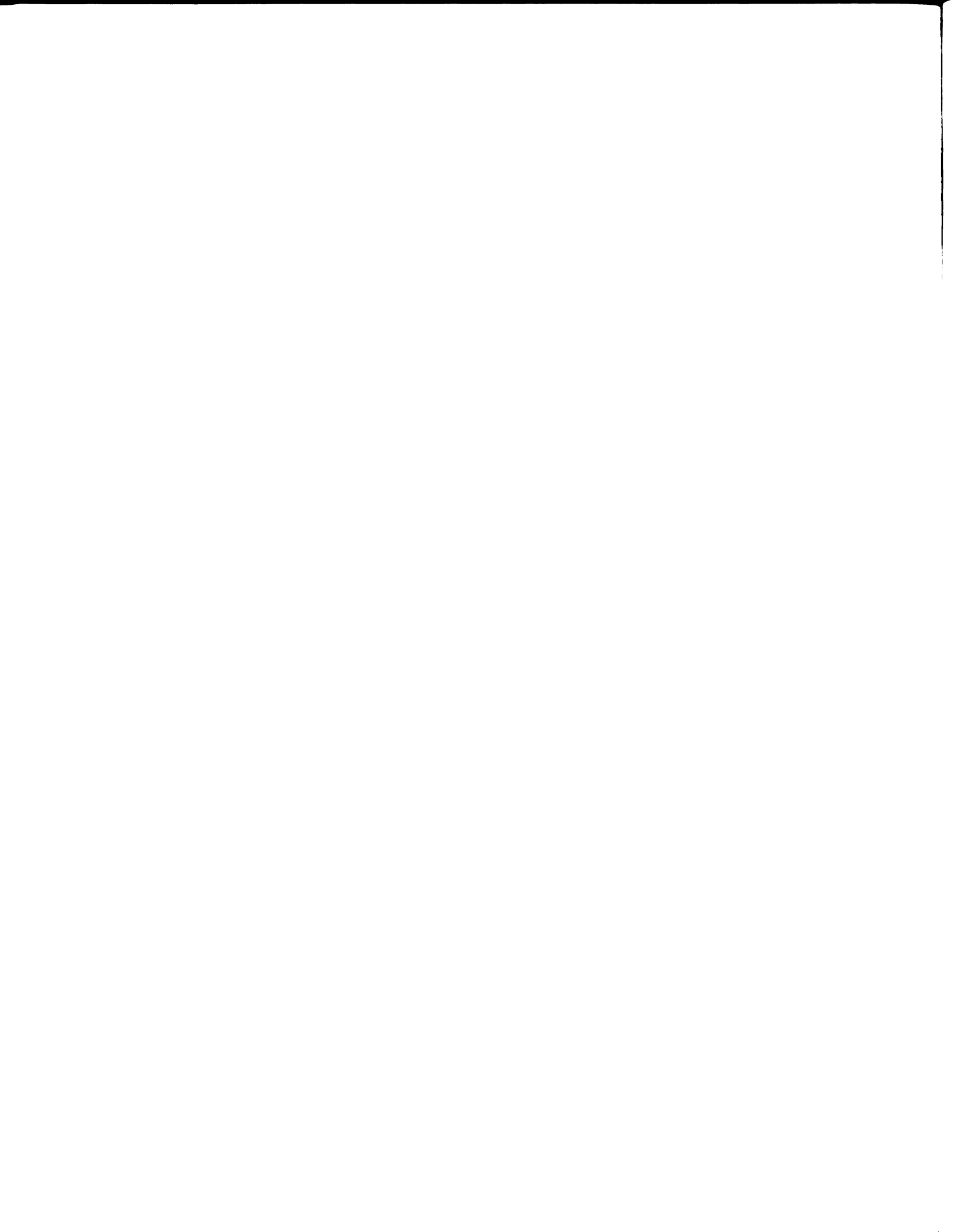
CO coexists with atop CO on Pt(335) [10-13] and on Pt(997) [16] over a wide range of CO coverage, but bridge CO is found on Pt(112) only near saturation CO coverage. [17] In the present work we find another difference: on Pt(112), H causes low-coverage CO to phase separate into one-dimensional islands along the step edge, but on Pt(335) H and CO form a mixed phase along the step edge.

This paper is organized as follows. We first discuss the experiment and our results. Next, a structural model for CO and H on the step edge is proposed that explains our observations. This is followed by a discussion of how *E*-field and coadsorbates affect CO's vibrational spectrum. We consider both the vibrational Stark effect and chemical explanations. We also compare our observations with previous electrochemical data.

2. Experiment

Our experiments were carried out in an ultrahigh vacuum (UHV) chamber with a base pressure of 2×10^{-10} torr. The sample was spot-welded to two Ta wires, which were also used for heating and cooling. The sample temperature could be controlled between 100 and 1400 K. The sample was cleaned by cycles of Ar ion bombardment, reacting at 1000 K with 2×10^{-8} torr O₂, and annealing at about 1300 K. The sample's cleanliness was checked by Auger spectroscopy before any ir spectra were taken. Also, to minimize the adsorption of residual hydrogen on the sample surface, both the cold trap at the bottom of the UHV system and the reservoir of the sample manipulator were filled with liquid N₂ before the sample was allowed to cool below 300 K. Cryopumping by the cold surfaces reduced the H₂ residual gas pressure by about a factor three. The sample temperature was kept at 105--110 K during dosing and data taking. The sample was dosed with CO or H₂ by simply leaking the gas into the chamber.

Detailed descriptions of the spectroscopy techniques are given elsewhere. [18] A single lead-salt diode laser, with a spectral range of 1947--2022 cm⁻¹, was used as the ir source for both reflection-absorption ir spectroscopy (RAIRS) and electroreflectance vibrational spectroscopy (EVS). We used ¹³C¹⁸O for the experiment so the C = O



stretch mode of the atop CO fell within the tuning range of the laser; the frequencies characteristic of bridge-bonded CO were not accessible. The RAIR spectra were obtained using a photoelastic modulator to modulate the polarization of the light. The measured quantity in RAIRS is the fractional change $\Delta R/R$ in *p*-polarized reflectivity (actually the fractional change in the difference between *p*- and *s*-polarized reflectivity) induced by the adsorbate.

The EV spectra were taken by applying an oscillating (100 kHz) high voltage between the sample and a spherical counter electrode, which created an oscillating electrostatic field normal to the surface. The measured quantity in EVS is S_E , the rms amplitude of the induced oscillation in reflectivity to *p*-polarized light, normalized by reflectivity. To interpret EVS spectra quantitatively, the applied field must be known. The applied field depends on the applied potential and the sample-to-electrode distance. The sample-to-electrode distance was determined by measuring the three-terminal capacitance between them.

The data discussed here were obtained on three different days, each with a fixed CO coverage. The angle of incidence of the light on the Pt(335) crystal was the same for both RAIRS and EVS on a given day. On the three days it was 86.4°, 86.4°, and 85.9°, and the rms static *E*-field at the surface was $\langle E \rangle = (3.1 \pm 0.2)$, (2.6 ± 0.2) , and $(3.0 \pm 0.2) \times 10^4$ V/cm, ordered by increasing CO coverage. These values of $\langle E \rangle$ are the average, weighted by the intensity of the focused ir beam, over the illuminated area of the sample. [19]

The CO overlayer was prepared by dosing the sample at 105 K, annealing at 420 K to remove H adsorbed from the background, and cooling back to 105 K; this procedure removed more than 95% of the H from the surface, while desorbing approximately 8% of the CO. During H₂ dosing the sample temperature was 103--110 K and it was kept in this range until the ir spectra with the highest H coverage had been taken. One EV and one RAIR spectrum were measured for each H coverage; each pair of spectra took about 90

minutes. After the ir spectra were completed at the highest H₂ dosage the sample was heated to 420 K while the partial pressures of H₂ and CO were monitored, to desorb the H without removing CO. The sample was then cooled back to 103--110 K and the final RAIR and EV spectra were taken.

We also performed experiments in which the sample was annealed to 198 K for 10 minutes after H₂ dosing. No significant difference was found between the ir spectra of the annealed and unannealed layers. This shows that at the coverages studied, both CO and H are sufficiently mobile at ~100 K to reach their equilibrium configuration, in agreement with Luo *et al.* [11] The experiments of Henderson and Yates [15] with CO and H on Pt(112) were done at 100 K.

The CO and final H coverages were determined with TPD after the last H₂ dose, referenced to the coverages obtained by dosing to saturation with CO or H₂ alone at 100--110 K. The saturation coverage of CO on Pt(335) is 0.63 ML. [9] (Here 1 ML is the coverage with an adsorbate on each surface atom of Pt.) The saturation coverage of H on Pt(S)[9(111) × (111)] is 1.0 ML. [20] We assume that the saturation coverage of H on Pt(335) is also 1.0 ML. The CO coverages on the three days were 0.06, 0.12 and 0.16 ML.

The other H coverages studied with ir were determined in separate experiments by repeating the CO and H₂ dosing sequences and performing TPD for each dosage. The background exposure to H₂ (approximately 0.1 L) that took place during a pair of ir spectra (one EVS and one RAIRS) was accounted for in replicating the coverages. The final coverages obtained by repeating the dosing schedule agreed with the post-ir coverages. For example, with 1.5 L CO, the post-ir TPD gave $\theta_{\text{CO}} = 0.16$ and $\theta_{\text{H}} = 0.30$ ML. After the repeated dosing schedule, TPD gave $\theta_{\text{CO}} = 0.15$ and $\theta_{\text{H}} = 0.29$ ML. Here θ_{CO} and θ_{H} are the coverages of CO and H, respectively.

We also used LEED to search for possible reconstruction of the Pt(335) surface or the formation of ordered overlayers that might be caused by H and CO adsorption. No

change from the clean surface was detected in the LEED pattern. In contrast, Pt(100) [21] and Pt(110) [22] do reconstruct.

3. Experimental results

3.1 TPD

Examples of TPD spectra for only CO on Pt(335) are shown in Fig. 3-1a. The initial CO coverages were saturation and the three θ_{CO} studied with ir. The high temperature TPD peak is from CO at step edges. [7] The low temperature peak is from CO on the terrace. With saturation θ_{CO} , our TPD spectrum taken at 10 K/s has peaks at 416 and 518 K, in agreement with previous studies. [7,11] To resolve the TPD curve into an edge peak and a terrace peak they are modeled as Gaussians, as shown in Fig. 3-1b. At saturation the edge peak is 40% of the total, in good agreement with Luo *et al.* [11] who found 43% edge CO. The TPD spectra in Fig. 3-2a show that at the CO coverages used for the ir spectra, without coadsorbed H, all of the CO was on the edge; none was on the terrace.

TPD spectra for H alone on clean Pt(335) are shown in Fig. 3-2. These spectra were also taken at 10 K/s. At low coverage, curve (a), there is only a single peak at 395 K. With increasing θ_{H} , this high temperature peak stays fixed and a second peak appears at about 315 K. The second peak shifts to lower temperature with increasing θ_{H} . At high θ_{H} (0.8--1.0 ML) a third peak appears as a shoulder at about 250 K. At saturation θ_{H} , the fraction of the total area under the low, intermediate, and high temperature peaks is 0.35, 0.39, and 0.26, respectively. With stepped Pt, the H₂ TPD peak at highest temperature is from chemisorbed H at edge sites. [23] Our data suggest that at saturation, 1/4 of the H is at edge sites, consistent with $\theta_{\text{H}} = 1.0$ ML.

There have been previous TPD studies of H on stepped single-crystal Pt surfaces: Pt(S)[3(111) × (100)], [15,24] Pt(S)[6(111) × (100)], [25] Pt(S)[6(111) × (111)], [25] and Pt(S)[9(111) × (111)]. [20] Surfaces with (100) oriented steps give H₂ TPD spectra with a high temperature peak that dominates at low θ_{H} and a lower temperature peak

with a shoulder, that increases in area with increasing θ_H . Surfaces with (111) oriented steps give H_2 TPD spectra that are more difficult to separate into a "step" and "terrace" contribution if the surface is well annealed. For example, the β_2 peak and β_1 shoulder seen for high- θ_H desorption from Pt(S)[9(111) \times (111)] [20] are very similar to the β_2 peak and β_1 shoulder seen for high- θ_H desorption from Pt(111). [3] For Pt(111) Christmann *et al.* [3] have argued that the peak and shoulder both come from the same state---the peak is distorted because the binding energy of H varies with θ_H .

It is interesting to compare the H_2 TPD spectra of Pt(S)[n(111) \times (100)] surfaces among Refs. 15, 20, 24, 25, and our experiments. The peak desorption temperatures seen in Refs. 20, 24, 25, and our experiments are generally consistent; the temperatures seen in Ref. 15 are lower. In Refs. 20, 24, and 25 the TPD peak of H_2 from Pt(111) stays at about 330 K even though the heating rates ranged from 10 K/s to 82 K/s. With low θ_H on Pt(S)[n(111) \times (100)], our experiments and those in Refs. 20, 24, and 25 consistently find a H_2 TPD peak at 400--430 K. As θ_H is increased, and H begins to occupy (111) terrace sites, a second H_2 peak appears at about 300 K. In contrast, Ref. 15 finds that for low θ_H on Pt(S)[3(111) \times (100)], the H_2 TPD peak is at 309 K, even lower than for H on Pt(111) in Refs. 20, 24, and 25. The same surface was studied in Ref. 24; at low θ_H the temperature of the H_2 TPD peak was 120 K higher than in Ref. 15. Only a small part of the discrepancy can be explained by the different heating rates used in the two experiments (3.9 K/s in Ref. 15 and 67 K/s in Ref. 24); for a first order TPD peak, the peak temperature should shift about 35 K. [26]

As shown in Fig. 3-3, the TPD curves of H on Pt(335) are significantly changed by predosing with CO. As initial θ_{CO} increases, the θ_H that results from a given H_2 dosage decreases. Figure 3-4, which shows edge site occupancy by H vs H_2 dosage for three values of θ_{CO} , further illustrates this point. (The mass spectrometer signals of both CO and H_2 were sampled during these desorptions.) The interaction between coadsorbed

H and CO is repulsive since increasing θ_{CO} monotonically reduces the temperature of the H_2 TPD peaks.

The data in Fig. 3-3 show that at constant θ_{H} , an increase in predosed CO transfers H from edge sites to terrace sites (compare curves a and d). The TPD data taken in conjunction with ir spectroscopy were also analyzed to determine the occupancy of edge sites by CO and H. For all three CO coverages studied, after saturation with H, the total occupancy of CO and H at edge sites was 1.1 ± 0.1 . Each CO at an edge site blocks one H from adsorbing at the edge.

3.2 ir Spectra

One set of EV and RAIR spectra (with $\theta_{\text{CO}} = 0.16$ ML) is shown in Fig. 3-5. The spectra taken at the other two CO coverages are similar. The resonant C-O stretch vibrational frequency vs total θ_{H} is shown in Fig. 3-6, and the integrated RAIR intensity S is shown in Fig. 3-7. Both the EV and RAIR spectra were used to determine the resonant frequency. Smooth cubic splines were first interpolated through the data. Since the EV spectra are proportional to $d(\Delta R/R)/d\nu$, where $(\Delta R/R)$ is the RAIR signal and ν is optical frequency, they were next integrated. The plotted peak frequency is the average from the RAIR and the integrated EV spectra.

The Stark tuning rate $(d\nu/dE)$ was determined by comparing the RAIR spectra with the integrated EV spectra. Two methods were used: comparison of peak heights and comparison of peak areas. The measured Stark tuning rate $(d\nu/dE)$ vs θ_{H} is plotted in Fig. 3-8 for each θ_{CO} . The data show that $(d\nu/dE)$ is independent of θ_{H} , but decreases with increasing θ_{CO} . The scatter in the data in Figs. 3-6--3-8 comes largely from interpolation errors. Mode hops in the diode laser's tuning curve leave gaps about 2 cm^{-1} wide that are later filled by interpolation. When the spectrum has important structure in a gap---a peak for example---some information is lost. This is especially serious for EVS.

4. Structural model of the CO + H overlayer

Let us first recall what is known about CO adsorption on clean Pt(335). It is well established that as CO's coverage builds up it occupies sites on the step edge first. Edge CO has a thermal desorption peak near 520 K (at 10 K/s) and an atop ν (for $^{12}\text{C}^{16}\text{O}$) between 2065 and 2080 cm^{-1} . As θ_{CO} continues to increase, terrace CO appears near 0.20 ML. Terrace CO has a thermal desorption peak near 420 K (at 10 K/s) and an atop ν between 2085 and 2100 cm^{-1} . At saturation (0.63 ML) all of the edge sites are occupied by atop CO, but on the terrace bridge and atop bonded CO coexist. [5,6,10-13] Bridge CO at the edge is also present in an intermediate coverage range. A comprehensive model of CO buildup on Pt(335) was proposed by Luo *et al.* [11]

The experimental evidence from previous studies of CO and H coadsorption on Pt surfaces in vacuum [15,16,27-38] points convincingly toward a strongly repulsive CO-H interaction despite early claims [27,29,30] to the contrary. On Pt(111), even though the CO-CO interaction is repulsive, CO is pushed into islands of high density pure CO as θ_{H} increases. [35-37] On Pt(112), Henderson and Yates observed similar behavior. [15] They used electron-stimulated desorption ion angular distribution (ESDIAD) to monitor edge CO. The same sequence of structures was observed as θ_{H} was increased at fixed θ_{CO} as when θ_{CO} was increased with $\theta_{\text{H}} = 0$. This shows that H and CO form segregated one-dimensional islands along the step edge. As θ_{H} increases the CO is compressed.

Suppose that coadsorbed H and CO on Pt(335) also formed separate islands. An increase in θ_{H} should have the same effect on CO's IR spectrum as an increase in θ_{CO} at $\theta_{\text{H}} = 0$. As θ_{H} increases we would expect to observe: (1) an increase in CO's resonant vibrational frequency ν , (2) little or no change in S , and (3) a reduction in $(d\nu/dE)$. Instead we see (Figs. 3-7--3-9) almost no change in ν , a strong reduction in S , ultimately to zero, and little or no change in $(d\nu/dE)$. Clearly, something different occurs on Pt(335), despite the strong structural similarity to Pt(112).

Our results are consistent with the following model: (1) Each CO blocks one H adsorption site. (2) H adsorbed at the edge forms compact one-dimensional islands of

mixed H and CO. Within the H/CO islands, atop CO shifts to an adjacent edge bridge site. (3) Atop CO outside the H/CO islands is unaffected by θ_H .

On polycrystalline Pt there is previous evidence that *both* a mixed phase and islands occur. [33] The coadsorption of H and CO on single-crystal surfaces has been reviewed by White [31] and again by White and Akhter. [39] A mixed phase of H and CO has previously been observed on relatively open surfaces like Ni(100), [40,41] Ni(110), [42,43] Fe(100), [44] and Rh(100) [45] near saturation coverage, but not on close-packed surfaces or at low coverage on any single-crystal surfaces. Our observation of a mixed phase for CO and H coadsorbed at a step edge, while unexpected, is generally consistent with previous experience. Sites at the edge are in an open environment. Also, even though the total coverage is below saturation the local coverage at the edge is still high; even at our lowest coverage 1/4 of the edge sites are occupied by CO.

Assumption (1) follows from our TPD measurements (Sec. 3.1) which show that at saturation θ_H there is one adsorbate (H or CO) per edge atom for all three θ_{CO} .

Assumptions (2) and (3) explain the ir spectra. Figure 3-7 shows that increasing θ_H strongly reduces the ir intensity of atop CO. Our model explains this: the CO is being shifted to an ir-silent site. The limited tuning range of our laser did not allow us to see the CO at bridge sites in the present experiment, but a subsequent electron energy loss spectroscopy (EELS) experiment [46] has confirmed that its coverage does increase with θ_H . The same effect has been observed in electrochemical experiments with coadsorbed CO and H on Pt(335), [5,6] and similarly in vacuum experiments on Rh(100) [45] and Ni(110). [42] Conversion of atop CO on the edge to bridge CO on the edge is also plausible on energetic grounds: with low θ_{CO} on Pt(111), atop CO is only 0.45 kcal/mol more strongly bound than bridge CO. [20]

Other explanations that we have considered for the disappearance of CO from the ir spectrum as H is coadsorbed on Pt(335) are less plausible. The CO does not move to atop sites on the terrace. Our ir spectra show that the terrace atop $\theta_{CO} < 0.008$ ML in the

range of total θ_{CO} and θ_{H} discussed here. The inability of H to displace CO from edge to terrace sites is consistent with the known binding energies of CO and H at the two sites: edge CO is 5--8 kcal/mol more strongly bound than terrace CO [14,15] but edge H is only 3 kcal/mol more strongly bound than terrace H. [23]

It is conceivable, but unlikely, that H causes a nearby CO to tilt nearly parallel to the surface (at least 77° from the surface normal to account for the observed loss of intensity). Tilted CO is commonly observed on stepped surfaces. [15,47-49] However, an explicit search [8] for tilted CO on Pt(335) found it to be vertical to within 10° . Even for CO on Pt(112), where CO does tilt, [15] the maximum tilt angle is only 20° .

Strong screening of the field at CO adsorption sites within islands is also unlikely. Generally, H adsorbs inside the image plane on metal surfaces. [50] On Pt(111) an explicit calculation shows that H is adsorbed at 3-fold hollow sites 0.95\AA above the top most Pt layer. [51] For CO on Pt(111) the distance from the topmost Pt layer to the center of the CO molecule is 2.43\AA from LEED. [52] There are several ways to estimate where the image plane is on the Pt(111) surface. [53] They all suggest that the center of the CO bond is outside the image plane. We believe that edge atop CO on Pt(335) is a comparable distance from the topmost Pt atoms. Thus the center of the CO bond is at least 1\AA above the H layer. Both experiment and theory suggest that coadsorbed H does not significantly screen the local E -field at the CO adsorption site.

Reduction of CO's vibrational polarizability α_{v} by nearby H can be ruled out. Since S is reduced from its original value by at least a factor 20, and since $\alpha_{\text{v}} \propto (e^*)^2$, the dynamic dipole e^* would need to be reduced by at least a factor 4.5 to explain the data. However, the measured (dv/dE) is expected to be proportional to e^* , so (dv/dE) should drop by a factor 4.5 with increasing θ_{H} . Instead, Fig. 3-8 shows that (dv/dE) does not change by more than about 20%.

Figures 3-6 and 3-8, which show the resonant frequency and (dv/dE) for the atop CO that remains ir-active, demonstrate that this CO is unaffected by coadsorbed H,

except at the very highest θ_H . In Sec. 5.2 we estimate the θ_H induced change in the local density of ir-active atop CO to be at most 0.02 ML. Since the total θ_{CO} on the edge remains constant with increasing θ_H , the average CO-CO distance in the mixed phase is about the same as in the pure phase. This observation indicates that the mixed H/CO islands are *compact*. A uniform or random distribution of H atoms would lead to a *gradual* decrease of the frequency and a gradual increase in (dv/dE) as the average distance between ir-active COs increased. Even though CO and H compete for sites, and the pairwise interactions are repulsive, the equilibrium state on the step edge has two phases---compact mixed islands and unaffected pure CO regions---with the same CO density in both.

Figure 3-9 provides further evidence that the local CO density is not affected by H. It shows S as a function of θ_H , *normalized to S at the lowest θ_H* . For all three θ_{CO} , a given θ_H eliminates the same *fraction* of the initial intensity, regardless of the initial θ_{CO} . If CO were expelled from growing H islands, more complicated behavior would be expected: one slope at low θ_H as the pure CO phase is compressed and a different, θ_{CO} - dependent slope at high θ_H as CO is incorporated into the growing H islands.

It is surprising that a mixed CO/H phase occurs on Pt(S) [4(111) \times (100)] but that an island phase occurs on Pt(S) [3(111) \times (100)] and on Pt(111). As discussed by White and Akhter, [39] in a situation with only pair interactions, a mixed phase between species A and B is energetically favored over an island phase if

$$\epsilon_{AB} < \frac{1}{2} (\epsilon_{AA} + \epsilon_{BB}) \quad (3-1)$$

Here ϵ_{AB} is the interaction energy between A and B, and similarly for ϵ_{AA} and ϵ_{BB} . Since H is inside the image plane, we do not expect its electrostatic interactions to be important. Generally, the strongest interaction between H and a coadsorbate is mediated by conduction electrons in the metal.

One explanation for the difference between the surfaces with three-atom and four-atom wide terraces is that molecules on adjacent terraces interact significantly, and this interaction changes the inequality in Eq.(3-1). In an extended Hückel calculation for CO and H on Rh(111), Ruckenstein and Halachev [54] showed that the through-metal interaction has a different dependence on separation for the CO-CO, H-H, and CO-H interactions. The length scale associated with the difference is a few lattice spacings. Although the computed energy difference is small, it could explain the qualitative change in behavior in going from three to four lattice spacings between edges.

Another explanation for the difference is that the local electronic structure near the edge is different on the two surfaces (without adsorbates), and this alters the interactions between adsorbates along an individual edge. A jellium calculation [55] shows that a single step has an associated dipole. The E -field from a line dipole decays as $1/d^2$ where d is the distance from the line. The induced surface charge at the nearest step consequently decreases by about a factor of two on going from Pt(112) to Pt(335). It is plausible that the extra charge could affect the CO-CO, H-H, and CO-H interactions differently, and this could change the equilibrium structure from a segregated phase to a mixed phase.

5. Vibrational Stark effect and coadsorbates

5.1 Background

Our experiments directly measure the vibrational Stark effect: the effect of a static E -field on a molecule's vibrational spectrum. The Stark effect with externally applied E -field has also been studied theoretically. Quantum mechanics has been used to express (dv/dE) for a molecule on a surface in terms of the molecule's dipole moment and potential energy functions. [19,56] (Here E is the *externally applied* electrostatic field.) The molecular properties needed for the calculation are measurable. There have also been *ab initio* calculations of (dv/dE) for a single molecule on a surface [57-60] or

in spatially uniform E -field. [61-67] In the limit of *low* adsorbate coverage the measurement-based and *ab initio* calculations of (dv/dE) agree, and both have successfully predicted the directly measured (dv/dE) . [10,53] With *saturation* CO coverage on Ni(100) good agreement was also found. [19] With *high* coverage CO on Pt(111) and Pt(335), however, our previous experiments have found discrepancies between theoretical prediction and experiment. [9,10,53]

There are diverse experiments in which a change in static E -field affects ν . Examples include the "chemical" shift $\Delta\nu_{\text{chem}}$ vs adsorbate coverage for a homogeneous layer, $\Delta\nu$ induced by a coadsorbate, and $\Delta\nu$ induced by varying the substrate electrode's potential in an electrochemical cell. One of our motivations is to examine how well the vibrational Stark effect explains such data.

In many experiments $\Delta\nu$ is proportional to the change in local static field E_{loc} :

$$\Delta\nu = \left(\frac{d\nu}{dE_{\text{loc}}} \right) \Delta E_{\text{loc}}. \quad (3-2)$$

For Eq.(3-2) to be useful, however, (dv/dE_{loc}) must be relatively insensitive to the environment, or at least the changes must be theoretically understood. For a single CO molecule on a metal surface, for example, theory predicts that (dv/dE) is approximately proportional to the dipole moment derivative e^* so some account must be taken of the molecular environment. [68] Since e^* can be estimated from EELS or ir intensities, it is relatively straightforward to take its variation into consideration. If other molecular properties of CO varied strongly with environment they would be more difficult to account for. There is evidence from an EELS experiment [14] that the important molecular properties of CO at edge and terrace sites on Pt(335) are similar, lending support to the usefulness of Eq.(3-2).

Coadsorption experiments provide strong evidence that CO's (dv/dE_{loc}) is relatively insensitive to the local chemical environment. Typically, experiments *do* find a linear correlation between ν and the estimated change in static E_{loc} caused by a given

coadsorbate. [69-72] This is seen, for example, in studies that correlate the coadsorbate-induced frequency shift with the change in work function $\Delta\phi$. For CO on Pt(111) both the chemical shift [73] $\Delta\nu_{\text{chem}}$ and the CO induced change in work function, [74-76] $\Delta\phi$, have been measured vs θ_{CO} . (Experimentally $\Delta\nu_{\text{chem}}$ is determined by varying the isotopic composition of the overlayer at constant total θ_{CO} .) At a temperature of 125 K, the measured $\Delta\nu_{\text{chem}}$ decreases from 0 at $\theta_{\text{CO}} = 0$ to -10 cm^{-1} at $\theta_{\text{CO}} = 0.33$ and then increases back to 0 at $\theta = 0.5$. Similarly, at 130 K the measured $\Delta\phi$ decreases from 0 at $\theta_{\text{CO}} = 0$ to $-0.295 \pm 0.038 \text{ eV}$ at $\theta_{\text{CO}} \approx 0.33 \text{ ML}$ and then increases back to 0 at $\theta_{\text{CO}} \approx 0.5 \text{ ML}$. (The θ_{CO} at which $\Delta\phi$ returns to zero is 0.50 ML in Ref. 75 but 0.40 ML in Ref. 76.) Both $\Delta\nu_{\text{chem}}$ and $\Delta\phi$ have the same functional form vs θ_{CO} . The proportionality constant between them is $(d\nu/d\phi) = 34 \pm 4 \text{ cm}^{-1}/\text{eV}$.

Other studies have given similar results. A study [72] of CO on Ni(111) found that ν has the same linear dependence on $\Delta\phi$ for coadsorbed O, CO, and Xe. The observed proportionality constant was $(d\nu/d\phi) = 35 \text{ cm}^{-1}/\text{eV}$. A linear correlation of $(d\nu/d\phi) \sim 45 \text{ cm}^{-1}/\text{eV}$ between $\Delta\phi$ and ν was found by Yamamoto and Nanba [77] for CO on Ag coadsorbed with Xe, Kr, O, and Cl.

Electrochemical experiments with CO on Pt(111) measure a similar quantity. [78-88] Here, the potential Φ of the Pt electrode relative to a reference electrode is controlled directly while ν is measured with ir spectroscopy. Again, the data show $\Delta\nu \propto \Delta\Phi$. The measured $(d\nu/d\Phi)$ depends on the solvent and solute of the electrolyte and on θ_{CO} . In aqueous 0.1 M HClO₄, with $\theta_{\text{CO}} = 0.1$ and 0.65 ML, $(d\nu/d\Phi) = 45$ and 30 cm^{-1}/V , respectively, for the spectral line of atop CO. The close quantitative agreement between $(d\nu/d\Phi)$ for the chemical shift of CO on Pt(111) in vacuum and $(d\nu/d\Phi)$ for CO at a Pt(111) electrode in an aqueous electrolyte suggests that they have a common origin.

Electrochemical experiments have also tried to distinguish between $\Delta\Phi$ and local E -field as the controlling variable for $\Delta\nu$ by varying either the solvent [86,87,89-94] or

the solute [79,95-98] in the electrolyte. The experiments suggest that the controlling variable is the potential drop across the CO molecule---the local E -field---not just Φ of the electrode.

However, other experiments suggest that (dv/dE_{loc}) varies significantly with local environment, and that Eq.(2), which focuses on E_{loc} , is less predictive than explicitly considering the chemical change of the molecule. In a study of CO on Rh(111) coadsorbed with Na, benzene, fluorobenzene, and ethylidyne, for example, Mate *et al.* [99] found that with equal concentrations of CO and the coadsorbate, Δv was proportional to the coadsorbate's dipole moment. They also tried to estimate E_{loc} at the CO adsorption site. The correlation between Δv and ΔE_{loc} was much worse than the correlation between Δv and the coadsorbate's dipole moment.

A previous comparison [53] of the effect of θ_{CO} on S and (dv/dE) , for CO on Pt(111), also called into question the assumptions involved in using E_{loc} for predictive purposes. As we discuss in Sec.5.2, $S \propto \theta_{CO} (\gamma_{ir} e^*)^2$, where γ_{ir} is an effective screening factor, and $(dv/dE) \propto \gamma_{dc}$, where γ_{dc} is the screening factor for the dc field. Within dipole coupling theory we expect $\gamma_{dc} \sim \gamma_{ir}$, so $(S/\theta_{CO})^{1/2}$ and (dv/dE) should have the same dependence on θ_{CO} *even if e^* varies with coverage*. Experimentally [53] this is *untrue* for CO on Pt(111). A similar comparison for CO on Pt(335) is discussed in Sec. 5.2.

Comparison between the Stark effect measured in vacuum and electrochemical data also raises doubts about the transferability of (dv/dE_{loc}) in Eq.(2) from one situation to another. The vacuum experiments directly measure (dv/dE) . At low θ_{CO} in vacuum, screening (by both the adsorbates and the metal's conduction electrons) is expected to be negligible so (dv/dE) should approach (dv/dE_{loc}) . For CO on Pt(111) in the limit of low θ_{CO} in vacuum, [53] $(dv/dE) = 75 \pm 9 \text{ cm}^{-1} /(\text{V/\AA})$.

In an electrochemical experiment the CO molecule is in the compact double-layer, and a model of the double-layer is required to relate ΔE_{loc} to change in electrode

potential Φ . There are many models of the double-layer. For an aqueous double-layer in the limit of low θ_{CO} , the model of Bockris *et al.* [100] implies that $(dE_{\text{loc}}/d\Phi) = 0.29$ (V/Å)/V. An alternative model---a CO monolayer---implies [19] that $(dE_{\text{loc}}/d\Phi) = 0.27$ (V/Å)/V. If we assume that the applied E -field is unscreened ($\gamma_{\text{dc}} = 1$ or $E = E_{\text{loc}}$) at the CO molecule in the vacuum experiment then the Bockris model and the CO monolayer model imply that $(d\nu/d\Phi) = 22$ and $20 \text{ cm}^{-1}/\text{V}$, respectively, while the measured value at low CO coverage is $45 \text{ cm}^{-1}/\text{V}$. To use these models to explain the $(d\nu/d\Phi)$ observed in the electrochemical experiments we would have to assume that $\gamma_{\text{dc}} \sim 0.5$ at the CO adsorption site on Pt(111) in vacuum. This is too small to be explained by presently accepted theory. [53] (Early analyses [19,68] that obtained better agreement for the CO on Pt electrochemical experiments extrapolated from vacuum measurements with CO on Ni surfaces. [19,101])

These conflicting results lead us to consider theories that focus on chemical interactions between adsorbates, rather than on E_{loc} . (There is no fundamental conflict between these alternatives. In some situations they are tied together by the Hellman-Feynman theorem. [102]) One chemical theory for the effect of coadsorbates on ν has been proposed by Ueba. [103] (Similar theories [104-106] had been proposed earlier.) Ueba starts with a Hamiltonian that includes the possibility of charge transfer between CO molecules, and between a CO molecule and the metal. Let $\Delta\nu$ be the difference between the observed ν at θ_{CO} and the singleton frequency. It consists of two parts: $\Delta\nu = \Delta\nu_{\text{dip}} + \Delta\nu_{\text{chem}}$ where $\Delta\nu_{\text{dip}}$ is from dipole-dipole coupling and $\Delta\nu_{\text{chem}}$ is from other effects. One prediction is that $\Delta\nu_{\text{chem}} \propto \Delta\phi$, the change in ϕ caused by adsorbing CO on the clean surface, consistent with the experimental results surveyed above. Another prediction is that CO's vibrational polarizability α_{ν} increases with increasing θ_{CO} .

In the following sections we analyze our data for CO + H on Pt(335) to see whether it is best described by the vibrational Stark effect and E_{loc} or by chemical interactions. We find that the Stark effect theory accurately predicts $(d\nu/dE)$ at low

coverage. However, the effect of coadsorbates is not readily explained by variations in E_{loc} . We also find qualitative support for Ueba's prediction of a coverage-dependent vibrational polarizability.

5.2 Our experiment

The Stark tuning rate (dv/dE) that we measure in terms of the externally applied E -field is given in Table I. With only CO on the clean Pt(335) surface, our data generally agree with previous UHV studies. [7-13] In particular, we find that $(dv/dE) = 88 \pm 9 \text{ cm}^{-1}/(\text{V}/\text{\AA})$ at low coverage (0.06 ML). In an earlier measurement at the same coverage in Ref.9: $(dv/dE) = 60 \pm 8 \text{ cm}^{-1}/(\text{V}/\text{\AA})$. There is also a theoretical relationship between (dv/dE) and the measured ir cross section. [68] At this θ_{CO} , theory predicts [9] $(dv/dE) = 70 \pm 11 \text{ cm}^{-1}/(\text{V}/\text{\AA})$. Theory and experiment are consistent at low CO coverage.

Dipole-dipole coupling is expected to affect the peak frequency ν , integrated intensity S , and Stark tuning rate (dv/dE). Our data at the three CO coverages are shown in Table I. The variation of ν with θ_{CO} is largely explained by dipole-dipole coupling.

We find that ν increases with θ_{CO} at $70 \pm 5 \text{ cm}^{-1}/\text{ML}$. For comparison, Hayden *et al.* [7] found a slope of $52 \text{ cm}^{-1}/\text{ML}$ for atop $^{12}\text{C}^{16}\text{O}$, corresponding to $48 \text{ cm}^{-1}/\text{ML}$ for $^{13}\text{C}^{18}\text{O}$, significantly smaller than we observe. Both in our experiment and in Ref. 7, S increased nearly linearly with total θ_{CO} in this coverage range.

A linear increase of S with θ_{CO} at low θ_{CO} would ordinarily be expected. However, in the present experiment *not* all the CO is atop CO---a θ_{CO} dependent fraction of it is bridge-bonded---so the linear relation between S and θ_{CO} is really a *non-linear* dependence of S on the CO population being observed. Evidence that the bridge-bonded fraction of θ_{CO} increases with θ_{CO} comes both from EELS [11] and ir [12,13] experiments. Since $S \propto \alpha_\nu$, the vibrational polarizability, one explanation for the data is that α_ν *increases* with θ_{CO} . The fraction of CO at atop sites is 1.0, 0.81, and 0.77 at

$\theta_{CO} = 0.06, 0.12, \text{ and } 0.16 \text{ ML}$, respectively. (These estimates come from Ref. 11, modified by recent evidence [46] that atop and bridge CO have the same EELS intensity on the step edge.) As total θ_{CO} increases from 0.06 to 0.16 ML, α_v would have to increase by $>20\%$ to keep S/θ_{CO} constant.

An increase in α_v with θ_{CO} was predicted by Ueba, [103] although the largest increase shown in his paper is only 13% at 1 ML. We are not aware of previous experimental evidence for this effect. The ir spectra of CO on Cu(100) and Ru(100) are well fit [107] by a dipole-dipole coupling model that assumes that α_v is coverage-independent.

Other explanations for the apparent increase in α_v with θ_{CO} that we have considered are less plausible. The inclusion of dipole screening does cause a non-linear dependence of S on θ_{CO} , but it has the wrong sign and only increases the need for α_v to increase with θ_{CO} . It is also possible that the ratio of bridge-to-atop CO is irreproducible; the data would be explained if α_v remained constant and all the CO was atop bonded in the present experiment and in Ref. 7, only in Refs. 10--14 was part of it bridge bonded. To support this explanation, bridge-bonded CO was looked for and not seen with ir in Ref. 7. However, data from the EELS experiments is very consistent and the same crystal was used in the present experiment and in Refs. 9--14.

Standard models of dipole coupling, [67,107] together with the assumption that the only coverage-dependent changes in (dv/dE_{loc}) are due to changes in α_v , predict:

$$S(\theta_{CO}) \propto (\gamma_{IR})^2 \alpha_v(\theta_{CO}) \theta_{atop},$$

$$\left(\frac{dv}{dE}\right)(\theta_{CO}) \propto \gamma_{dc} \sqrt{\frac{\alpha_v(\theta_{CO})}{\alpha_v(0)}} \left(\frac{dv}{dE}\right)(0), \quad (3-3)$$

where γ_{dc} is the screening factor for the static field and γ_{ir} is an effective ir screening factor. [107] Dipole-coupling theory [67,107] predicts $\gamma_{ir} \approx \gamma_{dc}$ for CO. (Previous derivations have been for a system with only one CO species; with multiple species, γ_{ir} and γ_{dc} are modified, but these conclusions are still correct. [108]) We find, however,

that for CO on Pt(335) γ_{dc} varies more rapidly with θ_{CO} than does γ_{ir} , similar to the results of Luo *et al.* [67] for CO on Pt(111). Fig. 3-10 shows γ_{ir} and γ_{dc} calculated from Eq.(3), assuming $\alpha_v(\theta_{CO})$ and $\theta_{atop}/\theta_{CO}$ are constant and $\gamma_{ir} = \gamma_{dc} = 1$ at the lowest coverage. If we instead take $\theta_{atop}/\theta_{CO}$ from Ref. 11, the discrepancy between γ_{ir} and γ_{dc} is even more pronounced. Allowing a coverage-dependent α_v will change the values of γ_{ir} and γ_{dc} in Fig. 3-10, but will not affect the disagreement between them. These results suggest either that dipole coupling theory is inadequate for the calculation of E_{loc} , or that (dv/dE_{loc}) exhibits coverage-dependence beyond that due to α_v .

The dependence of the C-O stretch frequency on work function, which is known from the experiments surveyed in Sec. 5.1 and expected from Ueba's theory, [103] can be used to analyze the small $\Delta\nu$ of CO vs θ_H . In particular, $\Delta\nu_{chem} \propto \Delta\phi$. The maximum H-induced $\Delta\phi$ for Pt(S)[6(111) \times (100)] is [109] 0.08 eV; we assume similar behavior for our surface, Pt(S)[4(111) \times (100)]. The H-induced $\Delta\phi$ is then proportional to θ_H at step sites and reaches 0.08 eV when all step sites are filled. With 0.06 ML CO, 21% of the step sites are blocked from H occupation so the maximum H-induced $\Delta\phi$ is 0.06 eV. If we assume that $\Delta\phi$ from θ_{CO} and θ_H have the same effect on ν and use $(dv/d\phi) = 30 \text{ cm}^{-1}/\text{eV}$, then $\Delta\nu = 2.0 \text{ cm}^{-1}$, more than half the observed shift. Since the measured $\Delta\phi$ is an average over the surface, the $\Delta\phi$ at the edge, and therefore the actual H-induced frequency shift, could be significantly larger. This estimate, though crude, suggests that most, and perhaps all of the observed $\Delta\nu$ could be caused by the H-induced $\Delta\phi$, rather than by changes in local θ_{CO} .

Figure 3-6 shows a slight decrease in ν for θ_H above 0.3 ML for the two lowest θ_{CO} . (For $\theta_{CO} = 0.16$ ML we were not able to reach such high θ_H .) At the highest θ_H , ν was $1973 \pm 1 \text{ cm}^{-1}$ with $\theta_{CO} = 0.06$ ML and $1975 \pm 1 \text{ cm}^{-1}$ with $\theta_{CO} = 0.12$ ML. Taking into account the H-induced chemical shift, these frequencies are close to that of an isolated atop CO molecule on the H-saturated edge (at $\theta_H = 0$ the singleton frequency [7] $\sim 1968 \text{ cm}^{-1}$). This is consistent with our model since at high θ_H nearly all of the atop

CO has been shifted to bridge sites. As the population of atop CO decreases its dipole interaction also decreases. This reduces ν for the CO that remains.

Comparison of the data of (dv/dE) vs θ_{CO} with the data of (dv/dE) vs θ_H also suggests that the local density of CO that contributes to the ir spectrum is independent of θ_H . At each θ_{CO} in Fig. 3-6, a straight line was fit to the data of (dv/dE) vs θ_H . The fit, expressed in terms of the effect of θ_{CO} on (dv/dE) , sets a limit to the effect of θ_H on local θ_{CO} . The estimated change in local θ_{CO} is 0--0.02 ML, consistent with the observed CO being in *the same local environment* at all but the highest H coverages.

5.3 Comparison with electrochemical experiments

Our experiments measure (dv/dE) where E is externally applied in vacuum. Electrochemical experiments measure $(dv/d\Phi)$, where Φ is the potential of the sample relative to a reference electrode. As discussed in Sec. 5.1, to explain both (dv/dE) measured in vacuum and $(dv/d\Phi)$ measured in an aqueous electrolyte for CO on Pt(111), the local E -field in the compact double-layer must be a factor two larger than predicted by two different models. However, as solvent and solute are changed there is good correlation between $(dv/d\Phi)$ and the expected $(dE_{loc}/d\Phi)$ in the compact double layer.

Our experiment also finds a discrepancy between (dv/dE) in vacuum and $(dv/d\phi)$ in an aqueous electrolyte. In the electrochemical experiments of Kim *et al.* [5,6] with CO on Pt(335) in 0.1 M HClO₄, $(dv/d\Phi)$ for atop CO was found to depend on Φ and θ_{CO} . At low θ_{CO} , there is a sharp transition between $(dv/d\Phi)$ with $\Phi < -0.1$ V and $\Phi > -0.1$ V (versus the saturated Calomel electrode). With $\Phi < -0.1$ V, $(dv/d\Phi)$ is zero. With $\phi > -0.1$ V, $(dv/d\Phi) \sim 75 \text{ cm}^{-1}/\text{V}$. At saturation θ_{CO} , the transition has disappeared and $(dv/d\Phi) = 33 \text{ cm}^{-1}/\text{V}$ over the entire potential range. A decrease in Stark tuning rate as θ_{CO} increases is seen both in the vacuum and electrochemical experiments. However, to explain the $(dv/d\phi)$ seen in the electrochemical experiment at low θ_{CO} (and for $\Phi > -0.1$ V) with (dv/dE) measured in vacuum at low θ_{CO} , we would

need to have $(dE/d\Phi) = 0.85 \text{ (V/\AA)/V}$. In contrast, models of the compact double layer discussed in Sec. 5.1 suggest that $(dE/d\Phi) \sim 0.28 \text{ (V/\AA)/V}$. These two estimates of $(dE/d\Phi)$ differ by a factor 3.0.

The sharp transition of $(dv/d\Phi)$ in the electrochemical experiment at $\Phi < -0.1 \text{ V}$ coincides with a peak in the cyclic voltammogram of the Pt(335) electrode. The peak is ascribed to H adsorption at the step edge. [110] Various models of H adsorption on single-crystal Pt have been proposed. [111] One interpretation of the electrochemical experiment is that coadsorbed H reduces CO's $(dv/d\Phi)$ to zero. In contrast, in our vacuum experiment coadsorbed H has no effect on CO's (dv/dE) . This difference is very surprising.

6. Summary

We have investigated the coadsorption of H and CO on the step edges of Pt(335). In striking contrast to the similar Pt(112) surface, [15] on Pt(335) H and CO form compact mixed H/CO islands, within which the CO occupies only bridge sites. The mixed islands coexist with a pure CO phase that is largely unaffected by the presence of H. A similar mixed phase has been observed previously for coadsorbed CO and H on polycrystalline Pt by Thrush and White. [33] Complete segregation of H and CO, however, occurred on the structurally similar Pt(112) surface. [15] The Pt(112) surface used in that experiment also gave, with low H coverage and no CO, an anomalously low temperature thermal desorption peak from edge H.

The Stark tuning rate that we measure for CO on Pt(335) is consistent with earlier measurements [9] in vacuum and with theoretical prediction, but is a factor 3.0 too small to account for the $(dv/d\Phi)$ seen for CO on Pt(335) in the electrochemical experiments of Kim *et al.* [5,6] Also, we find that H does not affect the Stark tuning rate of CO on Pt(335) in vacuum, but H is able to completely suppress $(dv/d\Phi)$ in the electrochemical experiment.

Our evidence for an increase in the vibrational polarizability of CO with increasing CO coverage lends qualitative support to Ueba's theory of coadsorbate effects. [103] The small shift of CO's resonant frequency with θ_H is also roughly consistent with the dependence of frequency on work function expected both from theory and from previous experiments.

TABLE I. Summary of the ir spectra with only CO on Pt(335). Here θ_{CO} is the CO coverage, ν is the frequency of the peak in the ir spectrum, $(\Delta R)/R$ is the maximum CO-induced reflectivity change in the RAIR spectrum, $S = \int (\Delta R) / R d\nu$, and $(d\nu/dE)$ is the Stark tuning rate in terms of the externally applied E -field.

θ_{CO} (ML)	ν (cm^{-1})	$(\Delta R)/R$ (10^{-2})	S (cm^{-1})	$(d\nu/dE)$ [$\text{cm}^{-1}/(\text{V}/\text{\AA})$]
0.060 ± 0.002	1974.4 ± 0.5	4.8 ± 0.3	0.24 ± 0.02	88 ± 9
0.120 ± 0.004	1976.8 ± 0.5	7.8 ± 0.2	0.50 ± 0.05	69 ± 7
0.160 ± 0.005	1981.8 ± 0.5	13.8 ± 0.3	0.61 ± 0.03	52 ± 5

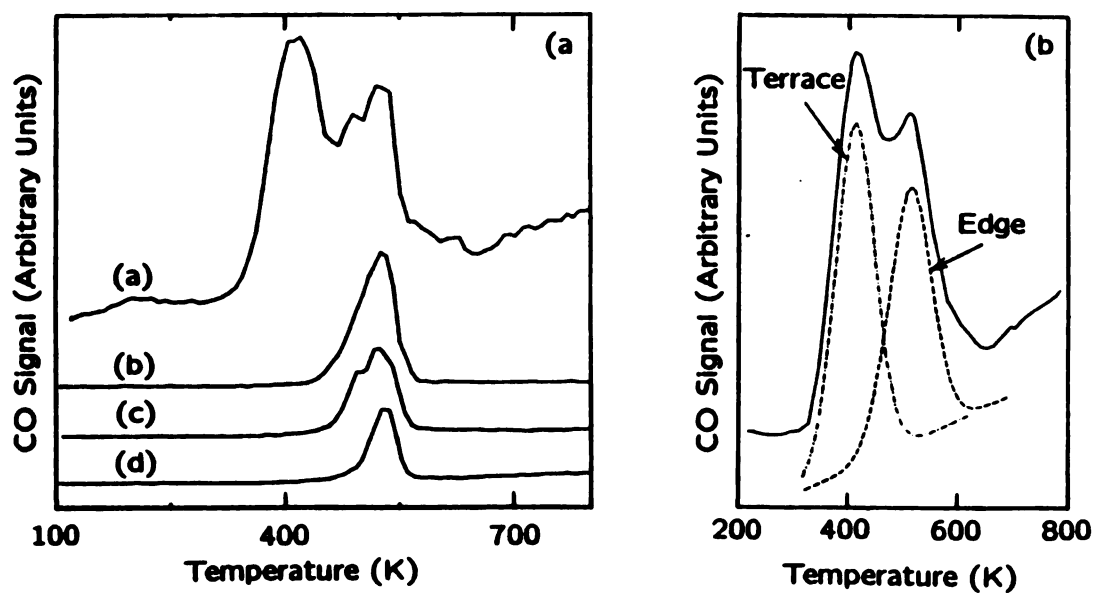


Figure 3-1. a) TPD spectra obtained by desorbing CO from the Pt(335) surface (without H). The CO dosages used to prepare (a)–(d) were 20, 1.5, 1.0 and 0.5 L, respectively. b) Fit of two Gaussians (one from edge CO and the other from terrace CO) to the 20 L TPD spectrum.

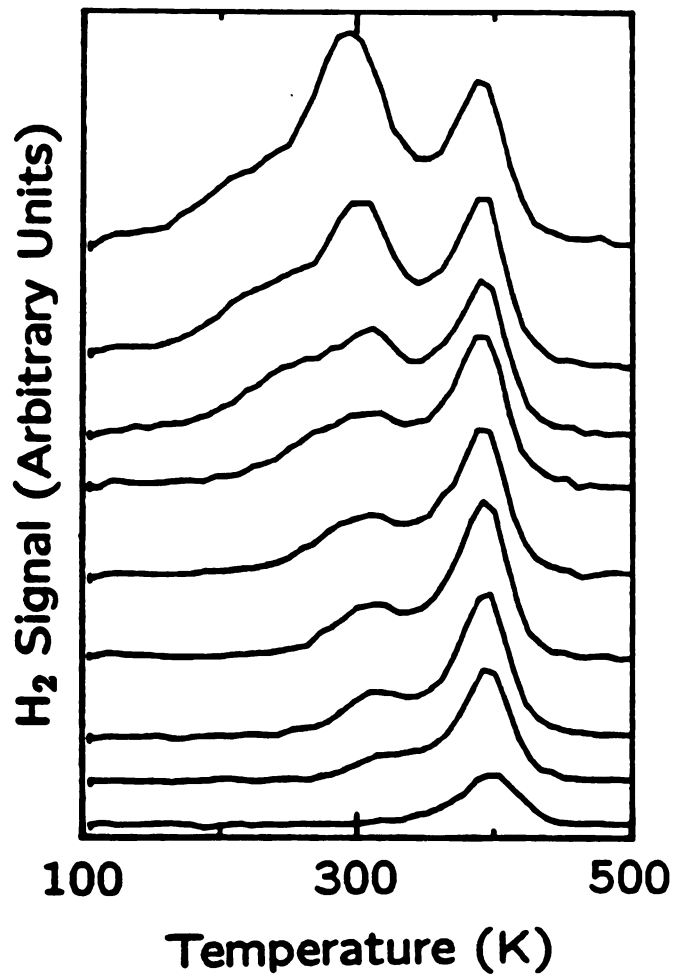


Figure 3-2. TPD spectra obtained by desorbing H₂ from the Pt(335) surface (without CO). From top to bottom the dosages used to prepare the surface were 40, 20, 10, 3, 1.5, 0.8, 0.5, 0.3 and 0.1 L.

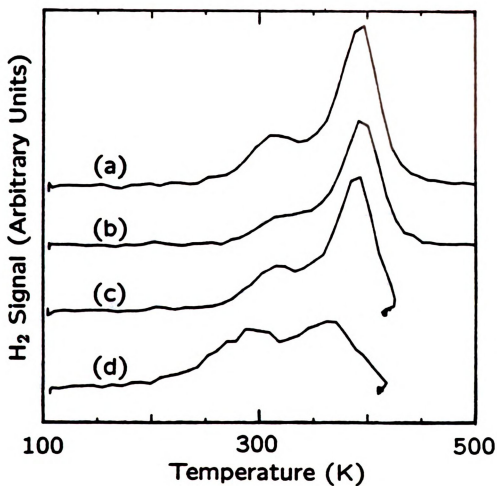


Figure 3-3. TPD spectra obtained by desorbing H₂ from the Pt(335) surface (with and without CO). In a) $\theta_{\text{CO}} = 0$, $\theta_{\text{H}} = 0.35$ ML; in b) $\theta_{\text{CO}} = 0$, $\theta_{\text{H}} = 0.25$ ML; in c) $\theta_{\text{CO}} = 0.05$ ML, $\theta_{\text{H}} = 0.31$ ML; and in d) $\theta_{\text{CO}} = 0.16$ ML, $\theta_{\text{H}} = 0.30$ ML. The hydrogen doses were a) 0.5 L, b) 0.3 L, c) 0.8 L and d) 4.5 L.

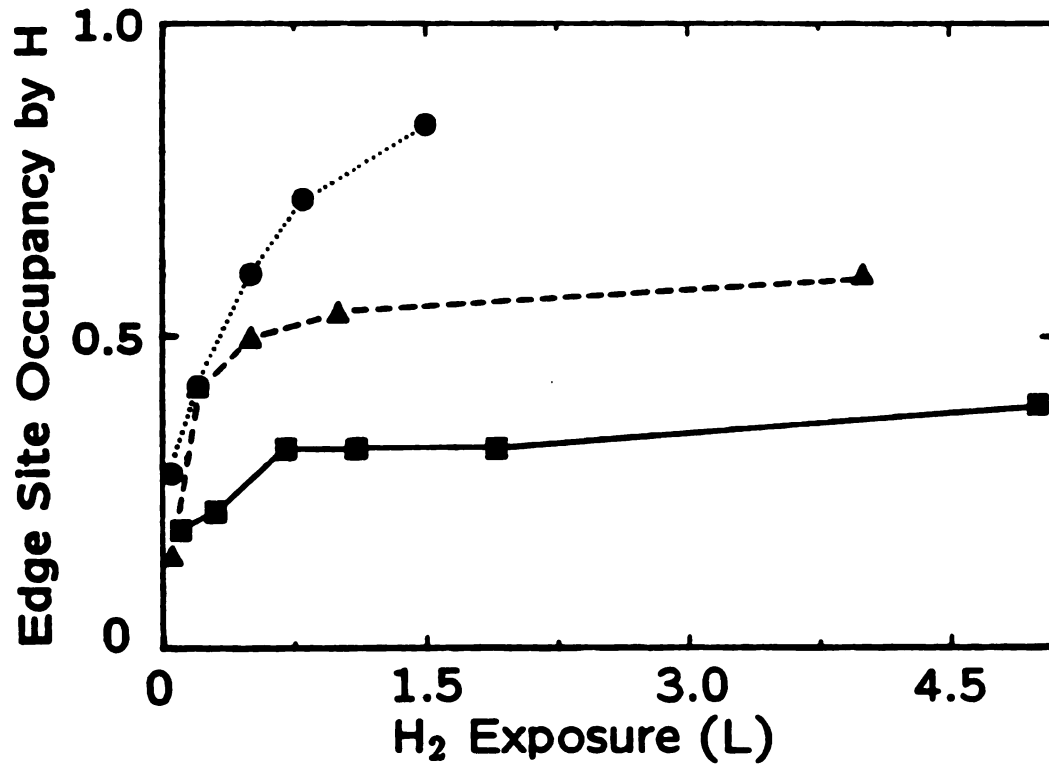


Figure 3-4. Measured H occupancy of edge sites vs H₂ dosage with various pre-coverages of CO. The data with ●, ▲ and ■ were obtained by pre-dosing with 0.5, 1.0 and 1.5 L of CO, respectively.

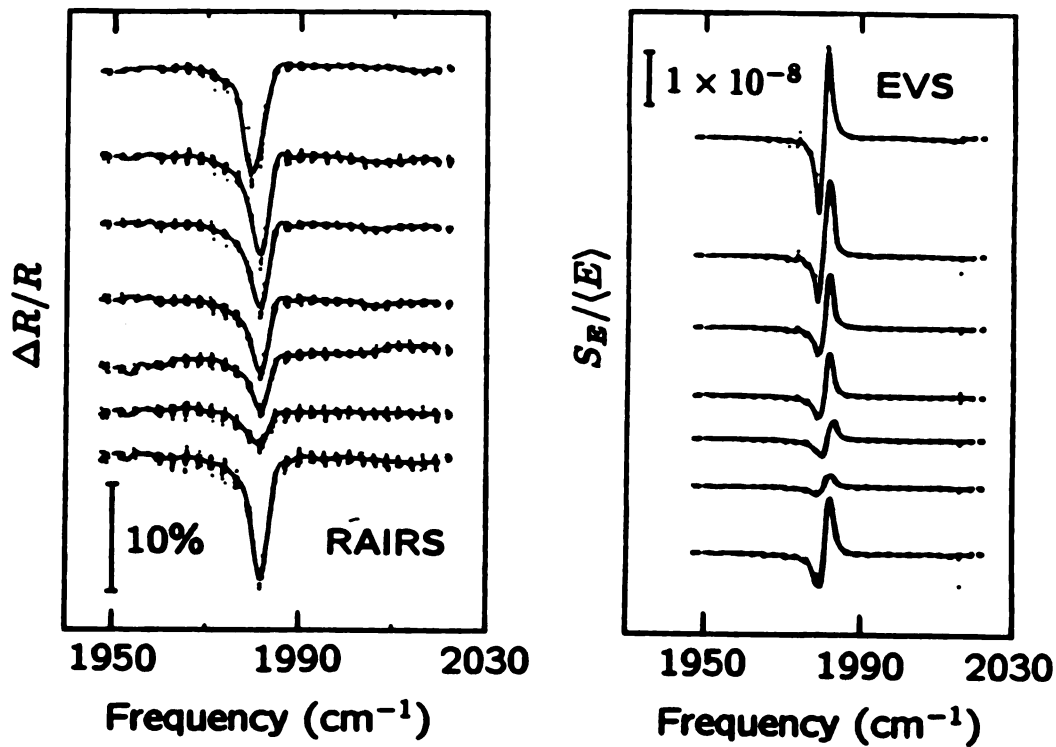


Figure 3-5. RAIR and EVS spectra of CO coadsorbed with H on Pt(335). The CO coverage was 0.16 ML for all of the spectra. From top to bottom the spectra are for $\theta_H = 0.06, 0.10, 0.16, 0.18, 0.21, 0.29,$ and 0.06 ML. The lowermost spectrum was obtained after the sample had been heated to 420 K to desorb the H but leave the CO in place.

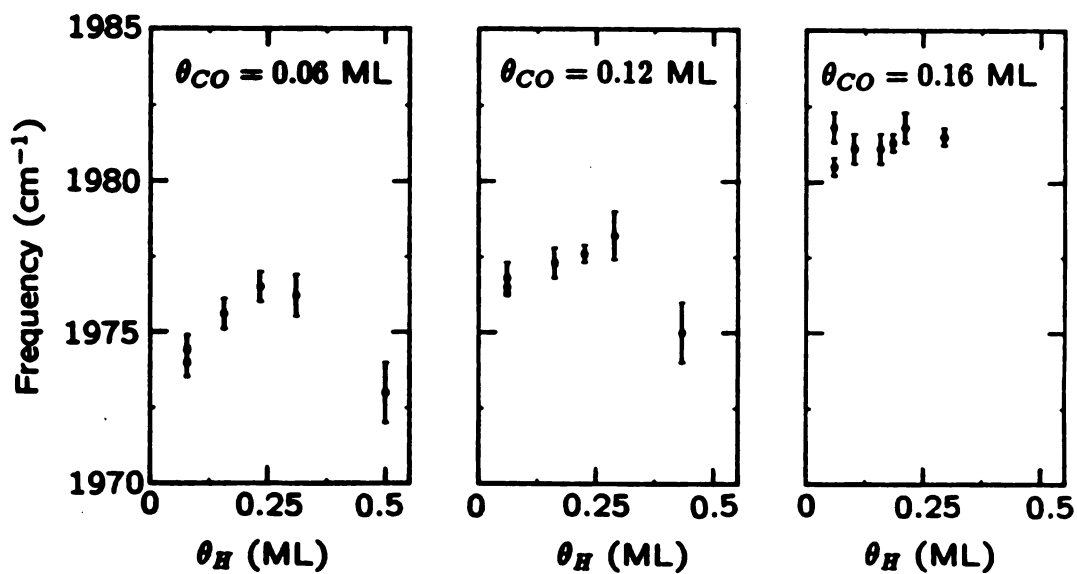


Figure 3-6. Data showing the effect of coadsorbed H on the resonant frequency of the C-O stretch vibration at atop sites, for CO and H coadsorbed on Pt(335).

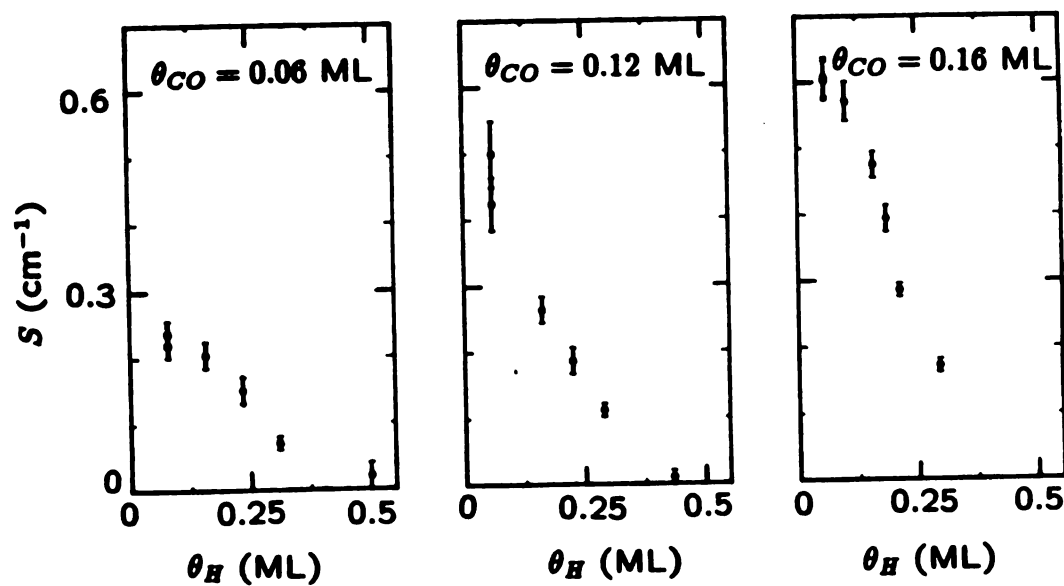


Figure 3-7. Data showing the effect of coadsorbed H on integrated intensity S of the C-O stretch vibration at atop sites, for CO and H coadsorbed on Pt(335).

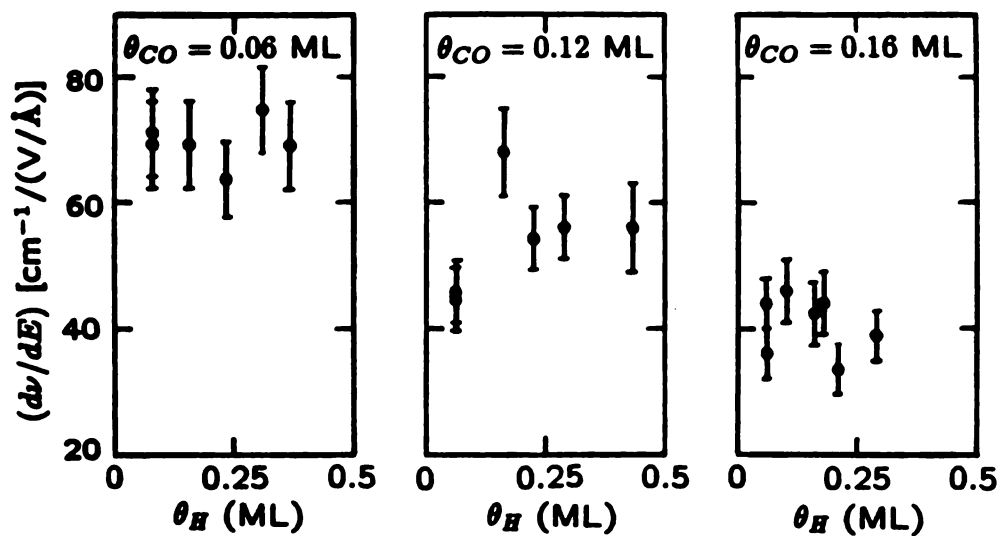


Figure 3-8. Data showing the effect of coadsorbed H on the Stark tuning rate (dv/dE) of the C-O stretch vibration at atop sites, for CO and H coadsorbed on Pt(335).

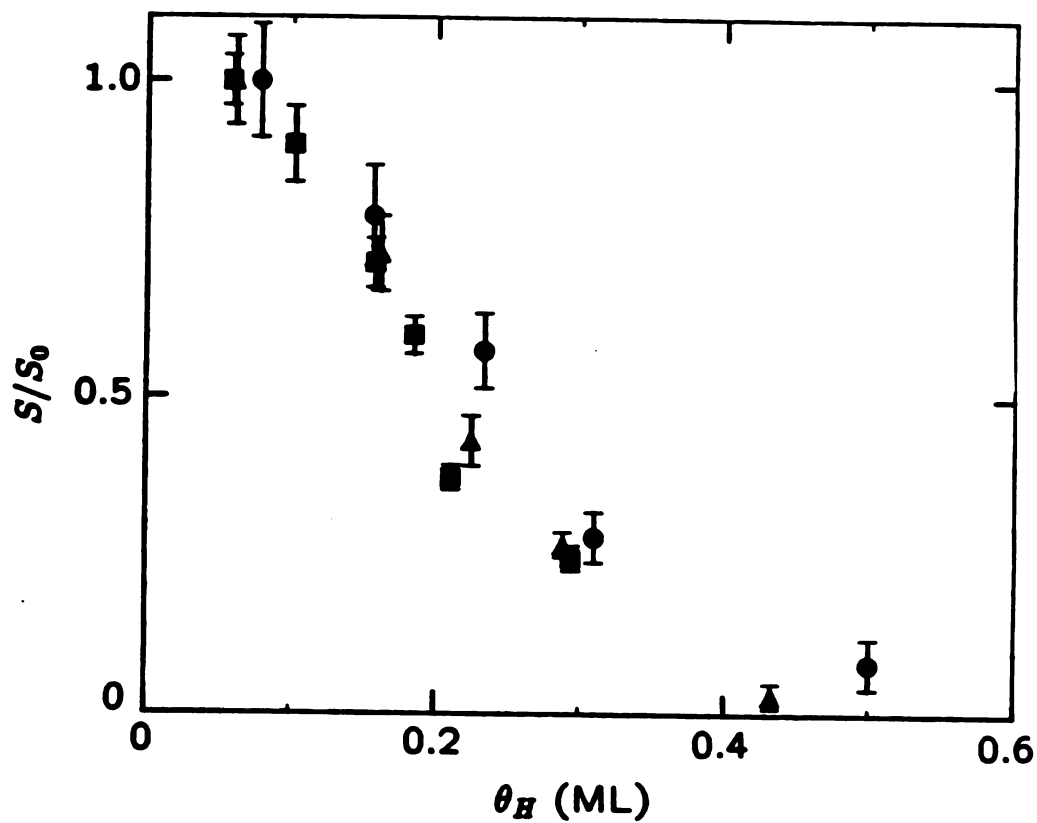


Figure 3-9. Data showing the effect of coadsorbed H on the integrated intensity S for atop CO on Pt(335). With each CO coverage, the data have been normalized by S_0 , the value of S at the lowest H coverage. The data with 0.06, 0.12 and 0.16 ML of CO are represented by ●, ▲ and ■, respectively.

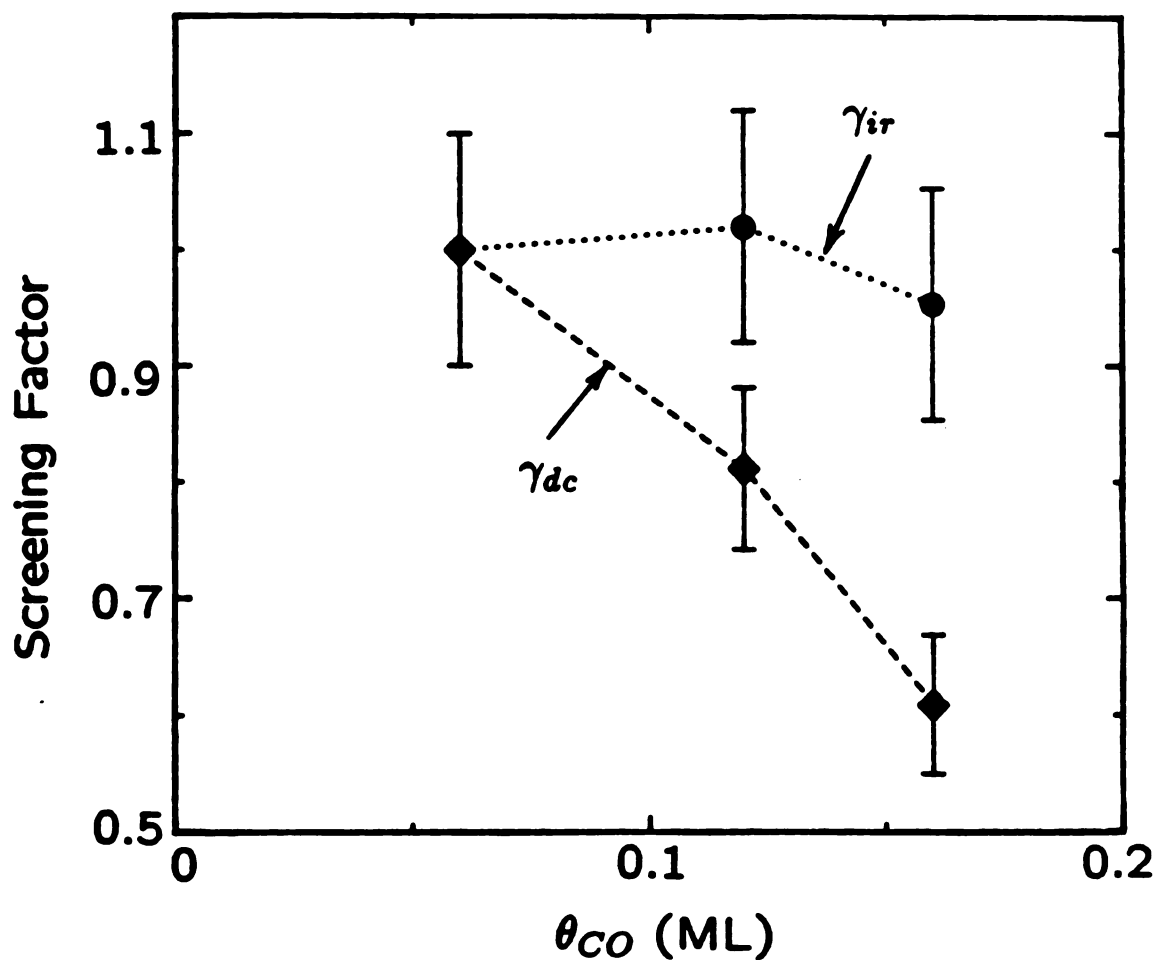


Figure 3-10. Data showing the effect of coadsorbed H on the screening factors (●) γ_{ir} and (◆) γ_{dc} for CO on Pt(335). We assume that $\gamma_{ir} = 1$ and $\gamma_{dc} = 1$ at the lowest coverage, and that $\gamma_{ir} \propto \sqrt{S/\theta_{cov}}$ and $\gamma_{dc} \propto (dv/dE)$.

References

1. K. C. Taylor, in *Catalysis Science and Technology*, edited by J. R. Anderson and M. Boudart (Springer-Verlag, Berlin, 1984), Vol. 5, Chap. 2, pp. 119--170.
2. G. Baier, V. Schüle, and A. Vogel, *Appl. Phys. A* **57**, 51 (1993).
3. K. Christmann, G. Ertl, and T. Pignet, *Surf. Sci.* **54**, 365 (1976).
4. K. Christmann, *Surf. Sci. Rep.* **9**, 1 (1988).
5. C. S. Kim, W. J. Tornquist, and C. Korzeniewski, *J. Phys. Chem.* **97**, 6484 (1993).
6. C. S. Kim, C. Korzeniewski, and W. J. Tornquist, *J. Chem. Phys.* **100**, 628 (1994).
7. B. E. Hayden, K. Kretzschmar, A. M. Bradshaw, and R. G. Greenler, *Surf. Sci.* **149**, 394 (1985).
8. J. S. Somers, T. Lindner, M. Surman, A. M. Bradshaw, G. P. Williams, C. F. McConville, and D. P. Woodruff, *Surf. Sci.* **183**, 576 (1987).
9. D. K. Lambert and R. G. Tobin, *Surf. Sci.* **232**, 149 (1990). Recent unpublished data shows that (dv/dE) for terrace CO on Pt(335) is actually larger than we saw here.
10. J. S. Luo, R. G. Tobin, D. K. Lambert, F. T. Wagner, and T. E. Moylan, *J. Electron Spectrosc. Relat. Phenom.* **54/55**, 469 (1990).
11. J. S. Luo, R. G. Tobin, D. K. Lambert, G. B. Fisher, and C. L. DiMaggio, *Surf. Sci.* **274**, 53 (1992).
12. J. Xu, P. Henriksen, and J. T. Yates, Jr., *J. Chem. Phys.* **97**, 5250 (1992).
13. J. Xu and J. T. Yates, Jr., *J. Chem. Phys.* **99**, 725 (1993).
14. J. S. Luo, R. G. Tobin, D. K. Lambert, G. B. Fisher, and C. L. DiMaggio, *J. Chem. Phys.* **99**, 1347 (1993).
15. M. A. Henderson and J. T. Yates, Jr., *Surf. Sci.* **268**, 189 (1992).
16. E. Hahn, A. Frike, H. Röder, and K. Kern, *Surf. Sci.* **297**, 19 (1993).
17. J. T. Yates, Jr., private communication.
18. D. K. Lambert, *Appl. Opt.* **27**, 3744 (1988).
19. D. K. Lambert, *J. Chem. Phys.* **89**, 3847 (1988).

20. K. Christmann and G. Ertl, *Surf. Sci.* **60**, 365 (1976).
21. B. Klötzer and E. Bechtold, *Surf. Sci.* **295**, 374 (1993).
22. C. S. Shern, *Surf. Sci.* **264**, 171 (1992).
23. B. Poelsema, G. Mechttersheimer, and G. Comsa, *Surf. Sci.* **111**, 519 (1981).
24. K. E. Lu and R. R. Rye, *Surf. Sci.* **45**, 677 (1974).
25. D. M. Collins and W. E. Spicer, *Surf. Sci.* **69**, 85 (1977).
26. C.-M. Chan and W. H. Weinberg, *Appl. Surf. Sci.* **1**, 377 (1978).
27. V. H. Baldwin, Jr. and J. B. Hudson, *J. Vac. Sci. Technol.* **8**, 49 (1971).
28. K. Kawasaki, T. Kodama, H. Miki, and T. Kioka, *Surf. Sci.* **64**, 349 (1977).
29. J. H. Craig, Jr., *Surf. Sci.* **111**, L695 (1981).
30. J. H. Craig, Jr., *Appl. Surf. Sci.* **10**, 315 (1982).
31. J. M. White, *J. Phys. Chem.* **87**, 915 (1983).
32. D. E. Peebles, J. R. Creighton, D. N. Belton, and J. M. White, *J. Catal.* **80**, 482 (1983).
33. K. A. Thrush and J. M. White, *Appl. Surf. Sci.* **24**, 108 (1985).
34. E. G. Seebauer and L. D. Schmidt, *Chem. Phys. Lett.* **123**, 129 (1986).
35. S. L. Bernasek, K. Lenz, B. Poelsema, and G. Comsa, *Surf. Sci.* **183**, L319 (1987).
36. K. Lenz, B. Poelsema, S. L. Bernasek, and G. Comsa, *Surf. Sci.* **189/190**, 431hfilbreak (1987).
37. D. Hoge, M. Tüshaus, and A. M. Bradshaw, *Surf. Sci.* **207**, L935 (1988).
38. D. H. Parker, D. A. Fisher, J. Colbert, B. E. Koel, and J. L. Gland, *Surf. Sci.* **258**, 75 (1991).
39. J. M. White and S. Akhter, *CRC Crit. Rev. Solid State Mater. Sci.* **14**, 131 (1988).
40. D. W. Goodman, J. T. Yates, Jr., and T. E. Madey, *Surf. Sci.* **93**, L135 (1980).
41. L. Westerlund, J. Jönsson, and S. Andersson, *Surf. Sci.* **199**, 109 (1988).
42. J. Bauhofer, M. Hock, and J. Küppers, *J. Electron Spectrosc. Relat. Phenom.* **44**, 55 (1987).

43. J. G. Love, S. Haq, and D. A. King, *J. Chem. Phys.* **97**, 8789 (1992).
44. M. L. Burke and R. J. Madix, *J. Am. Chem. Soc.* **113**, 1475 (1991).
45. L. J. Richter, B. A. Gurney, and W. Ho, *J. Chem. Phys.* **86**, 477 (1987).
46. H. Wang, R. G. Tobin, D. K. Lambert, G. B. Fisher, and C. L. DiMaggio, unpublished.
47. T. E. Madey, J. T. Yates, Jr., A. M. Bradshaw, and F. M. Hoffmann, *Surf. Sci.* **89**, 370 (1979).
48. P. Hofmann, S. R. Bare, N. V. Richardson, and D. A. King, *Solid State Comm.* **42**, 645 (1982).
49. M. D. Alvey, M. J. Dresser, J. T. Yates, Jr., *Surf. Sci.* **165**, 447 (1986).
50. J. R. Smith, S. C. Ying, and W. Kohn, *Phys. Rev. Lett.* **30**, 610 (1973).
51. P. J. Feibelman and D. R. Hamann, *Surf. Sci.* **182**, 411 (1987).
52. D. F. Ogletree, M. A. Van Hove, G. A. Somorjai, *Surf. Sci.* **173**, 351 (1986).
53. J. S. Luo, R. G. Tobin, and D. K. Lambert, *Chem. Phys. Lett.* **204**, 445 (1993).
54. E. Ruckenstein and T. Halachev, *Surf. Sci.* **122**, 422 (1982).
55. M. D. Thompson and H. B. Huntington, *Surf. Sci.* **116**, 522 (1982).
56. J. Martí and D. M. Bishop, *J. Chem. Phys.* **99**, 3860 (1993).
57. P. S. Bagus, C. J. Nelin, W. Müller, M. R. Philpott, and H. Seki, *Phys. Rev. Lett.* **58**, 559 (1987).
58. P. S. Bagus, C. J. Nelin, K. Hermann, and M. R. Philpott, *Phys. Rev. B* **36**, 8169 (1987).
59. P. S. Bagus and G. Pacchioni, *Surf. Sci.* **236**, 233 (1990).
60. M. Head-Gordon and J. C. Tully, *Chem. Phys.* **98**, 3179 (1993).
61. C. W. Bauschlicher, Jr., *Chem. Phys. Lett.* **118**, 307 (1985).
62. J. L. Andrés, M. Duran, A. Lledós, and J. Bertrán, *Chem. Phys.* **151**, 37 (1991).
63. J. L. Andrés, J. Martí, M. Duran, A. Lledós, and J. Bertrán, *J. Chem. Phys.* **95**, 3521 (1991).

64. J. Martí, A. Lledós, J. Bertrán, and M. Duran, *J. Comp. Chem.* **13**, 821 (1992).
65. Z. Xu, J. T. Yates, Jr., L. C. Wang, and H. J. Kreuzer, *J. Chem. Phys.* **96**, 1628 (1992).
66. D. M. Bishop, *J. Chem. Phys.* **98**, 3179 (1993).
67. K. Hermansson, *J. Chem. Phys.* **99**, 861 (1993).
68. D. K. Lambert, *Solid State Comm.* **51**, 297 (1984).
69. C. L. Angell and P. C. Schaffer, *J. Phys. Chem.* **70**, 1413 (1966).
70. K. J. Uram, L. Ng, and J. T. Yates, Jr., *Surf. Sci.* **177**, 253 (1986).
71. F. M. Hoffmann, N. D. Lang, and J. K. Nørskov, *Surf. Sci.* **226**, L48 (1990).
72. Z. Xu, M. G. Sherman, J. T. Yates, Jr., and P. R. Antoniewicz, *Surf. Sci.* **276**, 249 (1992).
73. M. Tüshaus, E. Schweizer, P. Hollins, and A. M. Bradshaw, *J. Electron Spectrosc. Rel. Phenom.* **44**, 305 (1987).
74. K. Horn and J. Pritchard, *J. Phys. (Paris)* **38**, C4--164 (1977).
75. G. Ertl, M. Neumann, and K. M. Streit, *Surf. Sci.* **64**, 393 (1977).
76. P. R. Norton, J. W. Goodale, and E. B. Selkirk, *Surf. Sci.* **83**, 189 (1979).
77. I. Yamamoto and T. Nanba, *Surf. Sci.* **202**, 377 (1988).
78. F. Kitamura, M. Takeda, M. Takahashi, and M. Ito, *Chem. Phys. Lett.* **142**, 318 (1987).
79. L.-W. H. Leung, A. Wieckowski, and M. J. Weaver, *J. Phys. Chem.* **92**, 6985 (1988).
80. N. Furuya, S. Motoo, and K. Kunimatsu, *J. Electroanal. Chem.* **239**, 347 (1988).
81. S.-C. Chang, L.-W. H. Leung, and M. J. Weaver, *J. Phys. Chem.* **93**, 5341 (1989).
82. F. Kitamura, M. Takahashi, and M. Ito, *Surf. Sci.* **223**, 493 (1989).
83. S.-C. Chang and M. J. Weaver, *J. Chem. Phys.* **92**, 4582 (1990).
84. Y. Kinomoto, S. Watanabe, M. Takahashi, and M. Ito, *Surf. Sci.* **242**, 538 (1991).
85. S.-C. Chang and M. J. Weaver, *J. Phys. Chem.* **95**, 5391 (1991).

86. S.-C. Chang, X. Jiang, J. D. Roth, and M. J. Weaver, *J. Phys. Chem.* **95**, 5378 (1991).
87. X. Jiang and M. J. Weaver, *Surf. Sci.* **275**, 237 (1992).
88. M. J. Weaver, *Appl. Surf. Sci.* **67**, 147 (1993).
89. M. R. Anderson, D. Blackwood, and S. Pons, *J. Electroanal. Chem.* **256**, 387 (1988).
90. M. R. Anderson, D. Blackwood, T. G. Richmond, and S. Pons, *J. Electroanal. Chem.* **256**, 397 (1988).
91. J. G. Love and A. J. McQuillan, *J. Electroanal. Chem.* **274**, 263 (1989).
92. J. D. Roth, S.-C. Chang, and M. J. Weaver, *J. Electroanal. Chem.* **288**, 285 (1990).
93. A. E. Russell, S. Pons, and M. R. Anderson, *Chem. Phys.* **141**, 41 (1990).
94. A. E. Russell, D. Blackwood, M. R. Anderson, and S. Pons, *J. Electroanal. Chem.* **304**, 219 (1991).
95. K. Ashley, M. G. Samant, H. Seki, and M. R. Philpott, *J. Electroanal. Chem.* **270**, 349 (1989).
96. L.-W. H. Leung, S.-C. Chang, and M. J. Weaver, *J. Chem. Phys.* **90**, 7426 (1989).
97. M. R. Anderson and J. Huang, *J. Electroanal. Chem.* **318**, 335 (1991).
98. J. D. Roth and M. J. Weaver, *Langmuir* **8**, 1451 (1992).
99. C. M. Mate, C.-T. Kao, and G. A. Somorjai, *Surf. Sci.* **206**, 145 (1988).
100. J. O'M. Bockris, M. A. V. Devanathan, and K. Müller, *Proc. R. Soc. London Ser. A* **274**, 55 (1962).
101. D. K. Lambert, *Phys. Rev. Lett.* **50**, 2106 (1983); **51**, 2233 (E) (1983).
102. R. P. Feynman, *Phys. Rev.* **56**, 340 (1939).
103. H. Ueba, *Surf. Sci.* **188**, 421 (1987).
104. N. K. Ray and A. B. Anderson, *J. Phys. Chem.* **86**, 4851 (1982).
105. H. S. Luftman and J. M. White, *Surf. Sci.* **139**, 369 (1984).
106. S. Holloway and J. K. Nørskov, *J. Electroanal. Chem.* **161**, 193 (1984).
107. B. N. J. Persson and R. Ryberg, *Phys. Rev. B* **24**, 6954 (1981).

108. H. Wang and R. G. Tobin, unpublished.
109. D. M. Collins and W. E. Spicer, *Surf. Sci.* **69**, 114 (1977).
110. A. Rodes, K. El Achi, M. A. Zamakhchari, and J. Clavilier, *J. Electroanal. Chem.* **284**, 245 (1990).
111. A. Wieckowski, P. Zelenay, and K. Varga, *J. Chim. Phys.* **88**, 1247 (1991).
112. H. Wang, R. G. Tobin, D. K. Lambert, *J. Chem. Phys.* **101**, 4277 (1994).

Chapter 4

H-CO interactions on the terraces and step edges of the Pt(335) surface

The material in this Chapter is largely based on a paper that has been submitted to Surface Science [53].

1. Introduction

Coadsorbed H and CO on stepped Pt is an interesting model system, relevant to such technologies as catalysts, chemical sensors and fuel cells. In this Chapter, I present a high resolution electron energy loss spectroscopy (EELS) and temperature-programmed desorption (TPD) investigation of CO and H on Pt(335).

As shown in Fig. 1-1, this surface is highly stepped with (111) terraces four atoms wide. In step-terrace notation it is Pt(S)[4(111) × (100)]. In a previous experiment [1] we used IR laser spectroscopy to study CO at step sites on Pt(335) with coadsorbed H. These results were presented in Chapter 3. However, that experiment was limited both by the restricted tuning range of the laser and by the range of CO coverage investigated so only atop bonded CO along the edge could be seen. In the present experiment, EELS allows *all* the CO to be seen, although it does not allow edge and terrace CO to be distinguished spectroscopically. Also, as an alternative to having CO just at edge sites, by blocking the edge sites with H before dosing with CO we are also able to put CO just at terrace sites.

To our knowledge, this is the first EELS study of coadsorbed CO and H on Pt. However, EELS has previously been used to obtain vibrational spectra of coadsorbed CO and H on Cr(111) [2], Cu₃Pt(111) [3], Fe(100) [4], Ir(110) [5], Ir(111) [5], Ni(100) [6-8], Ni(110) [9,10], Ni(111) [6], Pd(100) [8,11,12], and Rh(100) [13,14]. The coadsorption of CO and H on metal surfaces has been reviewed by White and Akhter[15]. Other experiments that have studied coadsorbed CO and H on Pt are discussed in Chapter 2

[Ref. 1]. In vacuum, IR vibrational spectra of coadsorbed CO and H have been obtained on Pt(111) [16] and Pt(S)[9(111) \times (111)] [17]. There have also been many electrochemical experiments that have used IR vibrational spectroscopy to study CO on Pt in situations where H must also have been present [1,18]. In particular the coadsorption of CO and H on Pt(335) in water has been studied [19,20].

As a matter of notation, we let θ_{CO} and θ_{H} be the CO and H coverages, respectively. Coverages are given in monolayers (ML), where 1 ML is 1 adsorbate per surface Pt atom. Previous experiments have shown that for clean Pt(335) covered only with CO, at saturation $\theta_{\text{CO}} = 0.63$ ML [21]. Experiments on a similar surface, clean Pt(S)[9(111) \times (111)], have shown that at H saturation $\theta_{\text{H}} = 1$ ML [22]. We assume that the same is true for H on Pt(335). On clean Pt(111) the saturation $\theta_{\text{H}} = 0.80$ ML [23].

2. Experiment

Our experiments were carried out in an ultrahigh vacuum (UHV) chamber with base pressure of 3.5×10^{-11} torr. The sample was spot-welded to two Ta wires, which were used for both heating and cooling. The sample temperature could be varied from 90 K to over 1400 K. The sample was cleaned by cycles of sputtering in Ar, cycling the sample temperature between 570 K and 1023 K in 1.0×10^{-8} torr oxygen and annealing at 1300 K for one minute. The sample cleanliness was always checked by Auger spectroscopy and EELS. The gases were dosed through individual dosers, with enhancement factors of about 100 over background dosing.

The EELS apparatus has been described elsewhere [24]. We scanned from 300 to 5000 cm^{-1} , which includes both the C-O internal stretch and the C-Pt stretch vibrations. The H-Pt stretch was too weak to be detected. All EEL spectra were measured at a sample temperature of 90 K.

The TPD scans reported here were taken at 10 K/s with the sample facing the mass spectrometer, as described in Chapter 2.

3. Results and Discussion

Our EELS and TPD results for CO alone on Pt(335) agree closely with those reported by Luo *et al.* [25], and are consistent with other IR and TPD data [1,21,26]. At low coverage, CO occupies only edge sites. At higher coverages, CO begins to occupy terrace sites as it continues to fill the edge sites. At saturation, all of the edge sites are occupied (one CO per edge Pt atom). In the model of Luo *et al.* [25] all of the CO at edge sites is atop bonded at saturation θ_{CO} . However, on the(111) terraces there is a mixture of atop and bridge-bonded CO. A similar CO structure occurs on Pt(111) at saturation [27].

Our TPD results for H alone on Pt(335) are shown in Fig. 4-1. As seen previously [1], at the lowest coverage there is one peak at 395K from H at edge sites. After the edge is saturated, H begins to fill terrace sites and a new peak appears at ~ 315 K. The only significant difference between Fig. 4-1 and the data in Chapter 3 [Ref. 1] is that in the present work we do not see a low temperature shoulder on the terrace peak. The low temperature shoulder may have been from H on the back or sides of the crystal; in the present work only the front face of the crystal was exposed to the mass spectrometer.

3.1 Coadsorption of H and CO on the step edge

At low θ_{CO} , in equilibrium, all of the CO is at edge sites. Figure 4-2 shows EEL spectra at various θ_H , for $\theta_{CO} = 0.07$ and 0.13 ML. The overlayer was prepared by dosing CO at 90 K and then annealing at 420 K for one minute, both to allow the layer to equilibrate and to desorb any H adsorbed from the background. The sample was cooled to 90 K and all H dosing and EEL spectra occurred at that temperature. Following each spectrum the sample was heated to 420 K while the partial pressure of H_2 was monitored to determine θ_H . A previous experiment [1] showed that throughout this range of θ_{CO} and θ_H , the coverage of atop CO on the terrace < 0.008 ML.

In Fig. 4-3a we plot the ratio I_B / I_{tot} vs. θ_H from the data in Fig. 4-2, where I_B is the integrated single-loss peak from bridge-bonded CO and I_{tot} is the total integrated single-loss peak (both bridge and atop-bonded). The data clearly show that coadsorbed H

shifts CO from atop to bridge sites. At the highest θ_H studied here the atop peak is reduced to about 25% of its original intensity. The IR data in Ref. 1 show that the elimination of the atop CO intensity is almost complete at higher θ_H .

The conversion of atop CO to bridge CO with increasing θ_H that we observe supports the model proposed in Chapter 3 [Ref. 1]. In the model, one-dimensional islands of mixed H and CO coexist with islands of pure CO. Both phases have equal CO concentrations. A mixed phase had previously been observed on relatively open surfaces of Ni [7,10,28-30], Fe [31], and Rh [13,14]. Both a mixed phase and islands occur on polycrystalline Pt [32]. The model for CO on Pt(335) explains the linear decrease of atop CO's IR intensity with increasing θ_H as a consequence of H displacing CO from atop to bridge sites within the mixed islands. Similar site shifting has been observed in other experiments [10,13,19,20].

Our EELS data and the IR results in Ref. 1 both show that the effect of θ_H on atop CO's vibrational frequency is small. In the IR spectra the change was $< 5 \text{ cm}^{-1}$. In the EEL spectra in Figs. 4-2a and 4-2b the atop frequency changes $\sim 20 \text{ cm}^{-1}$, less than the $\sim 60 \text{ cm}^{-1}$ instrumental linewidth.

Since the data in Figs. 4-2a and 4-2b were acquired at constant θ_{CO} , we can use them to compare the EELS cross sections of atop and bridge CO on the step edge, and to analyze the dependence of the cross sections on θ_H . Other studies [21,26,33-35] have examined the relative cross sections of edge atop and terrace atop CO, but to our knowledge this is the first measurement of the relative cross sections of atop and bridge CO on the step edge. On Pt(111), Mieher, Whitman and Ho [33] calibrated the populations with low-energy electron diffraction and found the EELS cross section of atop CO to be 1.8 times that of bridge CO. On Pt(335), however, it is immediately apparent from Fig. 4-2 that the cross sections of edge atop and edge bridge CO are comparable---at least when the bridge CO is in a H-rich environment. In both Fig. 4-2a

and Fig. 4-2b the bridge band intensity in the top spectrum is comparable to or greater than the atop intensity in the bottom spectrum.

Figure 4-3b displays I_{tot}/I_E vs θ_H , where I_E is the intensity of the elastic peak. The same qualitative behavior is found for both values of θ_{CO} . As θ_H increases, I_{tot}/I_E gradually drops, as we would expect if bridge CO has a smaller cross section than atop CO---as on Pt(111). At higher θ_H , although the fraction of bridge CO continues to increase, I_{tot}/I_E rises, and at the highest H-coverage is a factor 1.1 ± 0.2 greater than at $\theta_H = 0$.

The nonmonotonic behavior of I_{tot}/I_E shows that coadsorbed H has a strong effect on the EELS cross section of edge bridge CO. Further evidence comes from the spectra for 0.13 ML of CO with θ_H between 0.23 and 0.40 ML; in this range of H coverage I_{tot}/I_E increases by more than a factor of two, while I_B/I_{tot} (and thus the bridge coverage) barely changes. There is other evidence that coadsorbates affect CO's cross section. Reflection-absorption IR spectra [1,21,26] of CO alone on Pt(335) suggest that the IR cross section of edge atop CO increases by about 20% with increasing CO coverage. Such an increase is qualitatively consistent with a prediction by Ueba [36]. Nevertheless it is unexpected that H could cause a factor two increase in the cross section of edge bridge CO, particularly since the interaction between H and CO is relatively weak. For example, H induces only a small shift in CO's vibrational frequency, and on stepped Pt the work function changes due to H and CO are comparable [37].

We have found that intensity ratios like those in Fig. 4-3 are reproducible. While measuring the spectra in Figs.4-2a and 4-2b we did not change the settings of the EELS system. Moreover, the spectrum at $\theta_H = 0.10$ ML in Fig. 4-2b was measured twice---both before *and after* that at 0.40 ML---and both ratios, of I_{tot}/I_E and I_E/I_{tot} , varied by less than 10%. This consistency reinforces our belief that the increase in I_{tot}/I_E on going from $\theta_H = 0.23$ to 0.40 ML is not an artifact. The similarity of the I_{tot}/I_E at high θ_H to the initial

intensity for *both* CO coverages lends further support. We consider it likely, therefore, that the enhancement of the edge bridge CO cross section by coadsorbed H is real.

3.2 Coadsorption of H and CO on the terrace

Previous comparisons between adsorbates on Pt(335) and Pt(112) have shown that a difference of one row in terrace width has a profound effect [1,21,25,38,39]. It is therefore of interest to examine the coadsorption of H and CO on the terrace. It is difficult to isolate the properties of terrace CO because ordinarily edge CO is also present [1,21,25,26]. One approach to avoid edge CO is to block the edge sites with a different species [40].

In the present experiment, we use H to block the edge sites. We first saturate the step edge with 0.25 ML of H, dose with CO, and then add more H. The entire experiment is done at 90 K to prevent terrace CO from exchanging with H at the step edge. The H coverages were determined by repeating the dosing sequence and measuring TPD spectra in a separate experiment. The CO coverages were 0.05, 0.13 and 0.19 ML.

An IR experiment performed on the same crystal in a separate chamber demonstrates that this procedure gives terrace CO without edge CO---and in particular that CO does not exchange with edge H at this temperature. When the sample was predosed with 0.6 ML of H and then exposed to CO, the IR spectrum shows a peak at the frequency characteristic of terrace CO, and none at the frequency of edge CO. These results will be presented in the next Chapter and reported in a separate publication[41].

Our EELS and TPD measurements, with no H added after the CO dose, confirm that the CO is predominantly on the terrace, and also provide evidence that its behavior with the edge saturated with H is essentially the same as with CO on the edge. Figure 4-4 shows EEL spectra as a function of θ_{CO} , after predosing with 0.25 ML of H. Figure 4-5 shows $I_{\text{P}}/I_{\text{tot}}$ vs θ_{CO} , together with the bridge CO coverage calculated assuming the atop CO cross section is a factor 1.8 that of bridge CO, as on Pt(111) [33]. The bridge CO coverage < 0.03 ML for θ_{CO} up to 0.16 ML, and then increases almost linearly after that.

This behavior is essentially identical to that reported for terrace bridge CO on Pt(335) by Luo *et al.* (cf. Fig. 3 of Ref. 25), with the CO coverages offset by about 0.2 ML--- approximately the edge site coverage. We find from TPD that the saturation coverage of our postdosed CO is 0.36 ML, in agreement with the saturation coverage of terrace CO on the clean surface, 0.38 ML. Finally, our measured I_B/I_{tot} agrees with Ref. 25 if we make some reasonable assumptions: without H all edge CO is at atop sites [25], and the EELS cross section of terrace atop CO is 0.5 that of edge atop CO [41] and 1.8 that of terrace bridge CO [33].

Finally, as we show below, postdosed CO responds differently to additional H than does edge CO, providing further confirmation that at 90 K predosed H effectively blocks CO adsorption at edge sites.

Figure 4-6 shows EEL spectra of 0.05 ML of CO on the terrace and various amounts of postdosed H; our spectra (not shown) with $\theta_{CO} = 0.13$ and 0.19 ML on the terrace are similar. As θ_H on the terrace is increased the EEL spectra show only a slight shift of intensity from the atop to the bridge band with the first H postdose. The observed I_B/I_{tot} vs θ_H is plotted in Fig. 4-7 for all three θ_{CO} , and should be contrasted with the comparable data for edge CO in Fig. 4-3a. The small initial shift with 0.05 ML CO is consistent with a small amount of CO at the edge. Other than that, the total intensity, band frequencies, and line shapes are all independent of θ_H . In essence coadsorbed H on the terrace has *no observable effect* on the vibrational spectrum of terrace CO, in dramatic contrast to the site shift and intensity enhancement observed on the step edge.

The coadsorption behavior on the terrace is also very different from that seen on Pt(111), where compact islands containing pure CO are formed [17,42,43]. With 0.23 ML CO on Pt(111), dosing with H to saturation changes the single-loss EELS intensities for atop and bridge CO by factors of < 0.5 and > 2 , respectively; the peak shapes change significantly; and the vibrational frequencies of both atop and bridge CO shift $> 20 \text{ cm}^{-1}$ [17].

Figure 4-8 shows TPD spectra of a saturation coverage of H desorbing from Pt(335) with varying amounts of CO and 0.48 ML H on clean surface. As the sample temperature is increased the CO becomes mobile and replaces H at the edge sites. If there is enough CO to fill all the edge sites then no H desorption from edge sites is observed. Note that the peak desorption temperature of terrace H increases from 272 to 300 K as θ_{CO} increases from 0 to 0.19 ML. About 2/3 of this increase comes as θ_{CO} increases from 0 to 0.05 ML. Meanwhile, the bottom two spectra have similar H coverage but different CO coverage, 0.19 ML and 0 ML, yet there is no difference in terrace H desorption temperature.

In comparison, for CO and H on Pt(111), Peebles *et al.*[44] found that with 0.23 ML of CO and a saturation coverage of H, the peak desorption temperature was 260 K. Without CO it was 290 K. CO shifts the H desorption temperature down by 30 K. This is strong evidence for a repulsive interaction between coadsorbed H and CO, and is in sharp contrast with what happens on the terraces of Pt(335). The H₂ TPD data suggest that the interaction between coadsorbed terrace CO and H is very weak, in agreement with the EELS observation.

The difference in TPD data for CO and H on the two surfaces suggests that CO and H are not segregated on Pt(335) terraces as they are on Pt(111). The insensitivity of terrace CO vibrations on Pt(335) to coadsorbed H appears to support this. Our EELS data are similar in some respects to what is seen for atop CO on the edge. With all the CO on the edge, an increase in θ_{H} incorporates more CO in the mixed islands, and converts that CO from atop to bridge sites, *but the remaining CO is unaffected*. In particular, even though the H-CO interaction is repulsive, coadsorbed H on the edge does not compress the remaining atop CO. Similarly, on the terrace, coadsorbed H does not affect the local CO density; see the data for 0.19 ML of CO in Fig. 4-7. If H and CO were to segregate as they do on Pt(111), the local CO density at saturation θ_{H} would be 0.6 CO/Pt. But a comparison of $I_{\text{B}}/I_{\text{tot}}$ from Fig. 4-7 with Fig. 4-5 shows that the local CO density < 0.22

CO/Pt. On the other hand, if the two species were to mix uniformly on an infinite Pt(111) surface, at saturation θ_H each CO would have two nearest-neighbor sites occupied by H, two occupied by CO and two empty; in the mixed phase on the step edge, where both of the nearest-neighbor sites are occupied by H, complete conversion of atop to bridge is observed. It is surprising that a comparable H density on the terrace produces no discernible effect.

One explanation for our data is that the H added to the terrace goes to a subsurface location. This has previously been suggested to explain certain experiments involving H on Pt(111) [45,46] although that interpretation is not generally accepted [47,48]. There is also evidence that H on Pt(110) goes to a subsurface site associated with step troughs [49]. Some electrochemical experiments with H on Pt have also been explained with subsurface H [50,51]. In particular, a spectroelectrochemical study [19,20] of CO and H on Pt(335) found that CO's vibrational frequency is independent of electrode potential in the potential range where H adsorption occurs. However, our H₂ TPD spectra do not have an extra peak above the desorption temperature of edge H, as is seen on Pd(110) where there clearly is subsurface H [52].

A second interpretation for our data is that the H on the terrace has no effect on the CO on the terrace, even though they are fully mixed. This interpretation calls for an explanation of the apparent weakness of the H-CO interaction on the terrace. Also, since the terrace sites on Pt(335) are close-packed, H and CO would not be expected to form a mixed phase [15].

A third explanation is that H occupies sites on the surface that do not significantly affect the CO observed in the IR spectrum. For example, the CO could build up from the outside edge of the step while the H builds up from the trough. The finite step size would tend to leave voids in the CO pattern on the side of the step near the trough where extra H could be accommodated. Also, screening is expected to diminish the contribution to the IR spectrum of CO at sites down in the trough. An electrostatic model, presented in the

next Chapter [41], that successfully explains the enhanced relative IR cross section of CO at edge sites predicts that CO at the three atomic rows on the terrace have relative IR cross sections of 1.0, 0.57 and 0.03, respectively, as one moves away from the step edge toward the trough.

In our experiment, since the sample could not be annealed above 90K, the layer may not have equilibrated completely. Luo *et al.* [25] found that annealing was necessary to equilibrate the atop/bridge ratio for pure CO on Pt(335) at coverages where there was substantial terrace site occupation, but they speculated that rearrangement of edge CO at high coverage was the major barrier. Moreover, the coadsorption experiments on Pt(111), which showed segregation of H and CO, were performed at 100 K. This shows that H and CO are mobile enough on the flat surface to rearrange at that temperature.

4. Summary

We have studied the coadsorption of H and CO on both the edge and the terrace of Pt(335). For edge CO, we found that coadsorbed H continuously shifts CO from atop to bridge sites, confirming the model presented in Chapter 3, proposed by Wang *et al.*[1]. The site shift permits a direct comparison between the EELS cross sections of edge bridge and edge atop CO. The cross section of edge bridge CO in the presence of saturation H coverage is a factor 1.1 ± 0.1 that of edge atop CO without H; on Pt(111), the cross section of atop CO is a factor 1.8 that of bridge CO [33]. Coadsorbed H apparently has a large effect on the cross section of edge bridge CO.

We studied terrace CO by first saturating the step edges with H at 90 K. The EEL spectrum of terrace CO is *not changed* by increasing θ_H , even to saturation. This behavior is different from the segregation found on Pt(111) [17,42,43]. Evidently the nature of the H-CO interaction on Pt surfaces is very sensitive to the local surface structure.

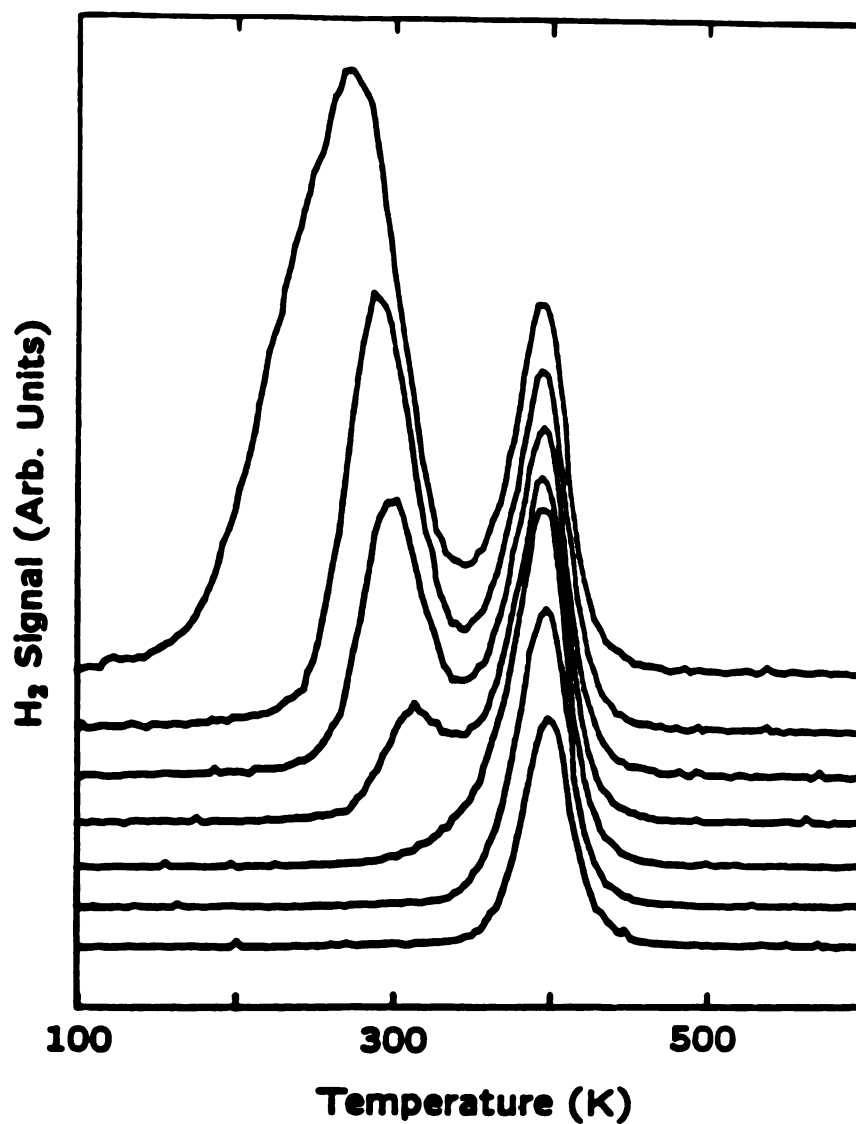


Figure 4-1. TPD spectra obtained by desorbing H₂ from the Pt(335) surface (without CO). From top to bottom, the relative dosages used to prepare the surface were 10, 5, 2.5, 1, 0.5, 0.25, and 0.1. The absolute dosages are uncertain because a doser was used, but a relative dose of 1 is approximately 1×10^{-6} torr s.

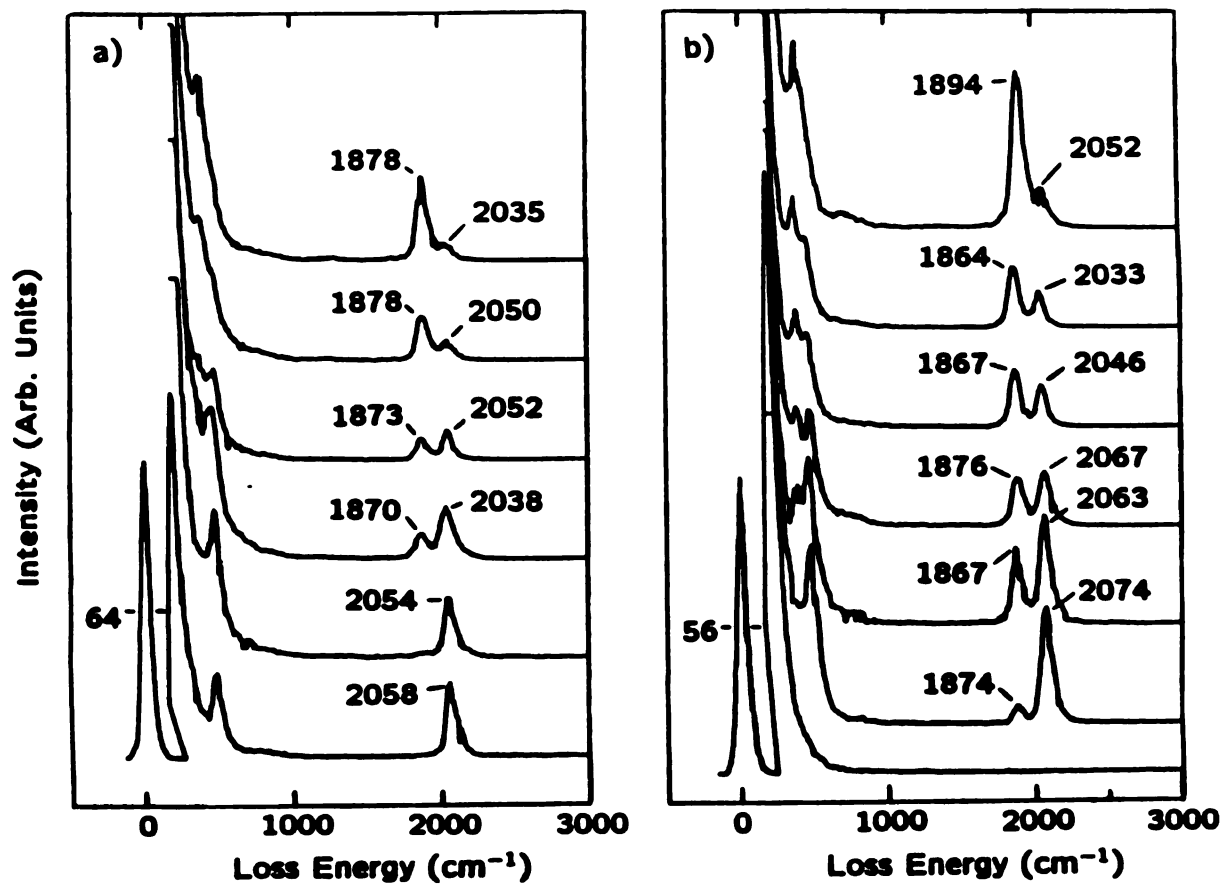


Figure 4-2. EEL spectra of edge CO on Pt(335) as a function of H coverage. The CO coverages in (a) and (b) are 0.07 and 0.13 ML, respectively. The spectra are arranged so H coverage increases up the page. In (a) the H coverages are 0.02, 0.10, 0.14, 0.18, 0.22, and 0.24 ML; in (b) 0 ($\theta_{\text{CO}} = 0$ also), 0.01, 0.06, 0.10, 0.13, 0.22, and 0.40 ML.

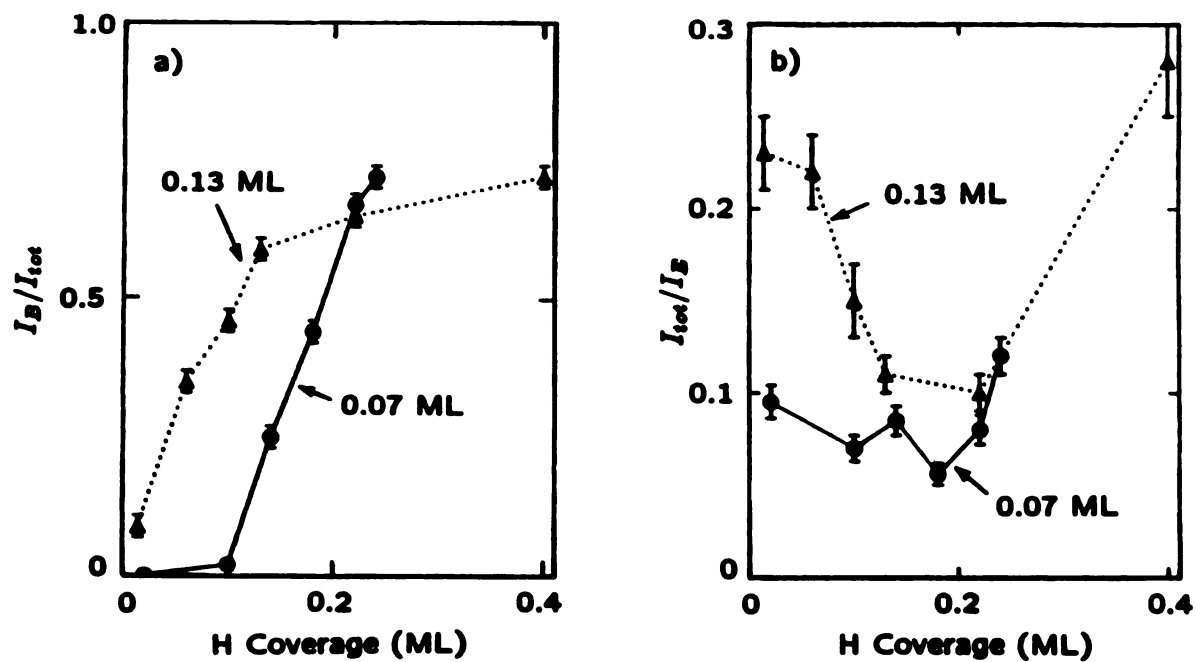


Figure 4-3. (a) Ratio I_B/I_{tot} of bridge to total (bridge +atop) single-loss EELS intensity as a function of H coverage, for the spectra in Fig. 4-2. (b) Ratio I_B/I_E where I_E is the elastic EELS intensity, as a function of H coverage, for the spectra in Fig. 4-2.

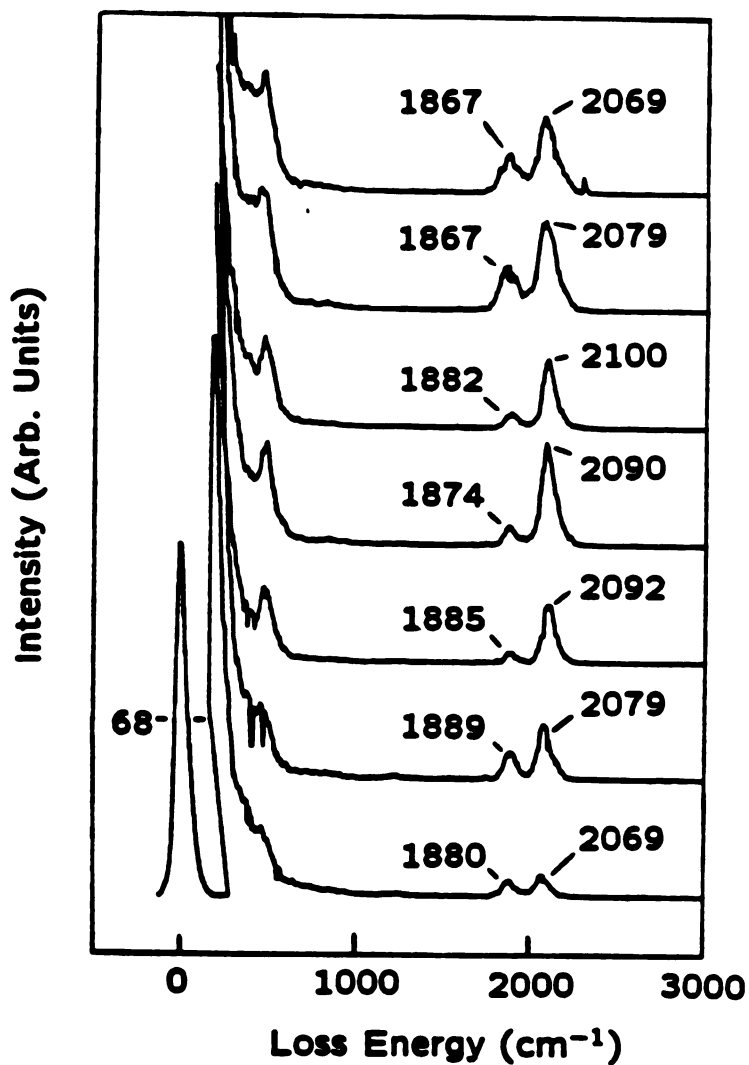


Figure 4-4. EEL spectra at various CO coverages after predosing with 0.25 ML H to block the edge sites. The spectra are arranged so CO coverage increases up the page: $\theta_{\text{CO}} = 0.05, 0.08, 0.13, 0.19, 0.28, \text{ and } 0.36 \text{ ML}$.

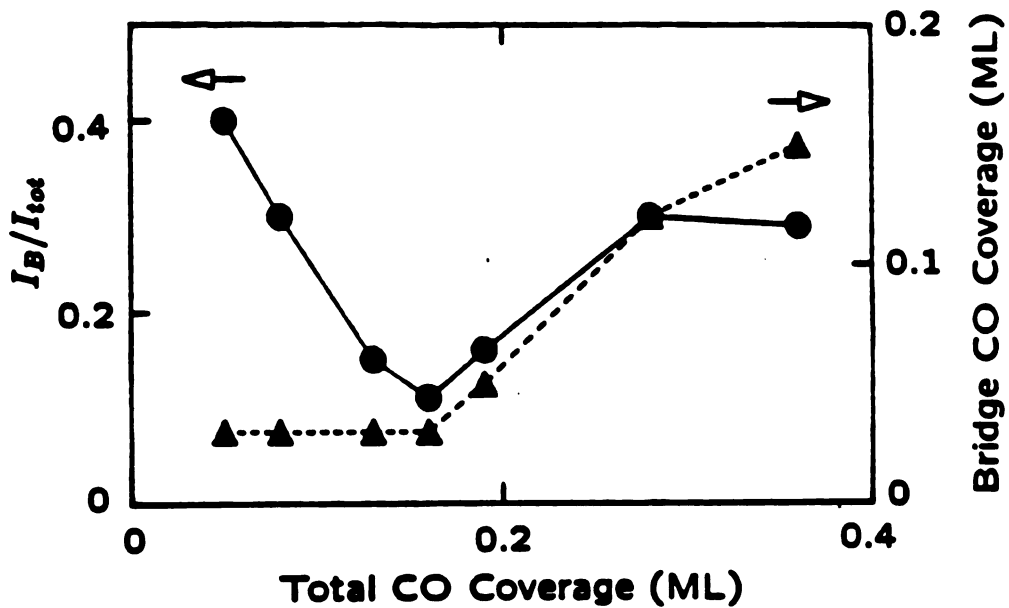


Figure 4-5. Ratio I_B/I_{tot} as a function of CO coverage, for terrace CO, with the edge saturated with H (for the EEL spectra in Fig. 4-4). Also shown is the bridge CO coverage, calculated assuming that the EELS cross section of terrace atop CO is a factor 1.8 times that of terrace atop CO.

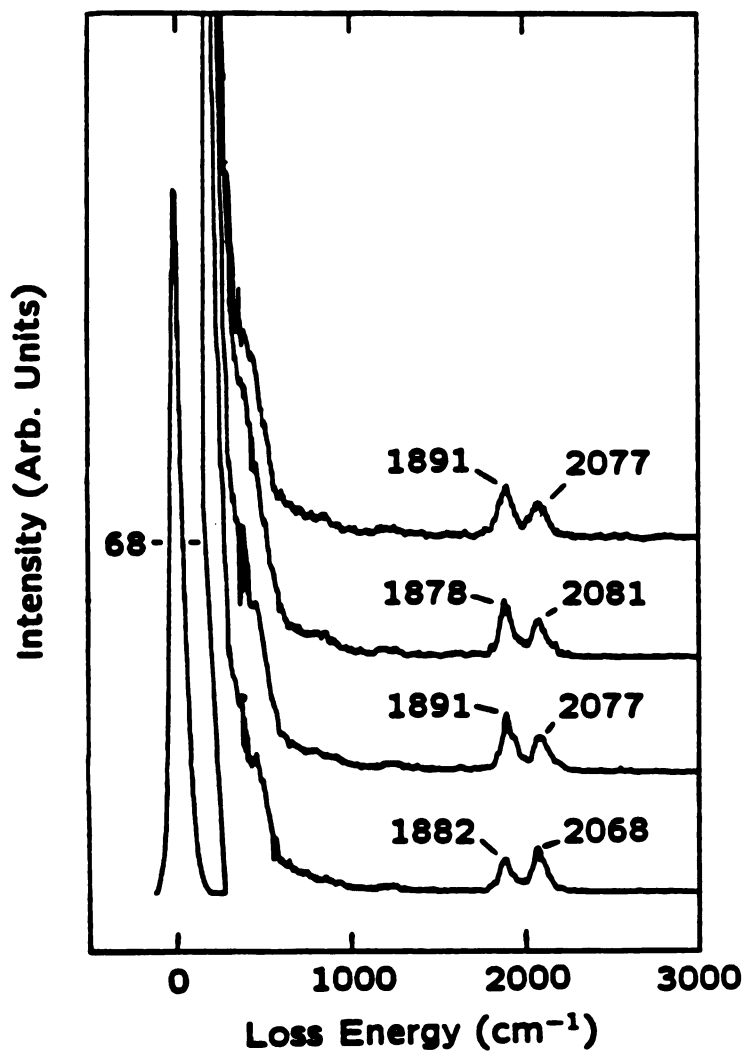


Figure 4-6. EEL spectra of 0.05 ML terrace CO as a function of postdosed H coverage.

The spectra are arranged so θ_H increases up the page: $\theta_H = 0.24, 0.46, 0.70,$ and 0.70ML .

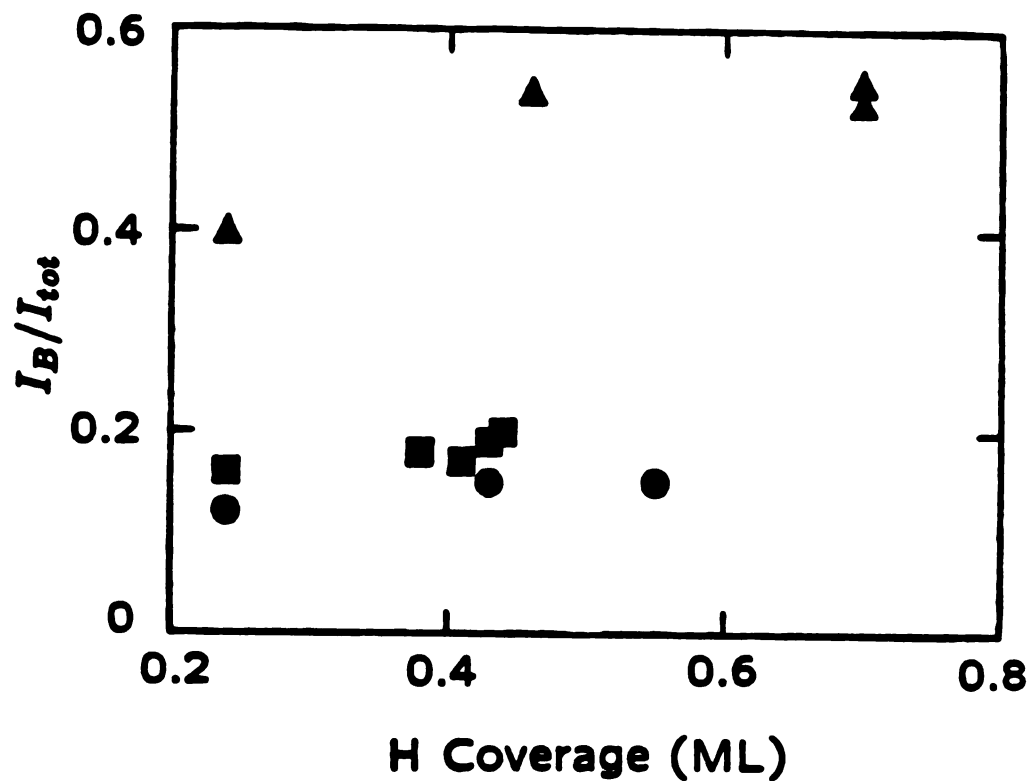


Figure 4-7. Ratio I_B/I_{tot} from EELS intensity for terrace CO, as a function of H coverage, for three CO coverages: Δ 0.05 ML, \bullet 0.13 ML, and \blacksquare 0.19 ML.

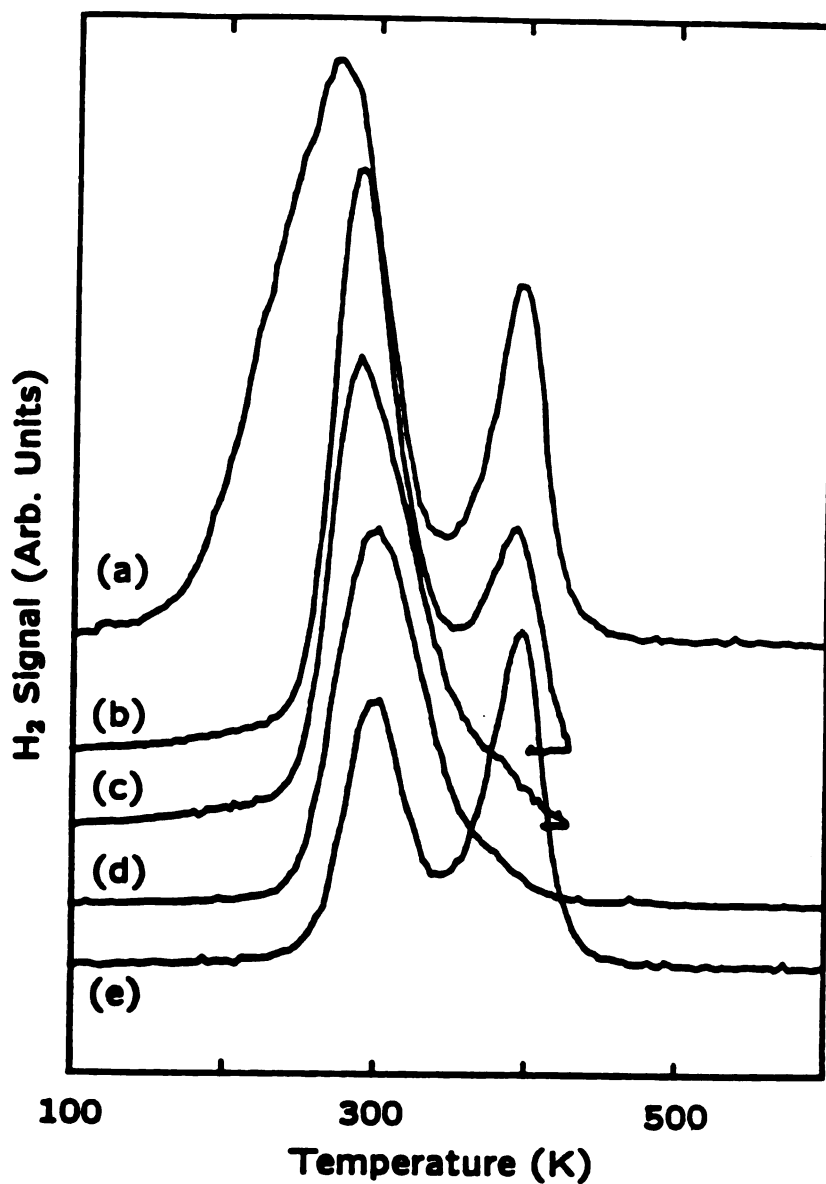


Figure 4-8. TPD spectra obtained by desorbing a saturation coverage H₂ from the Pt(335) surface and by desorbing 0.48 ML of H on clean surface. In (a) $\theta_{\text{CO}} = 0$ ML, $\theta_{\text{H}} = 1.0$ ML; in (b) $\theta_{\text{CO}} = 0.05$ ML, $\theta_{\text{H}} = 0.69$ ML; in (c) $\theta_{\text{CO}} = 0.13$ ML, $\theta_{\text{H}} = 0.55$ ML; and in (d) $\theta_{\text{CO}} = 0.19$ ML, $\theta_{\text{H}} = 0.45$ ML; (e) $\theta_{\text{CO}} = 0$ ML, $\theta_{\text{H}} = 0.48$ ML.

References

1. H. Wang, R. G. Tobin, and D. K. Lambert, *J. Chem. Phys.* **101**, 4277(1994).
2. M. Nagoshi and Y. Fukuda, *Appl. Surf. Sci.* **60/61**, 688(1992).
3. C. Becker, U. Schröder, G. R. Castro, U. Schneider, H. Busse, R. Linke, and K. Wandelt, *Surf. Sci.* **307–309**, 412(1994).
4. P. B. Merrill and R. J. Madix, *Surf. Sci.* **271**, 81(1992).
5. T. S. Marinova and D. V. Chakarov, *Surf. Sci.* **217**, 65(1989).
6. G. E. Mitchell, J. L. Gland, and J. M. White, *Surf. Sci.* **131**, 167(1983).
7. L. Westerlund, L. Jönsson, and S. Andersson, *Surf. Sci.* **199**, 109(1988).
8. C. Nyberg, L. Westerlund, L. Jönsson, and S. Andersson, *J. Electron Spectrosc. Relat. Phenom.* **54/55**, 639(1990).
9. N. D. S. Canning and M. A. Chesters, *Surf. Sci.* **175**, L811(1986).
10. J. Bauhofer, M. Hock, and J. Küppers, *J. Electron Spectrosc. Relat. Phenom.* **44**, 55(1987).
11. C. Nyberg and L. Westerlund, *Surf. Sci.* **256**, 9(1991).
12. C. Nyberg and L. Westerlund, *Chem. Phys. Lett.* **185**, 445(1991).
13. L. J. Richter, B. A. Gurney, and W. Ho, *J. Chem. Phys.* **86**, 477(1987).
14. L. J. Richter, T. A. Germer, and W. Ho, *Surf. Sci.* **195**, L182(1988).
15. J. M. White and S. Akhter, *CRC Crit. Rev. Solid State Mater. Sci.* **14**, 131(1988).
16. E. Hahn, A. Ficke, H. Röder, and K. Kern, *Surf. Sci.* **297**, 19(1993).
17. D. Hoge, M. Tüshaus, and A. M. Bradshaw, *Surf. Sci.* **207**, L935(1988).
18. For reviews of this work see K. Ashley and S. Pons, *Chem. Rev.* **88**, 673(1988); M. J. Weaver, *Appl. Surf. Sci.* **67**, 147(1993); and H. Seki, *IBM J. Res. Dev.* **37**, 227(1993).
19. C. S. Kim, W. J. Tornquist, and C. Korzeniewski, *J. Phys. Chem.* **97**, 6484(1993).
20. C. S. Kim, C. Korzeniewski, and W. J. Tornquist, *J. Chem. Phys.* **100**, 628(1994).
21. D. K. Lambert and R. G. Tobin, *Surf. Sci.* **232**, 149(1990).

22. K. Christmann and G. Ertl, *Surf. Sci.* **60**, 365(1976).
23. K. Christmann, G. Ertl, and T. Pignet, *Surf. Sci.* **54**, 365(1976).
24. B. A. Sexton, *J. Vac. Sci. Technol.* **16**, 1033(1979).
25. J. S. Luo, R. G. Tobin, D. K. Lambert, G. B. Fisher, and C. L. DiMaggio, *Surf. Sci.* **274**, 53(1992).
26. B. E. Hayden, K. Kretzschmar, A. M. Bradshaw, and R. G. Greenler, *Surf. Sci.* **149**, 394(1985).
27. G. Ertl, M. Neumann, and K. M. Streit, *Surf. Sci.* **64**, 393(1977).
28. D. W. Goodman, J. T. Yates, Jr., and T. E. Madey, *Surf. Sci.* **93**, L135(1980).
29. J. G. Love, S. Haq, and D. A. King, *J. Chem. Phys.* **97**, 8789(1992).
30. S. Haq, J. G. Love, and D. A. King, *Surf. Sci.* **275**, 170(1992).
31. M. L. Burke and R. J. Madix, *J. Am. Chem. Soc.* **113**, 1475(1991).
32. K. A. Thrush and J. M. White, *Appl. Surf. Sci.* **24**, 108(1985).
33. W. D. Miehler, L. J. Whitman, and W. Ho, *J. Chem. Phys.* **91**, 3228(1989).
34. J. E. Reutt-Robey, D. J. Doren, Y. J. Chabal, and S. B. Christman, *J. Chem. Phys.* **93**, 9113 (1990).
35. R. G. Greenler, J. A. Dudek, and D. E. Beck, *Surf. Sci.* **145**, L453(1984).
36. H. Ueba, *Surf. Sci.* **188**, 421(1987).
37. D. M. Collins and W. E. Spicer, *Surf. Sci.* **69**, 114(1977).
38. M. A. Henderson and J. T. Yates, Jr., *Surf. Sci.* **268**, 189(1992).
39. J. Xu, P. Henriksen, and J. T. Yates, Jr., *J. Chem. Phys.* **97**, 5250(1992).
40. A. Szabó, M. A. Henderson, and J. T. Yates, Jr., *J. Chem. Phys.* **96**, 6191(1992).
41. H. Wang, R. G. Tobin, D. K. Lambert, G. B. Fisher, and C. L. DiMaggio, unpublished.
42. S. L. Bernasek, K. Lenz, B. Poelsema, and G. Comsa, *Surf. Sci.* **183**, L319(1987).
43. K. Lenz, B. Poelsema, S. L. Bernasek, and G. Comsa, *Surf. Sci.* **189/190**, 431(1987).

44. D. E. Peebles, J. R. Creighton, D. N. Belton, and J. M. White, *J. Catal.* **80**, 482(1983).
45. W. Eberhardt, F. Greuter, and E. W. Plummer, *Phys. Rev. Lett.* **46**, 1085(1981).
46. C. M. Greenlief, S. Akhter, and J. M. White, *J. Phys. Chem.* **90**, 4080(1986).
47. P. R. Norton, J. A. Davies, and T. E. Jackman, *Surf. Sci.* **121**, 103(1982).
48. K. Christmann, *Surf. Sci. Rep.* **9**, 1(1988).
49. E. Kirsten, G. Parschau, W. Stocker, and K. H. Rieder, *Surf. Sci.* **231**, L183(1990).
50. A. Wieckowski, P. Zelenay, and K. Varga, *J. Chem. Phys.* **88**, 1247(1991).
51. I. M. Tidswell, N. M. Markovic, and P. N. Ross, *Phys. Rev. Lett.* **71**, 1601(1993).
52. R. J. Behm, V. Penka, M.-G. Cattania, K. Christmann, and G. Ertl, *J. Chem. Phys.* **78**, 7486 (1983).
53. H. Wang, R. G. Tobin, D. K. Lambert, G. B. Fisher, and C. L. DiMaggio, submitted to *Surf. Sci.*

*Chapter 5***Vibrational Intensity and Stark Tuning Rate of Edge and Terrace CO on Pt(335)**

This Chapter is largely based on a investigation that will be submitted to the Journal of Chemical Physics [26].

1. Introduction

Steps and other surface defects are important in heterogeneous catalysis at metal surfaces. A surface with defects has a wider variety of sites — some more exposed to the vacuum and some more tightly coupled to the metal — than does an atomically flat surface. Screening of an external electric field is one measure of site diversity. In this study we compare the vibrations of atop bonded CO at sites on the step edges and on the flat terraces of stepped Pt and try to explain our observations in terms of the electric field.

As shown in Fig. 1-1, the surface we use is Pt(335): Pt(S)[4(111)×(100)] in step-terrace notation. We compare the vibrational intensity of atop-bonded CO at step edge and terrace sites using reflection-absorption infrared spectroscopy (RAIRS) and high-resolution electron energy loss spectroscopy (HREELS). We also compare the Stark tuning rates (the change of vibrational frequency in an electrostatic field) of CO at the two sites, using electroreflectance vibrational spectroscopy (EVS). We manipulate the CO so it is either all on the edge or all on the terrace using coadsorbed H or O. This allows us to compare CO at the two sites with total CO coverage θ_{CO} held constant.

To get CO on the terrace, the surface is first dosed at low temperature (near 100 K) with enough O or H to fill the edge sites. If the H-predosed surface is later heated to 420 K the H desorbs and the CO moves to edge sites. Heating the O-predosed surface to 260 K causes the O to move to the terrace while the CO moves to the edge. Our use of

coadsorbed O to manipulate CO's site occupancy on stepped Pt follows Szabó *et al.* [1] Also, Hahn *et al.*[2] have used H on stepped Pt to prevent CO adsorption.

Previous experiments have also investigated the difference in vibrational cross section between edge and terrace CO. One approach has been to rely on the natural sequence of site filling as CO coverage builds up on the surface. At low coverage, CO preferentially occupies sites on the edge. At higher coverage it increasingly occupies terrace sites [3,4,5] In an earlier RAIRS study of CO on Pt(335), Hayden *et al.*[3] found that the rate of increase of integrated intensity with θ_{CO} at high coverage is 2.7 times higher than at low coverage. Greenler *et al* [6] estimated the *E*-field distribution on the same surface and found that at the center of the C=O bond the field at an edge site is 1.5 times greater than the average for the terrace sites, corresponding to a factor of 2.2 difference in IR cross-section. On the other hand, Lambert and Tobin found the cross-sections of edge and terrace CO to be nearly the same, and roughly equal to that of CO on Pt(111) [4]. Both of these analyses involve uncertainties, however. First, the terrace CO is not studied in isolation, since edge CO is always present, and the two vibrational bands are strongly dipole-coupled [3,4,6-8]. Moreover, both analyses assumed that all CO was on atop sites; it has now been established [5] that there is a substantial and coverage-dependent population of bridge-bonded CO. Inclusion of bridge CO in the analysis would tend to reduce the cross section ratio below the value of 2.7 found by Hayden *et al.*

A beautiful experiment of Reutt-Robey *et al.* [9,10] is not subject to these limitations. Using time-resolved IR spectroscopy and a pulsed molecular beam, they studied CO diffusion from the terrace to the step edges of Pt(S)[28(111)×(110)]. They found the cross-sections of edge and terrace atop CO to be equal within 5%.

Measurements of the Stark tuning rate also permit a straightforward interpretation, since they involve the ratio of an electroreflectance spectrum to an RAIR spectrum [11,12] and so do not require that the coverage be known. The Stark tuning rate of CO on Pt(111) was measured by Luo *et al.*[13], that of edge CO on Pt(335) was measured by

Lambert and Tobin [4] and by Wang *et al.* [14] Between Pt(111) and Pt(335), the estimated values differ by only 15% in the dilute limit, and are equal within experimental error. The calculation of Greenler *et al.* [6] would predict a 30% difference. On the other hand, Lambert and Tobin [4] found the Stark tuning rate of terrace atop CO on Pt(335) to be at least eight times smaller than that of edge CO, while an electrochemical study by Kim *et al.* [15,16] found a ratio of only 2.4.

2. Experiment

Details of the spectroscopy techniques and sample preparation procedures are given in Chapter 2 and elsewhere [11,14,17,18]. We used a single lead-salt diode laser, with a spectral range of 1947 to 2022 cm^{-1} , as the IR source for both RAIRS and EVS. The IR study used $^{13}\text{C}^{18}\text{O}$. This allowed atop CO to be seen with the laser, but not bridge CO. Since the present experiment is only concerned with ratios of Stark tuning rates, the normal measurement procedure [11] was simplified. Consequently, the EVS spectra we display have arbitrary, but consistent units. The HREEL spectra went from 300 to 5000 cm^{-1} with 60-70 cm^{-1} resolution. All of our measurements were repeated several times and were reproducible.

All spectroscopic measurements occurred with sample temperature 95 – 105 K. In the IR experiments, CO and H₂ were dosed by background filling while oxygen was dosed by an effusive doser placed one sample diameter away from the sample. The doser enhanced the effective pressure at the sample by a factor of about 20. In the HREELS experiments, each gas was dosed through an individual doser, with enhancement factors of about 100 over background dosing. The H and CO coverages were determined by temperature-programmed desorption (TPD). For CO the saturation coverage was assumed [4] to be 0.63 monolayer (ML); for H it was assumed [14] to be 1 ML (Here, one ML corresponds to one adsorbate per surface Pt atom.) Our TPD results for all three adsorbates are in agreement with previous measurements on stepped Pt [1,3,4,5,18,19]. The CO coverage was kept below 0.2 ML to avoid populating terrace sites [5]. The O₂

dosage was chosen to just saturate the edge sites (as seen with TPD). On Pt(335), terrace and edge O exhibit TPD peaks near 750 and 850 K, respectively [18].

For the H coadsorption experiments, the surface was first dosed with H₂ near 100 K, (0.72 ML for the IR experiments; 0.25 ML for HREELS) and then with CO. Infrared (RAIR and EV) or EEL spectra were next measured, and the sample was heated to 420 K. A TPD spectrum taken as the sample temperature was raised showed that this desorbed all the H, but 95% of the CO remained. After the sample cooled back to 100 K, one more set of IR or EEL spectra was acquired. Finally the sample was heated enough to desorb all the CO. During this desorption CO coverage was determined with TPD.

The procedure for the O coadsorption was similar. The initial O₂ dose was 0.1 L (1 L = 10⁻⁶ torr sec) and the sample temperature was 190 K. This saturated the edge sites with O and ensured that the O₂ all dissociated [18]. Next, 3.0 L of CO was dosed at 150 K, giving a CO coverage of 0.19 ML. This overlayer was studied. To get the CO to migrate to edge sites, the overlayer was annealed for five minutes at 260 K. On Pt(112) [1], terrace CO and edge O switch position at 230 K. On Pt(335) we observed a partial switch at 230 K but it was not complete until 260 K. On Pt(335), the switching procedure caused about 15% of the CO to react with O. As the switch took place, the CO₂ signal showed a minor peak at 180 K, with about 10% of the main peak's area, and some desorption at 260 K as a precursor to the main CO₂ desorption peak at 320 K.

3. Results

3.1. RAIRS and EVS

Figure 5-1 shows RAIR and EV spectra of 0.16 ML CO on a sample precovered with 0.72 ML of H, and again after heating to 420 K to desorb the H. Desorbing the H decreases the CO band's peak frequency ν and increases its intensity. With H, $\nu = 1995 \text{ cm}^{-1}$; after the H desorbs, $\nu = 1984 \text{ cm}^{-1}$. It is well established [3,4,14] that on Pt(335), for ¹³C¹⁸O on the edge, $1975 < \nu < 1985 \text{ cm}^{-1}$ and on the terrace $1987 < \nu$

$<2000\text{ cm}^{-1}$. We therefore attribute the frequency shift to the movement of CO from terrace to edge sites. Annealing increases the integrated area of the RAIRS band a factor of 1.6 ± 0.2 . Any loss of CO during annealing would *reduce* the intensity. We estimate that <0.003 ML of background $^{13}\text{C}^{18}\text{O}$ adsorbs during the annealing and cooling.

The EV spectra are proportional to $d(\Delta R/R)/d\nu$ where $\Delta R/R$ is the RAIRS signal and ν is the frequency. The Stark tuning rate ($d\nu/dE$) is proportional to the ratio of the integrated EV spectrum to the RAIR spectrum, and can be estimated by comparing either peak heights or integrated areas. The values given here are obtained from the average of the two methods. We find, from the data in Fig. 5-1, that desorbing the H and shifting the CO from terrace to edge sites increases the Stark tuning rate by a factor of 2.0 ± 0.2 .

Figure 5-2 shows RAIR and EV spectra for 0.19 ML CO adsorbed on a surface predosed with 0.1 L O_2 , before and after annealing at 260 K to move the CO to edge sites. As in the H-coadsorption experiment, annealing reduces ν from 2004 to 1986 cm^{-1} , and increases the intensity. Again, we attribute the shift to CO movement from terrace to edge sites. The unusually high terrace-CO frequency is explained by the effect that O on the step edge has on the work function, as discussed below. For the data in Fig. 5-2 we find that annealing increases the intensity is by a factor of 1.4 ± 0.2 and increases the Stark tuning rate by a factor of 2.0 ± 0.2 . The smaller intensity enhancement with O as opposed to H is attributable largely to loss of CO during annealing (see below).

3.2. HREELS

Figure 5-3 shows a set of EEL spectra (with $\theta_{\text{CO}}=0.05, 0.08, 0.13$ and 0.16 ML) on a Pt(335) surface precovered with 0.24 ML of H at 95 K. The spectra in Fig. 5-3a were taken before annealing, in Fig. 5-3b after annealing to 420 K to desorb the H. As with the IR spectra, H-desorption tends to decrease ν and increase the intensity of the atop CO band. For 0.05, 0.08, 0.13 and 0.16 ML, $\Delta\nu = 8, 0, 32,$ and 27 cm^{-1} , respectively. The apparent absence of a shift at 0.08 ML could be due to uncertainty in

identifying the peak position; the spectrum before annealing is noisier than most and the atop peak exhibits an unusual and probably spurious asymmetry. The spectra also show that H affects the intensity of the band due to bridge-bonded CO. We account for this as we estimate the change in atop CO's cross section.

3.3. Analysis of the atop intensity

Table II summarizes our experimental data. The intensity ratios are obtained by directly comparing the integrated intensity of the atop CO band before and after annealing. Of greater interest is the cross section ratio, which represents the ratio of integrated intensity *per CO* for edge CO compared to terrace CO. The two ratios differ because the amount of atop CO changes upon annealing. First, some CO is lost during the anneal; for the IR experiments we estimate this loss at 5% for H coadsorption and 15% for O coadsorption; for EELS the loss was less than 5%. Second, annealing causes CO to migrate from atop to bridge sites, and from terrace to edge sites. This effect is visible in the EEL spectra of Fig. 5-3.

To determine the relative populations of bridge and atop CO from the EEL spectra, we need the cross section ratio between atop and bridge CO. In Table II we give our best estimate for this quantity and its uncertainty (including both random and systematic error). For the IR experiments we use the bridge CO correction determined from the EELS data at $\theta_{\text{CO}} = 0.16$ ML.

Before annealing, the bridge CO is presumed to be on the H-saturated step edge — terrace bridge sites are not occupied at these coverages [5,18]. Previous EELS measurements have shown that the cross sections of edge bridge and edge atop CO are equal [18]. Any bridge CO on the terrace would, by analogy with Pt(111) [20], be expected to have an EELS cross section 1.8 times smaller than that of terrace atop CO. It is clear from TPD that all the CO *after* annealing is on the step edge, but without H, so

again the bridge CO cross section is between 1.0 and 1.8 times smaller than the atop CO cross section. Since the amount of bridge CO is relatively small, the value of the atop cross section ratio is rather insensitive to our assumption about the bridge CO cross section, as reflected in the uncertainties in Table II.

All the data in Table II show that the vibrational cross section of edge CO is larger than that of terrace CO. We estimate that the vibrational cross section of edge atop CO is 2.0 ± 0.2 times that of terrace atop CO.

The Stark tuning rate data in the last column of Table II are unaffected by loss of CO or migration between sites. To get (dv/dE) , a peak in the integrated electroreflectance spectrum is divided by a peak in the RAIR spectrum. Since both of these are proportional to the atop CO coverage, the coverage cancels out. We find that the Stark tuning rate of edge atop CO is also 2.0 ± 0.2 times that of terrace atop CO.

4. Discussion

We have developed an electrostatic screening model that explains much of our data. Before describing our model, we consider alternative explanations.

One possibility is that CO is chemically different at edge and terrace sites. A previous EELS experiment [21] that looked at the coverage dependence of overtone intensities was unable to find any chemical difference between edge and terrace CO.

Since coadsorbates are used to control CO's binding site, it is possible that the effects we observe are caused by a direct interaction of H or O with CO. Coadsorbed H and CO on Pt(335) has been studied with RAIRS, HREELS and TPD [14,18]. Edge CO is strongly affected by coadsorbed H. In the present work, however, the H is all gone when the CO is at edge sites. The vibrational properties of terrace CO are *completely insensitive* [18] to the presence of terrace H. The effect of edge H on terrace CO is also expected to be negligible. We believe that H desorption affects CO's vibrational intensity and Stark tuning rate primarily through the CO's change in adsorption sites.

We have less information about the effects of coadsorbed O, but the strong similarity we see between the effects of H and O is consistent with a shift of CO from terrace to edge sites also being the most important effect. As seen in Fig. 5-2a, coadsorbed O does cause an unusually high ν for terrace CO, but this is easily explained. It is well established [14] that a change in work function ϕ induces a proportional $\Delta\nu$ for CO, as discussed in Chapter 3, with a tuning rate $(d\nu/d\phi) = 34 \pm 4 \text{ cm}^{-1}/\text{eV}$. Collins and Spicer [22] found that filling the edge sites with O on Pt(S)[6(111) \times (100)] causes a 0.4 eV increase in ϕ , while saturating the terrace sites with O increases ϕ by about 0.1 eV, and filling the edge sites with CO increases ϕ by only 0.03 eV. With the step edge saturated with O, we would expect an O-induced $\Delta\nu$ of $+13 \text{ cm}^{-1}$ for the terrace CO. The observed $\Delta\nu$ is $10 \pm 2 \text{ cm}^{-1}$ (the estimated ν for no O takes θ_{CO} into account). After annealing, with O on terrace sites, the expected $\Delta\nu$ for the edge CO is only 3 cm^{-1} , the observed $\Delta\nu = 3 \pm 2 \text{ cm}^{-1}$.

Our electrostatic model is similar to a model for the Pt(335) surface described by Greenler *et al.* [6]. We know that the step height between (111) terraces is 2.26 Å. For CO on Pt(111) Ogletree *et al.* [23] used LEED to show that center of the CO bond is 2.43 Å outside the top layer of Pt atoms. However, the electrical surface is at the image plane, not at the outside layer of Pt atoms. On Pt(100), spectroscopic studies [24] of image potential-induced image states have shown that the image plane is 1.05 Å outside the outermost Pt atoms. This suggests that on Pt the center of the CO bond is approximately 1.38 Å outside the image plane. In our model we represent the stepped surface by an ideal conductor with sharp, perfectly rectangular steps. The electrostatic field is applied by an equipotential plane, parallel to the average (335) surface and 100 step-heights away. We consider the field component normal to the average surface plane. The field is evaluated at points along a line parallel to the terrace, and half a step height (1.13 Å) above it as shown in the inset in Fig. 5-4. The results are not strongly sensitive to the height assumed. Greenler *et al.* [6] studied the enhancement dependence on the height of

the center of the C=O bond to the image plane; from 0.9 to 1.23 Å, or from 1.23 to 1.4 Å, the result only changes by 5%. Our model ignores smoothing of the electron density, variation of the field over the spatial extent of the CO and possible tilts of the molecules. On the other hand, an explicit study found that CO does not tilt by more than 10° on Pt(335) [30]. Greenler *et al.* also considered the effects of tilting in their model. A tilting of 10° is only going to make a difference of 5%. The abrupt metal-vacuum interface and sharp step edge used in the model tend to overestimate the field enhancement near the edge.

Figure 5-4 shows the calculated magnitude of the electric field normal to the average surface plane as a function of distance from the step edge, for two surfaces, with ratios of terrace-width to step-height of 3.87 and 29.2, which simulate Pt(335) and the surface used by Reutt-Robey *et al.* [9,10], respectively. The field is normalized to the field on a flat surface, so a value smaller than 1 means screening, bigger than one means enhancement.

For the (335) surface, the field at the step edge is enhanced by 15% relative to the flat surface, while the field in the center of the terrace is suppressed by 12%; thus the effects of "lightning rod" enhancement at the edge and screening on the terrace are comparable. The field at the edge is 1.3 times larger than at the center of the terrace, in good agreement with the value of 1.31 found in Ref. 6. This difference in field between edge and terrace sites implies a factor of 1.5 – 2 difference in vibrational cross section, in good agreement with our observations. Also, a factor of 1.3 difference is expected between the IR cross sections of edge CO on Pt(335) and CO on Pt(111); this is consistent with the observation of Lambert and Tobin [4] that these two cross sections are roughly equal. Our field calculation also agrees with the observed difference (~15%) in Stark tuning rate between edge CO on Pt(335) [4,13], and CO on Pt(111) [12]. In the dilute limit these tuning rates were found to be $8.8 \pm 0.9 \text{ cm}^{-1}/(\text{V}/\text{Å})$ and $7.6 \pm 1.6 \text{ cm}^{-1}/(\text{V}/\text{Å})$, respectively.

For the surface with wide terraces, the calculated screening on the terrace is much smaller than it is for the (335) surface. At the height of a CO molecule, the field at the step edge and at the center of the terrace differ by 18%, which corresponds to 1.4 times difference in the cross section. Because the field at the step of this surface varies rapidly around the step edge, it is conceivable that if we round off the sharp step edge in our model, the enhancement will be reduced. It is possible that the field induced cross section on that surface is only 1.2, that is still bigger than the limit set by Reutt-Robey *et al.* Another possibility is that they have edge bridge CO that is not observed in their spectrum, but at the very low coverages they used, it is quite unlikely. Nevertheless, our calculation shows that the cross section difference between edge and terrace CO decreases with increasing terrace width.

The electrostatic model explains: (1) The enhancement of the IR and EEL cross sections, and the Stark tuning rate, of edge CO relative to terrace CO on Pt(335) (this work); (2) The small difference in cross section and Stark tuning rate between edge CO on Pt(335) and CO on Pt(111) [4,13,14]. The model also partly explains the lack of any significant cross section enhancement for edge CO on a surface with 28-atom-wide terraces [9,10]. The strong dependence of the cross section enhancement on terrace width is particularly strong evidence for an electrostatic mechanism, since a chemical mechanism would be expected to have shorter range.

Despite the model's success, not all of the Stark tuning rate results are explained. Our EVS data (see Figs. 5-1 and 5-2 and Table II) show that the Stark tuning rate of edge CO is a factor of 2 greater than that of terrace CO — a ratio as large as the enhancement of the IR intensity. The electrochemical experiments of Kim *et al.* [15,16] also indicate a tuning rate enhancement of at least a factor of 2; with aqueous electrolyte they found a tuning rate (with electrode potential) of 75-80 cm^{-1}/V at low coverage (edge CO) and 33 cm^{-1}/V at high coverage (both edge and terrace CO); in contrast, Ref. 25 shows that on Pt(111) at low CO coverage the tuning rate with aqueous electrolyte is 40-44 cm^{-1}/V .

(Discrepancies in absolute Stark tuning rate between electrochemical and vacuum studies are discussed in Refs. 13 and 14.)

Since the Stark shift of adsorbed molecules is linear in the applied field while the IR absorption is quadratic, a simple electrostatic model would predict that the tuning rate ratio should be equal to the square root of the cross section ratio, *i.e.* smaller, not equal as we find. Our results therefore suggest a difference in screening between the static and IR fields. Similar differences have been noted previously. Both Luo *et al.* [13] and Wang *et al.* [14] have presented evidence that the suppression of the Stark tuning rate by coadsorbates is significantly stronger than would be predicted from the suppression of the IR intensity due to dipole screening.

One possible explanation for the discrepancy in observed ratios lies in the fact that the local electric field varies strongly with position at a metal surface. The field used to calculate IR absorption or the Stark effect should actually be a weighted average over the molecule, perhaps including even nearby regions of the metal. The field is averaged in different ways for IR absorption and the Stark effect. Instead of interacting with the local field at the center of the C-O bond, the molecule interacts with the local field at the positions of the C and O nuclei. It has been shown theoretically that IR absorption really does depend on the local field at the nuclear positions *in the actual molecule*. [27,28] This makes sense since we are looking at molecular vibrations that occur as the nuclei move. The nuclei move because an electric field acts on the nuclear charge. Most theoretical treatments, however, consider the local field at the nuclear positions *with the molecule removed*. For the vibrational Stark effect, an argument that relates the field with the molecule removed to the molecule's response is given by Lambert [29]. Presumably the vibrational Stark effect could also be expressed in terms of the local field at the nuclei. As an extreme example, suppose that the local field at the C and O nuclei contribute equally, both for the vibrational Stark effect and for IR absorption. Then our data would be consistent with equal screening at all of the O sites and at the C site on the edge, but

complete screening at the C site on the terrace. Since screening, whether by a nearby step or by neighboring adsorbates, can affect not only the magnitude but also the spatial variation of the field, it is possible for screening to have different effects on these different properties, as we observe.

In order for C nucleus to be completely screened, it has to be inside the image plane. There are several ways to estimate the relative position of the C nucleus and the image position on Pt(111). For atop CO, a LEED study [23] found that the C-Pt bond length is 1.85 Å, and the C-O bond length is 1.15 Å.

The jellium edge on Pt(111) is 1.13 Å outside the topmost Pt layer. By linear extrapolation from Lang and Kohn's calculation [31] (for $r_s > 2$ a.u.) to 1.45 a.u., the radius of a Pt atom containing one valence electron, the image plane is 0.89 Å outside the jellium edge. So the C nucleus is 0.17 Å inside the image plane while the O nucleus is 0.98 Å outside the image plane. It is easily conceivable that the image plane will be closer to the metal at the step site. Screening of an external electric field at Al(100) [32] and Ag(100) [33] has been calculated by the surface embedding method. The screening charge is found lay on top of the surface atoms, which means the effective image plane position is lower in the open area of the surface. The difference on the flat Ag(100) surface is in 0.23 Å at 1.85 Å outside the topmost atom layer. Moreover, a calculation based on the surface states energies [24] have found that image plane moves closer to the metal by just going from (111) to (100) faces. The difference is in the order of 0.1 to 0.2 Å for Ni, Ag, and Au. So it is possible that at the step site, the C nucleus is just outside the image plane. That can explain our data for same enhancement ratio for both IR cross section and the Stark tuning rate.

On the other hand, there are several quite different estimates about the position of the image plane. One comes from fits of the standard model to RAIR spectra of CO on Pt(111). The fit is best if the center of the C=O bond is 1.1 Å outside the image plane, which means that the C nucleus is 0.52 Å outside the image plane. Ref. 24 gives that on

Pt(100) the image plane is 1.05 Å outside the topmost Pt atoms, while the distance should be larger on Pt(111) by about 0.1 to 0.2 Å. This means that the C nucleus is about 0.6 to 0.7 Å outside the image plane. If this is true, then there should be no big difference in the level of screening of the applied field at terrace or edge site at C nucleus other than what is calculated in our model.

We want to point out that even if the first estimation is true and the big difference in CO's Stark tuning rate at the two sites is caused by the change in C nuclei's relative position to the image plane, that still would not explain the different screening of IR and DC field on Pt(111) [13] and Pt(335) [14], because in those experiments all the CO stays in equivalent sites.

Finally we discuss an unresolved experimental discrepancy. The Stark tuning rate of terrace atop CO measured in this study, as well as in the electrochemical work of Kim *et al.* [15,16] is much larger than reported by Lambert and Tobin [4], who used the same apparatus and the same crystal as we did here. Figure 5-5 shows our RAIR and EV spectra for 0.26 ML CO on Pt(335). At a comparable coverage Lambert and Tobin's RAIR spectrum looked similar, with edge and terrace CO peaks of comparable intensity. Their EV spectrum, however, showed a strong EVS peak corresponding to edge CO, but *no* EVS signal from terrace CO. In fact they observed a small peak at the terrace CO vibrational frequency, where a zero-crossing would ordinarily be expected. They concluded that the Stark tuning rate of terrace CO is at least a factor of eight smaller than that of edge CO. Our EV spectrum shows EVS peaks of comparable size for both CO species, and we find only a factor of two difference in Stark tuning rates.

We have no firm explanation for this discrepancy. Both Lambert and Tobin's result and ours were reproduced many times. We investigated coadsorption with O and H, as well as C contamination, but were unable to reproduce Lambert and Tobin's results. We offer two observations: the sample was repolished between the two sets of experiments, and Lambert and Tobin observed Sn contamination — although the Sn

concentration was below the limit of Auger detection for their final experiments. We note that the EELS experiments of Luo *et al.* [21], which were aimed at explaining the large difference in Stark tuning rate between edge and terrace CO, were performed before the crystal was repolished.

5. Conclusion

We have compared the vibrational cross section and the Stark tuning rate for terrace and edge atop CO on Pt(335) using RAIRS, EVS and HREELS. The CO adsorption site was controlled by coadsorption of H and O. The cross section of edge atop CO is 2.0 ± 0.2 times greater than that of terrace atop CO and the ratio of the Stark tuning rates is also 2.0 ± 0.2 . The cross section ratio agrees semiquantitatively with a classical *E*-field calculation. The model is able to partly account for the much smaller difference in cross sections observed by Reutt-Robey *et al.* [9,10] on a Pt surface with much wider terraces. We conclude that there is little chemical difference between edge and terrace atop CO, and that the difference in *E*-field strength between edge and terrace sites largely accounts for the variation in vibrational intensity and Stark tuning rate.

The ratio of the Stark tuning rates at the two sites is larger than would be expected from a simple model and the observed ratio of IR intensities. This discrepancy is consistent with other experiments that have found a significant difference in the screening of static and IR fields [13,14]. It is possible that IR intensity and Stark tuning rate measurements are probing different aspects of the *E*-field distribution on the surface.

Our determination that the Stark tuning rate for terrace atop CO on Pt(335) is only two times smaller than that of edge atop CO is in agreement with an electrochemical study [15,16], but contradicts the previous experiments of Lambert and Tobin [4]. This difference remains unexplained, but suggests that the Stark tuning rate of terrace CO may be sensitive to surface preparation.

Table II. Ratios of vibrational intensity, vibrational cross section, and Stark tuning rate of edge atop CO compared to terrace atop CO. The intensity and Stark tuning rate ratios are determined directly from the experimental data. The cross section ratios include corrections for loss of CO during annealing and for migration between bridge and atop sites, as discussed in the text.

Experiment	Intensity ratio	Cross section ratio	Stark tuning rate ratio
IR — H coadsorption			
$\theta_{\text{CO}} = 0.16$	1.6 ± 0.2	2.1 ± 0.3	2.0 ± 0.2
IR — O coadsorption			
$\theta_{\text{CO}} = 0.19$	1.4 ± 0.2	2.0 ± 0.4	2.0 ± 0.2
HREELS — H coadsorption			
$\theta_{\text{CO}} = 0.05$	2.3	1.4 ± 0.4	
$\theta_{\text{CO}} = 0.08$	2.6	1.8 ± 0.4	
$\theta_{\text{CO}} = 0.13$	2.2	2.3 ± 0.3	
$\theta_{\text{CO}} = 0.16$	1.7	2.1 ± 0.2	
Average:		2.0 ± 0.2	2.0 ± 0.2

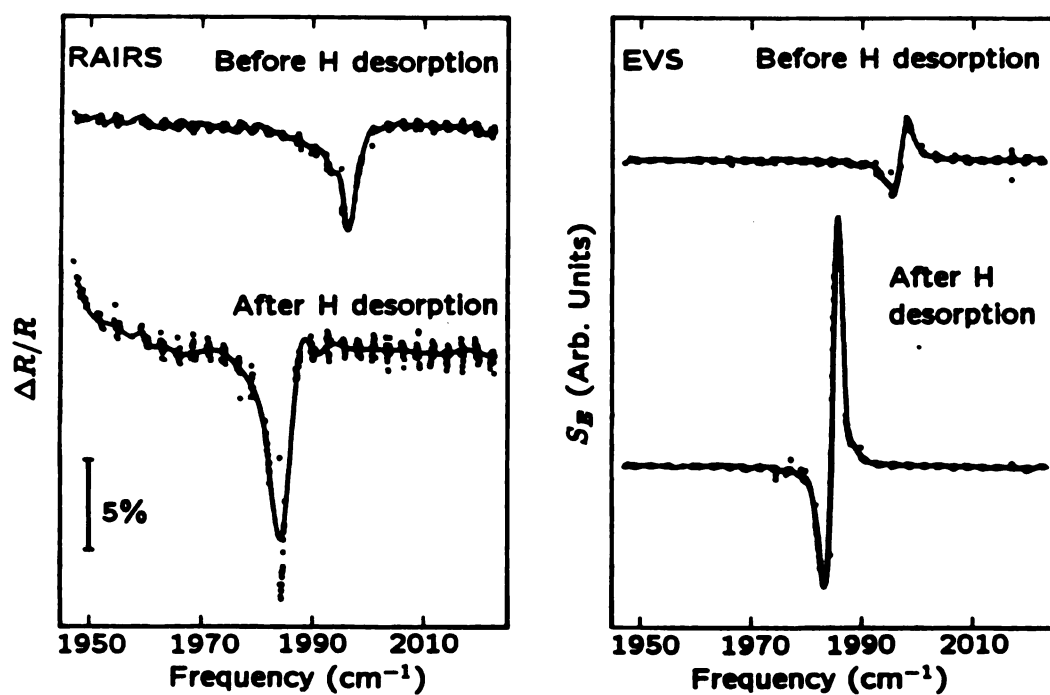


Figure 5-1. RAIR and EV spectra for 0.16 ML CO on a Pt(335) surface precovered with 0.72 ML of H, before and after annealing the sample at 420 K. Upon H desorption, the CO moves to edge sites.

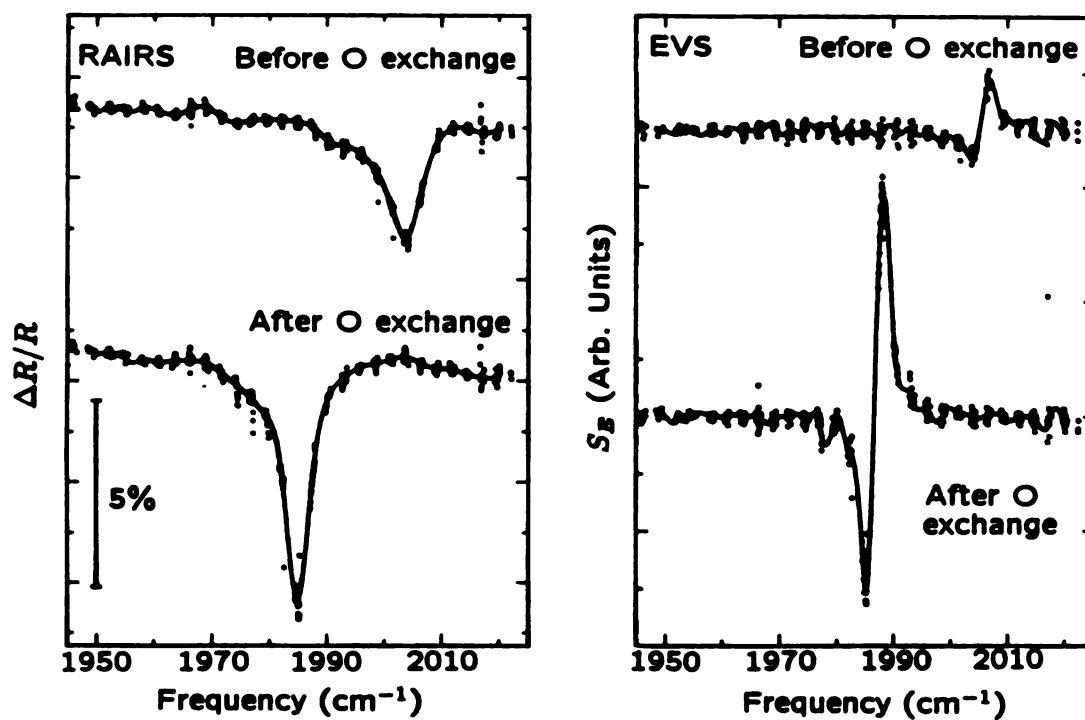


Figure 5-2. RAIR and EV spectra for 0.14 ML CO on a Pt(335) surface predosed with 0.1 L O_2 , before and after annealing the sample at 260 K. Upon annealing, the CO moves from terrace sites to edge sites, while the O moves to terrace sites.

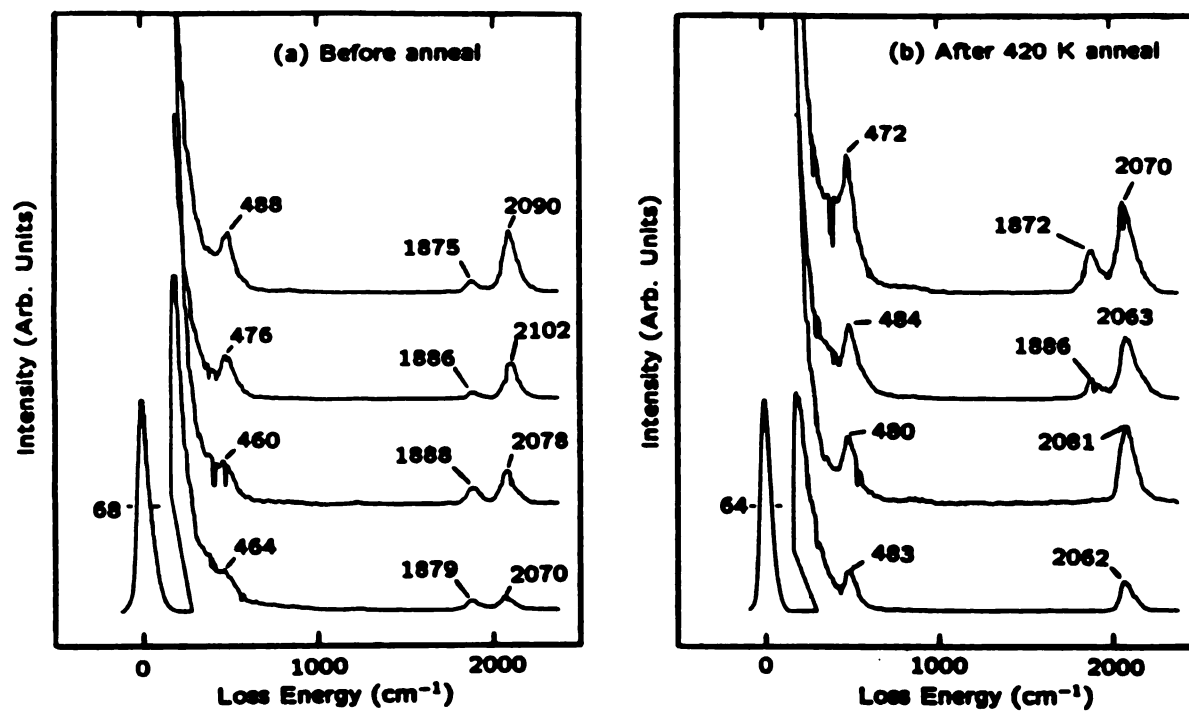


Figure 5-3. HREEL spectra for 0.16, 0.13, 0.08, 0.05 ML CO (from top to bottom) on a Pt(335) surface precovered with 0.25 ML of H, before and after annealing at 420 K.

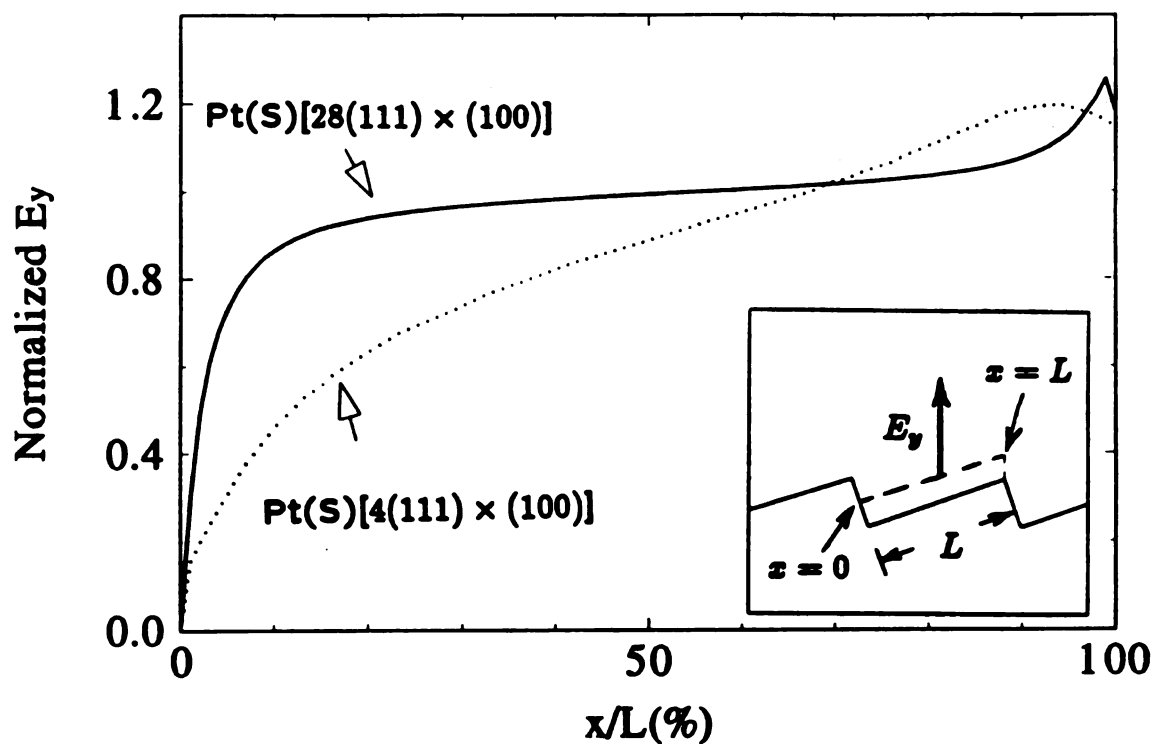


Figure 5-4. Calculated E field normal to the average surface plane, as a function of fractional distance across the terrace. The field is normalized to the field on a flat surface, and is calculated along a line one-half step height above the terrace, as shown in the inset. The dotted curve represents a surface with narrow terraces similar to Pt(335); the solid curve represents a surface with much wider terraces, similar to that used in Refs. 8 and 9.

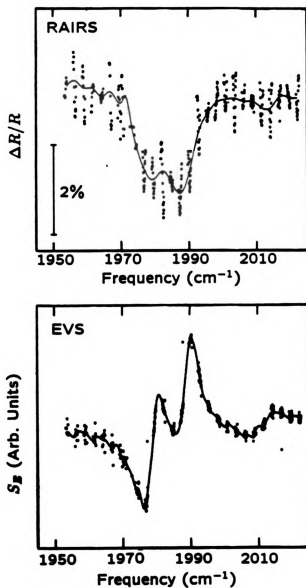


Figure 5-5. EV and RAIR spectrum for 3.5 L (0.26 ML) CO on clean surface. Strong EV features are seen corresponding to both of the peaks in the RAIR spectrum, indicating that edge and terrace CO have comparable Stark tuning rates. The zero-crossings in the EV spectrum occur at the same frequencies as the peaks in the RAIR spectrum. These results are in contrast to those reported in Ref. 4.

References

1. A. Szabó, M. A. Henderson, and J. T. Yates, Jr., *J. Chem. Phys.* **96**, 6191(1992).
2. E. Hahn, A. Fricke, H. Röder, and K. Kern, *Surf. Sci.* **297**, 19 (1993).
3. B. E. Hayden, K. Kretzschmar, A. M. Bradshaw, and R. G. Greenler, *Surf. Sci.* **149**, 394 (1985).
4. D. K. Lambert and R. G. Tobin, *Surf. Sci.* **232**, 149 (1990).
5. J. S. Luo, R. G. Tobin, D. K. Lambert, G. B. Fisher, C. L. DiMaggio, *Surf. Sci.* **274**, 53 (1992).
6. R. G. Greenler, J. A. Dudek, and D. E. Beck, *Surf. Sci.* **145**, L453 (1984).
7. F. M. Leibsle, R. S. Sorbello, and R. G. Greenler, *Surf. Sci.* **179**, 101 (1987).
8. R. K. Brandt and R. G. Greenler, *Chem. Phys. Lett.* **221**, 219 (1994).
9. J. E. Reutt-Robey, Y. J. Chabal, D. J. Doren, and S. B. Christman, *J. Vac. Sci. Technol. A* **7**, 2227 (1989).
10. J. E. Reutt-Robey, D. J. Doren, Y. J. Chabal, and S. B. Christman, *J. Chem. Phys.* **93**, 9113 (1990).
11. D. K. Lambert, *Appl. Optics* **27**, 3744 (1988).
12. D. K. Lambert, *J. Chem. Phys.* **89**, 3847 (1988).
13. J. S. Luo, R. G. Tobin, and D. K. Lambert, *Chem. Phys. Lett.* **204**, 445 (1993).
14. H. Wang, R. G. Tobin, and D. K. Lambert, *J. Chem. Phys.* **101**, 4277 (1994).
15. C. S. Kim, W. J. Tornquist and C. Korzeniewski, *J. Phys. Chem.* **97**, 6484 (1993).
16. C. S. Kim, C. Korzeniewski, and W. J. Tornquist, *J. Chem. Phys.* **100**, 628 (1994).
17. B. A. Sexton, *J. Vac. Sci. Technol.* **16**, 1033 (1979).
18. H. Wang, R. G. Tobin, D. K. Lambert, G. B. Fisher, and C. L. DiMaggio, unpublished.
19. D. M. Collins and W. E. Spicer, *Surf. Sci.* **69**, 85 (1977).
20. W. D. Mieher, L. J. Whitman and W. Ho, *J. Chem. Phys.* **91**, 3228 (1989).

21. J. S. Luo, R. G. Tobin, D. K. Lambert, G. B. Fisher, and C. L. DiMaggio, *J. Chem. Phys.* **99**, 1347 (1993).
22. D. M. Collins and W. E. Spicer, *Surf. Sci.* **69**, 114 (1977).
23. D. F. Ogletree, M. A. Van Hove, and G. A. Somorjai, *Surf. Sci.* **173**, 351 (1986).
24. N. V. Smith, C. T. Chen, and M. Weinert, *Phys. Rev. B* **40**, 7565 (1989).
25. L.-W. H. Leung, A. Wieckowski, and M. J. Weaver, *J. Phys. Chem.* **92**, 6985 (1988).
26. H. Wang, R. G. Tobin, D. K. Lambert, G. B. Fisher, C. L. DiMaggio, to be submitted to *J. Chem. Phys.*
27. P. Lazzretti, and R. Zanasi, *Phys. Rev. A* **24**, 1696 (1981).
28. P. W. Fowler and A. D. Buckingham, *Chem Phys.* **98**, 167 (1985).
29. D. K. Lambert, *Solid State Comm.* **51**, 297 (1984).
30. J. S. Sommers, T. Lindner, M. Surman, A. M. Bradshaw, G. P. Williams, C. F. McConville, and D. P. Woodruff, *Surf. Sci.* **183**, 576 (1987).
31. N. D. Lang, and W. Kohn, *Phys Rev. B*, **7**, 3541 (1973).
32. J. E. Inglesfield, *Surf. Sci.* **188**, L701 (1987).
33. G. C. Aers, J. E. Inglesfield, *Surf. Sci.* **217**, 367 (1989).

Chapter 6

Conclusions

In conclusion, by using RAIRS, EVS, and HREELS techniques, I obtained several significant results about the influence of substrate morphology on the relative interaction strength among the adsorbates on the surface, as well as the field distribution on stepped surfaces.

First, I demonstrated that coadsorbed edge CO and H do not segregate on this surface, even though the interaction between them is still repulsive. This is in sharp contrast to earlier results of coadsorption of H and CO on both Pt(111) and on the step edge of Pt(112), two surfaces structurally similar to Pt(335). Instead, H and CO mix into one dimensional islands along the step edges on Pt(335). Within such islands, CO is shifted by H from atop to bridge sites.

The different overlayer structures show that the relative interaction strength is strongly influenced by the substrate morphology. A small change in the substrate can introduce drastic change in the overlayer structure. The difference between the (335) and (112) results may be related to the idea of "quantum corrals" [1]. As the H-CO interaction is mostly indirect, through metal, the strength depends strongly on the perturbation of the substrate charge density. When we put CO and H together, how much the changes they produce in the substrate charge density match one another is the deciding factor of their interaction. The match can be modulated by the terrace width, as the perturbation wave will be reflected at the next step edges.

I confirmed the proposed site shifting of CO by H with HREELS experiment. I found that coadsorbed H continuously shifts edge CO from atop to bridge sites; this process is almost complete. With this site shifting, I compared the cross section of edge atop and bridge CO. Surprisingly, first, H has a big effect on the cross section of edge

bridge CO; second, edge bridge CO has almost the same cross section as edge atop CO, at least in a H-rich environment. This is very different from the well established result that on Pt(111), atop CO has a cross section 1.8 times bigger than that of bridge CO. I also found that edge atop CO's cross section increases by about 20% with increasing CO coverage; this is in qualitative agreement with a theory of coadsorbate effects. On the other hand, the effect expected from theory is much smaller than 20%, let alone the huge difference in edge bridge CO's cross section observed by us. Our results demonstrate that the coverage-dependent cross section is much more complex than current theory predicts.

I also studied the coadsorption of terrace CO with H on Pt(335). Coadsorbed H has no observable effect on the HREEL spectrum of terrace CO. This is very surprising, since coadsorbed H and CO segregate on Pt(111) and Pt(112), and even on the step edges of Pt(335) coadsorbed H has big effects on edge CO. Our TPD data also suggest that the interaction between terrace CO and terrace H is very weak. The reason for this is not clear. We offered several possibilities: H may go to subsurface sites, H and CO may occupy different rows on the surface naturally, and H may influence some of the CO that is not observed by our spectroscopy tools. This result again demonstrates the strong influence of substrate morphology on overlayer structure.

This study is also significant for its direct comparison of the vibrational cross section and the Stark tuning rate for terrace and atop CO. We found that the cross section of edge atop CO is 2.0 ± 0.2 times greater than that of terrace atop CO and the ratio of the Stark tuning rate is also 2.0 ± 0.2 . The cross section ratio is in qualitative agreement with a classical *E*-field calculation. In contrast to previous belief that only field enhancement at the step edges is important, this model shows that the screening of the field on the terraces is equally significant. The model is also able to partly account for the much smaller difference in cross sections for CO on Pt surfaces on much wider terraces observed by others. This agreement demonstrates that there is little chemical difference between edge and terrace CO, in agreement with a previous HREELS study [2].

The ratio of the Stark tuning rate for CO at the two sites is larger than would be expected from the E -field calculation and the observed ratio of IR intensities. Our data also show that the coverage-dependent screening of the DC and IR field is different, in agreement with a previous finding for CO on Pt(111). It is possible that on step surfaces, the screening and enhancement of applied fields vary significantly over the size of the CO molecule, and the CO response in RAIRS and EVS, depends on different spatial averages. On the other hand, this still would not explain the difference in coverage-dependent screening, which is in contradiction with current models of depolarization within the overlayer.

This work is also significant in providing another direct comparison of the Stark tuning rate measurement between vacuum and electrochemical experiments. I observed the Stark tuning rate for edge CO at low coverage to be $88 \pm 9 \text{ cm}^{-1} (\text{V}/\text{\AA})$, in agreement with a previous vacuum study, but 3 times smaller compared to electrochemical results if conventional double layer models are used. This is similar to with a previous comparison between UHV and electrochemical studies for CO on Pt(111). Coadsorption of H also produces different results. In vacuum, CO's Stark tuning rate is not changed by coadsorbed H but in an electrochemical cell it goes to zero in classical hydrogen region. These results indicate that the electrochemical double layer is probably more complex than we thought. A better understanding of it can be achieved by models that can explain the difference between the UHV and electrochemical studies.

In summary, I found and analyzed several intriguing results in the overlayer structure, relative interaction strength among the coadsorbates, and field distribution on the surface because of the existence of the steps. I have modeled the results, with overlayer structure and electrostatic calculations and offered speculative explanations for still unexplained results. These results will be interesting both as a model for practical catalysis or in distinguishing between electrostatic and chemical effects in chemisorbed systems. They are also very useful for theorists working on the understanding of

chemisorption and interactions among coadsorbates, as well as on the understandings the complex response of metal surface to applied electric fields, and the understanding of electrochemical double layers.

Future experiments can be carried out in several directions that address the unanswered questions and significantly enhance our understanding in the two areas. For example, edge CO and H coadsorption could be studied on a series of samples with various terrace width. A Detailed STM study could examine the perturbation of the local surface density of states by adsorbates on high index surface. UHV water coadsorption experiments have been used to model the electrochemical double layer [3], but CO's response to applied field has not been probed under such conditions. An EVS study of water's influence on CO's Stark tuning rate could be very useful in understanding the different results and gaining a better understanding of the electrochemical double layer. Stark tuning rate measurement of other species would also contribute to the understanding of how admolecules respond to applied fields. Isotope mixture experiments could also help clarify the origin of the different screening of IR and DC fields.

References

1. M. F. Crommie, C. P. Lutz, and D. M. Eigler, *Nature*, **V363**, 524 (June 10, 1994).
2. J. S. Luo, R. G. Tobin, D. K. Lambert, G. B. Fisher, and C. L. DiMaggio, *J. Chem. Phys.* **99**, 1347 (1993).
3. F. T. Wagner, in "*The Structure of Electrified Interfaces*," Vol. 2 in the series "*Frontiers of Electrochemistry*," edited by J. Lipkowski and P. N. Ross, Jr., VCH Publishers.

MICHIGAN STATE UNIV. LIBRARIES



31293014098663